

SLICED WASSERSTEIN REGRESSION

Han Chen and Hans-Georg Müller

Department of Statistics, University of California, Davis
Davis, CA 95616 USA

ABSTRACT

While statistical modeling of distributional data has gained increased attention, the case of multivariate distributions has been somewhat neglected despite its relevance in various applications. This is because the Wasserstein distance, commonly used in distributional data analysis, poses challenges for multivariate distributions. A promising alternative is the sliced Wasserstein distance, which offers a computationally simpler solution. We propose distributional regression models with multivariate distributions as responses paired with Euclidean vector predictors. The foundation of our methodology is a slicing transform from the multivariate distribution space to the sliced distribution space for which we establish a theoretical framework, with the Radon transform as a prominent example. We introduce and study the asymptotic properties of sample-based estimators for two regression approaches, one based on utilizing the sliced Wasserstein distance directly in the multivariate distribution space, and a second approach based on a new slice-wise distance, employing a univariate distribution regression for each slice. Both global and local Fréchet regression methods are deployed for these approaches and illustrated in simulations and through applications. These include joint distributions of excess winter death rates and winter temperature anomalies in European countries as a function of base winter temperature and also data from finance.

KEY WORDS: Distributional data analysis, Multivariate distributional data, Radon transform, Slice-wise Wasserstein distance, Fréchet regression

arXiv:2306.10601v2 [stat.ME] 12 Mar 2024

1 INTRODUCTION

It is increasingly common for statisticians to encounter data that consist of samples of multivariate distributions. Examples include distributions of anthropometric data (Hron et al., 2023), stock price returns for multiple stocks or indices (Guégan and Iacopini, 2018) and systolic and diastolic blood pressure data (Fan and Müller, 2021). Distributional data differ from functional data in that they do not form a vector space. In the emerging field of distributional data analysis, the focus has been on approaches designed for univariate distributions (Matabuena et al., 2021; Ghosal et al., 2023; Petersen et al., 2022) while there is a lack of methodology for the case where samples feature multivariate distributions (Dai, 2022). In this paper, we propose a new regression approach for situations where responses are multivariate distributions and predictors are Euclidean vectors. Our approach is based on a novel general slicing transform framework with the Radon transform as a prominent example and we also introduce a new slice-wise Wasserstein distance. The regression models are developed for both the previously established sliced (in the following referred to as slice-average) Wasserstein (Bonneel et al., 2015) and the new slice-wise Wasserstein paradigms.

For the case of univariate distributions, global bijective transformations, including the log quantile density transform and log hazard transform, have been used to map univariate distributions to a Hilbert space L^2 (Petersen and Müller, 2016), where established functional regression methods can then be deployed. Alternative transformations evolved in the field of compositional data analysis, referred to as Bayes Hilbert space (Hron et al., 2016; Menafoglio et al., 2018). When using the Wasserstein metric in the space of one-dimensional distributions the quasi-Riemannian structure of this space has been exploited by deploying log maps to tangent bundles. One can then develop principal component analysis (Bigot et al., 2017) and regression models (Chen et al., 2023a) in tangent spaces, which are Hilbert spaces so that classical functional data analysis regression models can be applied. This approach comes with some caveats as the inverse exp maps are not defined on the entire tangent space (Pegoraro and Beraha, 2022) and its extension to multivariate distributions has only been considered for the special case of multivariate Gaussian distributions (Okano and Imaizumi, 2023).

An alternative approach for distributional regression is based on learning optimal transports between distributions, where [Ghodrati and Panaretos \(2022\)](#) directly targeted transport maps from predictor to response distributions, and provided a theoretical study of potential extensions of this approach to the multivariate case without discussing or illustrating actual implementations in [Ghodrati and Panaretos \(2023\)](#), while [Zhu and Müller \(2023a\)](#) used rudimentary algebraic operations on the space of optimal transports to build optimal transport regression models, which were demonstrated with the autoregressive modeling of time series of one-dimensional distributions. Fréchet regression is yet another approach that provides an asymptotically consistent regression method for univariate distributions as responses with scalar- or vector-valued predictors ([Petersen and Müller, 2019](#)), but this approach lacks theoretical guarantees for the case of multivariate distributions. Overall, much less is known about regression models for multivariate distributional data. In addition to [Ghodrati and Panaretos \(2023\)](#), a Bayes Hilbert space approach to model bivariate density functions has been discussed ([Guégan and Iacopini, 2018](#); [Hron et al., 2023](#)), without any theoretical guarantees.

Due to the computational and theoretical difficulties when applying optimal transport and Wasserstein distances for multivariate distributions, the sliced Wasserstein distance ([Bonneel et al., 2015](#)), a computationally more efficient alternative to the Wasserstein distance, has gained popularity in statistics and machine learning ([Courty et al., 2017](#); [Kolouri et al., 2019](#); [Rustamov and Majumdar, 2023](#); [Tanguy et al., 2023](#); [Quellmalz et al., 2023](#)). To the best of our knowledge, current studies employing the sliced Wasserstein distance for regression have been limited to the application of kernel methods in machine learning ([Kolouri et al., 2016](#); [Meunier et al., 2022](#); [Zhang et al., 2022](#)) and lack a focus on statistical data analysis and asymptotic convergence.

These considerations motivate the development of a generalized regression framework utilizing the sliced Wasserstein distance based on a slicing transform from the multivariate distribution space to the slicing space. We implement this novel framework with multivariate distributions as responses with two regression techniques, the first of which utilizes the sliced Wasserstein distance in the multivariate distribution space, while the second slice-wise approach utilizes a regression step for each slice, followed by an inverse transform from the sliced space to the original distribu-

tion space. These approaches come with theoretical guarantees on the convergence of the fitted regressions under suitable regularity conditions. Our results build on the strengths of univariate distribution regression while accounting for the effects of the inverse transform. We provide additional assumptions and details for the case where the response distributions need to be recovered from random samples generated by the underlying distributions in section S.3 of the Supplement.

The paper is organized as follows. We introduce analytical tools for slicing transforms with emphasis on the Radon transform in Section 2 and delineate the slicing space in Section 3. In Section 4 we present the two regression models as outlined above, where corresponding estimates are discussed in Section 5. Asymptotic convergence results are presented in Section 6 and practical algorithms in Section 7. We report the results of simulation studies in Section 8 and illustrate the proposed methods with data on excess winter mortality in European countries and also data on weekly returns of the S&P500 index and VIX index in the United States in Section 9, followed by a discussion in Section 10. Additional results and proofs are in the Supplement.

2 SLICING TRANSFORMS FOR MULTIVARIATE DISTRIBUTIONS

2.1 Preliminaries

We denote by $\|\cdot\|_2$ the L^2 norm and by $\|\cdot\|_\infty$ the sup norm for vectors or functions and throughout use C_0, C_1, \dots to denote various constants and their dependence on relevant quantities R will be indicated by writing $C_0(R), C_1(R), \dots$. All notations are listed in Section S.1 of the Supplement. We assume that the multivariate distributions under consideration possess density functions and share a common support set D , assumed to be known or diligently chosen, usually from subject-matter considerations, where

(D1) The support set $D \subset \mathbb{R}^p$ is compact and convex.

Denote the space of multivariate density functions on \mathbb{R}^p with compact support D by

$$\mathcal{F} = \left\{ f \in L^1(\mathbb{R}^p) : f(z) \geq 0, \int_{\mathbb{R}^p} f(z) dz = 1, \text{ support}(f) = D, f \text{ satisfies (F1)} \right\}, \quad (1)$$

where

(F1) There exists a constant $M_0 > 0$ and an integer $k \geq 2$ such that for all $f \in \mathcal{F}$, $\max\{\|f\|_\infty, \|1/f\|_\infty\} \leq M_0$ on D and f is continuously differentiable of order k on D and has uniformly bounded partial derivatives.

(F2) $k > p/2$.

(F3) $k \geq p + 1$.

Smoothness of higher order leads to faster decay rate of Fourier-transformed functions and conditions (F2)-(F3) will be utilized to obtain rates of convergence. We also require a set

$$\mathcal{G} = \left\{ g \in L^1(\mathbb{R}) : g(u) \geq 0, \int_{\mathbb{R}} g(u) du = 1, g \text{ satisfies (D2) and (G1)} \right\}$$

of univariate density functions. Denoting the support set of $g \in \mathcal{G}$ by $I(g)$, we also require

(D2) For all $g \in \mathcal{G}$, the support set $I(g)$ is compact and $\bigcup_{g \in \mathcal{G}} I(g)$ is bounded.

(G1) For k as in (F1), there exists a constant $M_1 > 0$ such that for all $g \in \mathcal{G}$, $\max\{\|g\|_\infty, \|1/g\|_\infty\} \leq M_1$ on $I(g)$; g is continuously differentiable of order k on $I(g)$ with uniformly bounded derivatives.

Throughout, we utilize the unit sphere to denote a slicing parameter set in \mathbb{R}^p ,

$\Theta = \{z \in \mathbb{R}^p : \|z\|_2 = 1\}$. Defining the density slicing space Λ_Θ as a family of maps from Θ to \mathcal{G} ,

$$\Lambda_\Theta = \left\{ \lambda : \Theta \rightarrow \mathcal{G}, \int_{\Theta} \int_{\mathbb{R}} [\lambda(\theta)(u)]^2 dud\theta < \infty \right\},$$

Λ_Θ can be endowed with a L^2 metric,

$$d_2(\lambda_1, \lambda_2) = \left(\int_{\Theta} \int_{\mathbb{R}} (\lambda_1(\theta)(u) - \lambda_2(\theta)(u))^2 dud\theta \right)^{1/2}, \quad \text{for all } \lambda_1, \lambda_2 \in \Lambda_\Theta, \quad (2)$$

where we note that the integral is well defined because of the Cauchy-Schwarz inequality. Two maps λ_1, λ_2 will be considered to be identical if they coincide except on a set of measure zero.

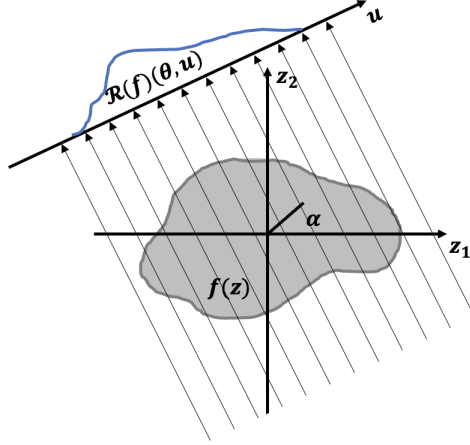


Figure 1: Scheme for the two-dimensional Radon transform. For each unit vector $\theta(\alpha) = (\cos(\alpha), \sin(\alpha))$, the Radon transform integrates along the line $\langle z, \theta \rangle = u$ for each $u \in \mathbb{R}$.

2.2 Radon Transform and Slicing Transforms

The Radon transform \mathcal{R} (Radon, 1917) is an integral transform, which maps an integrable p -dimensional function to the infinite set of its integrals over the hyperplanes of \mathbb{R}^p . Following the notation in Epstein (2007), let θ be a unit vector in Θ , u be an element in \mathbb{R} , and $l_{u,\theta}$ the affine hyperplane represented as $l_{u,\theta} = \{z \in \mathbb{R}^p : \langle z, \theta \rangle = u\}$. Employing an orthonormal basis $\{\theta, e_1, \dots, e_{p-1}\}$ for \mathbb{R}^p with $\langle \theta, e_j \rangle = 0$ and $\langle e_j, e_l \rangle = \delta_{jl}$, for $j, l = 1, \dots, p-1$, the p -dimensional Radon transform $\mathcal{R} : \mathcal{F} \rightarrow \Lambda_\Theta$ is defined through integrals over $l_{u,\theta}$,

$$\mathcal{R}(f)(\theta, u) = \int_{\mathbb{R}^{p-1}} f\left(u\theta + \sum_{j=1}^{p-1} s_j e_j\right) ds_1 \cdots ds_{p-1}, \quad \text{for } \theta \in \Theta \text{ and } u \in \mathbb{R}, \quad (3)$$

where we write $\mathcal{R}(f)(\theta, u)$ for $\mathcal{R}(f)(\theta)(u)$; see Figure 1 for a schematic illustration of the two-dimensional Radon transform. Since $l_{u,\theta}$ and $l_{-u,-\theta}$ are the same line, the Radon transform is an even function that satisfies $\mathcal{R}(f)(\theta, u) = \mathcal{R}(f)(-\theta, -u)$.

The inverse Radon transform is related to the Fourier transform. The p -dimensional Fourier transform $\mathcal{J}_p : L^1(\mathbb{R}^p) \rightarrow \mathbb{C}$ is

$$\mathcal{J}_p(f)(\iota) = \int_{\mathbb{R}^p} e^{-i\langle z, \iota \rangle} f(z) dz, \quad \text{for all } \iota \in \mathbb{R}^p,$$

with the one-dimensional Fourier transform $\mathcal{J}_1 : L^1(\mathbb{R}) \rightarrow \mathbb{C}$ given by $\mathcal{J}_1(g)(r) = \int_{\mathbb{R}} g(u)e^{-iur} du$ for all $r \in \mathbb{R}$. The connection between the Fourier transform and the Radon transform is as follows.

Proposition 1 (Central Slicing Theorem ([Bracewell, 1956](#))). *Assume $f \in \mathcal{F}$. For any real number r and a unit vector $\theta \in \Theta$, $\mathcal{J}_1(\mathcal{R}(f)(\theta))(r) = \mathcal{J}_p(f)(r\theta)$.*

The inverse Radon transform has been well investigated both theoretically and numerically ([Abeida et al., 2012](#); [Herman, 2009](#); [Mersereau and Oppenheim, 1974](#)). A common device to reconstruct the original multivariate function from its Radon transform is the filtered back-projection,

$$\mathcal{R}^{-1}(\lambda)(z) = \frac{1}{2(2\pi)^p} \int_{\Theta} \int_{\mathbb{R}} \mathcal{J}_1(\lambda(\theta))(r) e^{ir\langle\theta, z\rangle} |r|^{p-1} dr d\theta, \quad (4)$$

which satisfies $\mathcal{R}^{-1}(\mathcal{R}(f)) = f$ for any $f \in \mathcal{F}$ ([Natterer, 2001](#); [Epstein, 2007](#)). The inversion formula can be decomposed into two steps. The first step acts as a high-pass filter, suppressing low-frequency components and amplifying high-frequency components. The second step implements an angular integral which can be interpreted as a back-projection of the filtered Radon transform ([Epstein, 2007](#); [Helgason, 2010](#)). However, \mathcal{R}^{-1} is not a continuous map, and small errors in the reconstruction of $\mathcal{R}(f)$ are amplified ([Epstein, 2007](#)). Therefore, regularization is usually applied when reconstructing the original function from its Radon transform ([Horbelt et al., 2002](#); [Qureshi et al., 2005](#); [Shepp and Vardi, 1982](#)), often through the use of a ramp filter that has a cut-off in the high-frequency domain ([Epstein, 2007](#); [Kak and Slaney, 2001](#)).

Defining a regularizing function $\phi_{\tau}(r)$ with tuning parameter τ as $\phi_{\tau}(r) = 1$ for $|r| \leq \tau$ and $\phi_{\tau}(r) = 0$ for $|r| > \tau$, the regularised inverse map $\tilde{\mathcal{R}}_{\tau}^{-1} : \Lambda_{\Theta} \rightarrow L^1(\mathbb{R}^p)$ is obtained by cutting off the high-frequency components in the filtered back-projection (4) through

$$\tilde{\mathcal{R}}_{\tau}^{-1}(\lambda)(z) = \frac{1}{2(2\pi)^p} \int_{\Theta} \int_{\mathbb{R}} \mathcal{J}_1(\lambda(\theta))(r) e^{ir\langle\theta, z\rangle} |r|^{p-1} \phi_{\tau}(r) dr d\theta. \quad (5)$$

As this regularized inverse is not guaranteed to be a multivariate density function, normalization

is applied to map the resulting L^1 function into the multivariate density space \mathcal{F} via

$$\mathcal{R}_\tau^{-1}(\lambda)(z) = \begin{cases} |\check{\mathcal{R}}_\tau^{-1}(\lambda)(z)| / \int_D |\check{\mathcal{R}}_\tau^{-1}(\lambda)(z)| dz & \text{if } \int_D |\check{\mathcal{R}}_\tau^{-1}(\lambda)(z)| dz > 0, \\ 1/|D| & \text{otherwise,} \end{cases} \quad (6)$$

where $|D|$ is the Lebesgue measure of the domain set D . Note that $\mathcal{R}_\tau^{-1}(\lambda)(z)$ satisfies the differentiability assumption in (F1) while the boundedness assumption can be enforced by projecting to the space \mathcal{F} where (F1) is satisfied.

If $\mathcal{R}(f)$ is approximated by $\widetilde{\mathcal{R}}(f)$, the reconstruction function $\tilde{f}_\tau = \mathcal{R}_\tau^{-1} \circ \widetilde{\mathcal{R}}(f)$ will approximate the original function f with the reconstruction error represented as the sum of two error terms

$$\Delta_\tau = f - \tilde{f}_\tau = (f - \mathcal{R}_\tau^{-1} \circ \mathcal{R}(f)) + \mathcal{R}_\tau^{-1} \circ (\mathcal{R}(f) - \widetilde{\mathcal{R}}(f)).$$

Let $\Delta_{\tau,1} = f - \mathcal{R}_\tau^{-1} \circ \mathcal{R}(f)$ and $\Delta_{\tau,2} = \mathcal{R}_\tau^{-1} \circ (\mathcal{R}(f) - \widetilde{\mathcal{R}}(f))$.

Theorem 1. *Assume (D1), (F1) and (F3). If $f \in \mathcal{F}$, as $d_2(\mathcal{R}(f), \widetilde{\mathcal{R}}(f)) \rightarrow 0$ and $\tau \rightarrow \infty$,*

$$\begin{aligned} \|\Delta_{\tau,1}\|_\infty &= O(\tau^{-(k-p)}), & \|\Delta_{\tau,2}\|_\infty &= O(\tau^p d_2(\mathcal{R}(f), \widetilde{\mathcal{R}}(f))), \\ \|\Delta_\tau\|_\infty &= O(\tau^{-(k-p)} + \tau^p d_2(\mathcal{R}(f), \widetilde{\mathcal{R}}(f))). \end{aligned}$$

The first error term $\Delta_{\tau,1}$ arises from the regularised inverse map and decreases with τ . The convergence of $\Delta_{\tau,1}$ relies on the smoothness assumption for densities, where higher order smoothness corresponds to a faster convergence rate of the Fourier transform in the frequency domain. The second error term $\Delta_{\tau,2}$ results from the approximation of $\mathcal{R}(f)$ and increases with τ . The value of the tuning parameter τ is then ideally chosen to minimize the total error Δ_τ . While the focus of this paper is primarily on the Radon transform, there are other transforms that may also be of interest such as the circular Radon transform (Kuchment, 2006) and the generalized Radon transform (Beylkin, 1984; Ehrenpreis, 2003); see Section S.6 in the Supplement for further details.

Next, we consider a general *slicing transform* $\psi : \mathcal{F} \rightarrow \Lambda_\Theta$ that maps a multivariate density

function on D into a density slicing function indexed by the slicing parameter set Θ and satisfies

(T0) ψ is injective.

(T1) For a constant C_0 , $d_2(\psi(f_1)(\theta), \psi(f_2)(\theta)) \leq C_0 d_2(f_1, f_2)$, for all $f_1, f_2 \in \mathcal{F}$ and $\theta \in \Theta$.

(T2) An inverse transform ψ^{-1} exists such that $\psi^{-1} \circ \psi(f) = f$, for all $f \in \mathcal{F}$.

(T3) There exists a sequence of approximating inverses ψ_τ^{-1} and constants $C_1(\tau), C_2(\tau)$ such that

$$d_\infty(\psi_\tau^{-1} \circ \psi(f), f) \leq C_1(\tau) \text{ for all } f \in \mathcal{F} \text{ and}$$

$$d_\infty(\psi_\tau^{-1} \circ \psi(f), \psi_\tau^{-1}(\lambda)) \leq C_2(\tau) d_2(\psi(f), \lambda) \text{ for all } \lambda \in \Lambda_\Theta, f \in \mathcal{F}, \text{ as } d_2(\psi(f), \lambda) \rightarrow 0, \text{ where}$$

$C_1(\tau)$ and $C_2(\tau)$ depend only on τ , and $C_1(\tau)$ is decreasing to 0 while $C_2(\tau)$ is increasing as $\tau \rightarrow \infty$.

Assumption (T1) is concerned with the continuity of the forward transform, while assumption (T2) provides the existence of an inverse transform from the image set $\psi(\mathcal{F})$ to \mathcal{F} . Note that $\psi(\mathcal{F})$ is not required to cover the entire space Λ_Θ and the inverse transform ψ^{-1} is only defined on the image space $\psi(\mathcal{F})$ of \mathcal{F} . The sequence of approximating inverses ψ_τ^{-1} in assumption (T3) is required when mapping elements in Λ_Θ that are not in $\psi(\mathcal{F})$ back to \mathcal{F} . To be able to make use of a slicing transform for both forward and inverse transformations we require an additional property and call a slicing transform *valid* if in addition to (T1)-(T3) it satisfies

(T4) Under (D1) and (F1), it holds that $\psi(\mathcal{F}) \subset \Lambda_\Theta$ and (D2), (G1) are satisfied for all $\lambda(\theta)$ for which $\lambda \in \psi(\mathcal{F})$.

Proposition 2. *The Radon transform \mathcal{R} is a valid slicing transform, i.e., it satisfies assumptions (T0)-(T4) where $C_1(\tau) = O(\tau^{-(k-p)})$ and $C_2(\tau) = O(\tau^p)$ as $\tau \rightarrow \infty$.*

3 DISTRIBUTION SLICING AND SLICED DISTANCE

As a formal device we use a map φ that assigns to any given distribution its associated density function, while its inverse φ^{-1} maps a density function to its corresponding distribution. Consider the metric space (\mathcal{F}, d) , where $\mathcal{F} = \{\mu \in \mathcal{F}: \mu \text{ has a density function } \varphi(\mu) \in \mathcal{F}\}$ and d is a metric on \mathcal{F} . Many metrics can be considered, including the Fisher-Rao metric (Dai, 2022; Zhu and Müller, 2023c) or the Wasserstein metric (Gibbs and Su, 2002), which is closely connected

with the optimal transport problem (Kantorovich, 2006; Villani, 2003). The L^2 -Wasserstein metric between two random distributions is defined as

$$d_W^2(\mu_1, \mu_2) = \inf_{\substack{\mu \in \mathcal{P}(\mu_1, \mu_2), \\ (Z_1, Z_2) \sim \mu}} E(\|Z_1 - Z_2\|_2^2), \quad \text{for all } \mu_1, \mu_2 \in \mathcal{F}, \quad (7)$$

where Z_1 and Z_2 are random variables on \mathbb{R}^p , μ_1 and μ_2 are random distributions supported on D and $\mathcal{P}(\mu_1, \mu_2)$ is the space of joint probability measures on $D \times D$ with marginal distributions μ_1 and μ_2 . We use the notations $\mathcal{G} = \{\nu \in \mathcal{G} : \nu \text{ has a density function } \varphi(\nu) \in \mathcal{G}\}$ for a space of univariate distributions, G for the map that maps univariate distributions to their corresponding quantile function, with G^{-1} mapping a quantile function to its corresponding distribution and $\mathcal{Q} = \{Q \in \mathcal{Q} : \text{There exists a univariate distribution } \nu \in \mathcal{G} \text{ such that } Q = G(\nu)\}$.

The L^2 -Wasserstein metric (7) can be equivalently expressed in terms of quantile functions,

$$d_W^2(\nu_1, \nu_2) = \int_0^1 (G^{-1}(\nu_1)(s) - G^{-1}(\nu_2)(s))^2 ds, \quad \text{for all } \nu_1, \nu_2 \in \mathcal{G}.$$

When the dimension p of the random distribution is larger than 1, i.e., $p \geq 2$, one does not have an analytic form of the Wasserstein distance and the algorithms to obtain it are complex (Rabin et al., 2011; Peyré et al., 2019). The sliced Wasserstein distance (Bonneel et al., 2015) is a computationally more efficient alternative that utilizes the Radon transform. It has become increasingly popular for multivariate distributions due to its attractive topological and statistical properties (Nadjahi et al., 2019, 2020; Kolouri et al., 2016).

We define the quantile slicing space Γ_Θ as a family of maps from Θ to \mathcal{Q} ,

$$\Gamma_\Theta = \left\{ \gamma \in \Gamma_\Theta : \Theta \rightarrow \mathcal{Q}, \int_\Theta \int_{[0,1]} \gamma(\theta)(s)^2 ds d\theta < \infty \right\}$$

and introduce a map $\varrho : \Gamma_\Theta \rightarrow \Lambda_\Theta$ as $\varrho(\gamma)(\theta) = \varphi(G^{-1}(\gamma(\theta)))$, $\gamma \in \Gamma_\Theta$, which sends a quantile function $\gamma(\theta)$ to its corresponding density function. Similarly, ϱ^{-1} can be defined through $\varrho^{-1}(\lambda)(\theta) = G \circ \varphi^{-1}(\lambda(\theta))$, $\lambda \in \Lambda_\Theta$; see Figure 2 for a schematic illustration. A slicing transform

ψ between \mathcal{F} and Λ_Θ can be naturally extended to a transform $\tilde{\psi}$ between $\tilde{\mathcal{F}}$ and Γ_Θ ,

$$\tilde{\psi}(\mu) = \varrho^{-1} \circ \psi \circ \varphi(\mu), \quad \mu \in \tilde{\mathcal{F}}. \quad (8)$$

The inverse transform $\tilde{\psi}^{-1}$ and regularized inverse transform $\tilde{\psi}_\tau^{-1}$ can be extended as

$$\tilde{\psi}_\tau^{-1}(\gamma) = \varphi^{-1} \circ \psi_\tau^{-1} \circ \varrho(\gamma), \quad \gamma \in \Gamma_\Theta \text{ and } \tilde{\psi}^{-1}(\gamma) = \varphi^{-1} \circ \psi^{-1} \circ \varrho(\gamma), \quad \gamma \in \tilde{\psi}(\tilde{\mathcal{F}}). \quad (9)$$

Note that the space of Γ_Θ is closed and convex. Define the distribution-slicing Wasserstein

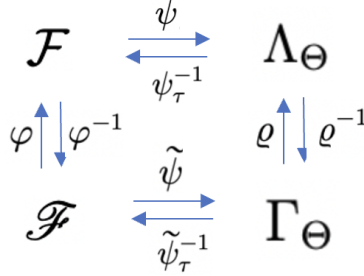


Figure 2: Schematic of maps involved in the slicing transform. Here φ maps the multivariate distribution space $\tilde{\mathcal{F}}$ to the multivariate density space \mathcal{F} and ϱ maps the quantile slicing space Γ_Θ to the density slicing space Λ_Θ . A slicing transform ψ and its inverse ψ_τ^{-1} with a tuning parameter τ between \mathcal{F} and Λ_Θ can be naturally extended to a slicing transform between $\tilde{\mathcal{F}}$ and Γ_Θ through the induced maps $\tilde{\psi}$ and $\tilde{\psi}_\tau^{-1}$.

metric on Γ_Θ through the aggregated Wasserstein distance across the slices

$$\begin{aligned} d_{DW}(\gamma_1, \gamma_2) &= \left(\int_{\Theta} d_W^2(G^{-1}(\gamma_1(\theta)), G^{-1}(\gamma_2(\theta))) d\theta \right)^{1/2} \\ &= \left(\int_{\Theta} \int_{[0,1]} (\gamma_1(\theta)(s) - \gamma_2(\theta)(s))^2 ds d\theta \right)^{1/2}, \quad \gamma_1, \gamma_2 \in \Gamma_\Theta. \end{aligned} \quad (10)$$

Here the integral is well defined because of the Cauchy-Schwarz inequality. We then define the slice-averaged Wasserstein distance as

$$d_{SW}(\mu_1, \mu_2) = d_{DW}(\tilde{\psi}(\mu_1), \tilde{\psi}(\mu_2)), \quad \text{for all } \mu_1, \mu_2 \in \tilde{\mathcal{F}}. \quad (11)$$

Proposition 3. *The slice-averaged Wasserstein distance is a distance over \mathcal{F} if and only if (T0) is satisfied.*

4 SLICED WASSERSTEIN REGRESSION FOR MULTIVARIATE DISTRIBUTIONS

A general approach for the regression of metric-valued responses and Euclidean predictors is Fréchet regression with both global and local versions (Petersen and Müller, 2019; Chen and Müller, 2022), where its application to distributional data extensively discussed in recent studies (Fan and Müller, 2022; Zhou and Müller, 2023). We extend Fréchet regression to the case of multivariate distributions by providing two types of sliced regression models. The first model applies Fréchet regression to the multivariate distribution space \mathcal{F} equipped with the slice-averaged Wasserstein distance, while the second model applies a Fréchet regression step for each slice, followed by the regularized inverse transform.

Suppose $(X, \mu) \sim F$ is a random pair, where predictors X and responses μ take values in \mathbb{R}^q and \mathcal{F} and F is their joint distribution. Denote the marginal distributions of X and μ as F_X and F_μ respectively, and assume that mean $E(X)$ and variance $\text{Var}(X)$ exist, where $\text{Var}(X)$ is positive definite. The conditional distributions $F_{\mu|X}$ and $F_{X|\mu}$ are also assumed to exist. Given any metric d on \mathcal{F} , Fréchet mean and Fréchet variance of the random distribution μ are defined as

$$\omega_\oplus = \underset{\omega \in \mathcal{F}}{\operatorname{argmin}} E [d^2(\mu, \omega)], \quad V_\oplus = E [d^2(\mu, \omega_\oplus)]. \quad (12)$$

The conditional Fréchet mean, i.e., the regression function of μ given $X = x$, targets

$$m(x) = \underset{\omega \in \mathcal{F}}{\operatorname{argmin}} M(\omega, x), \quad M(\cdot, x) = E [d^2(\mu, \cdot) | X = x], \quad (13)$$

where $M(\cdot, x)$ is the conditional Fréchet function. The global Fréchet regression given $X = x$ is

$$m_G(x) = \underset{\omega \in \mathcal{F}}{\operatorname{argmin}} M_G(\omega, x), \quad M_G(\cdot, x) = E [s_G(X, x) d^2(\mu, \cdot)], \quad (14)$$

where the weight $s_G(X, x) = 1 + (X - E(X))^T \text{Var}(X)^{-1}(x - E(X))$ is linear in x .

The proposed slice-averaged Wasserstein (SAW) regression employs Fréchet regression over the multivariate distribution space \mathcal{F} equipped with the slice-averaged Wasserstein distance

$$m^{SAW}(x) = \underset{\omega \in \mathcal{F}}{\operatorname{argmin}} M^{SAW}(\omega, x), \quad M^{SAW}(\cdot, x) = E \left[d_{SW}^2(\mu, \cdot) | X = x \right]. \quad (15)$$

The global slice-averaged Wasserstein (GSAW) regression given x is defined as

$$m_G^{SAW}(x) = \underset{\omega \in \mathcal{F}}{\operatorname{argmin}} M_G^{SAW}(\omega, x), \quad M_G^{SAW}(\cdot, x) = E \left[s_G(X, x) d_{SW}^2(\mu, \cdot) \right]. \quad (16)$$

The second proposed model is the slice-wise Wasserstein (SWW) regression, where Fréchet regression is applied over the quantile slicing space Γ_Θ , equipped with the distribution-slicing Wasserstein metric, followed by the regularized inverse transform,

$$m_\tau^{SWW}(x) = \tilde{\psi}_\tau^{-1} \left[\underset{\gamma \in \Gamma_\Theta}{\operatorname{argmin}} M^{SWW}(\gamma, x) \right], \quad M^{SWW}(\cdot, x) = E \left[d_{DW}^2(\tilde{\psi}(\mu), \cdot) | X = x \right]. \quad (17)$$

The global slice-wise Wasserstein (GSWW) regression given $X = x$ is

$$m_{G,\tau}^{SWW}(x) = \tilde{\psi}_\tau^{-1} \left[\underset{\gamma \in \Gamma_\Theta}{\operatorname{argmin}} M_G^{SWW}(\gamma, x) \right], \quad M_G^{SWW}(\cdot, x) = E \left[s_G(X, x) d_{DW}^2(\tilde{\psi}(\mu), \cdot) \right]. \quad (18)$$

We note that for SAW based models the minimization is carried out over the space \mathcal{F} and thus is automatically a multivariate distribution, while for SWW based models the minimization is carried out slicewise and as the slice-wise minimizers are not guaranteed to be situated in $\psi(\mathcal{F})$, a regularized inverse is needed since the inverse ψ^{-1} is only defined on $\psi(\mathcal{F})$.

Proposition 4. *Let $\gamma_{G,x} = \underset{\gamma \in \Gamma_\Theta}{\operatorname{argmin}} M_G^{SWW}(\gamma, x)$, see (18). It can be characterized as*

$$\gamma_{G,x}(\theta) = \underset{\nu \in \mathcal{G}}{\operatorname{argmin}} E \left[s_G(X, x) d_W^2 \left(G^{-1} \left(\tilde{\psi}(\mu)(\theta) \right), \nu \right) \right], \quad \text{for almost all } \theta \in \Theta.$$

This characterization of SWW regression provides a practical implementation of this method.

Proposition [S6](#) in the Supplement demonstrates that the search space of SAW is a subset of the search space of SWW. Note that besides global Fréchet regression as described above one can analogously develop more flexible local Fréchet regression based models for both SAW and SWW regression approaches. These combine SAW and SSW with local Fréchet regression rather than the above described global regression and are referred to as LSAW for the local version of SAW and LSWW for the local version of SWW. Details about the implementation of these local versions can be found in Section [S.4](#) in the Supplement. So overall the proposed methodology encompasses four regression approaches (GSWW, GSAW, LSWW, LSAW).

5 ESTIMATION

Suppose we have a sample of independent random pairs $\{(X_i, \mu_i)\}_{i=1}^n \sim F$. Sample mean and covariance can be obtained as

$$\bar{X} = n^{-1} \sum_{i=1}^n X_i, \quad \hat{\Sigma} = n^{-1} \sum_{i=1}^n (X_i - \bar{X})(X_i - \bar{X})^T.$$

If random distributions μ_i are fully observed on domain D , sample-based estimators for GSAW and GSWW are given by

$$\check{m}_G^{SAW}(x) = \operatorname{argmin}_{\omega \in \mathcal{F}} \check{M}_G^{SAW}(\omega, x), \quad \check{M}_G^{SAW}(\cdot, x) = n^{-1} \sum_{i=1}^n [s_{iG}(x) d_{SW}^2(\mu_i, \cdot)], \quad (19)$$

$$\check{m}_{G,\tau}^{SWW}(x) = \tilde{\psi}_\tau^{-1} \left[\operatorname{argmin}_{\gamma \in \Gamma_\Theta} \check{M}_G^{SWW}(\gamma, x) \right], \quad \check{M}_G^{SWW}(\cdot, x) = n^{-1} \sum_{i=1}^n [s_{iG}(x) d_{DW}^2(\tilde{\psi}(\mu_i), \cdot)], \quad (20)$$

where $s_{iG}(x) = 1 + (X_i - \bar{X})^T \hat{\Sigma}^{-1} (x - \bar{X})$ is the sample version of $s_G(X, x)$.

An additional challenge in many statistical applications is that random distributions $\{\mu_i\}_{i=1}^n$ are not directly observed and instead one has available only the observations that they generate. For such scenarios, we implement a preliminary density estimation step, with further details on this provided in Section [S.3](#) in the Supplement, where also extended assumptions for this scenario are listed that aim at avoiding the interference of boundary effects and also at dealing with

distribution-specific domains, in which case the target distributions are considered to correspond to the truncated distributions on a common domain D . Employing kernel density estimates as provided in $\hat{\mu}_i$ (S.1) of Section S.3, one obtains

$$\hat{m}_G^{SAW}(x) = \underset{\omega \in \mathcal{F}}{\operatorname{argmin}} \hat{M}_G^{SAW}(\omega, x), \quad \hat{M}_G^{SAW}(\cdot, x) = n^{-1} \sum_{i=1}^n [s_{iG}(x) d_{SW}^2(\hat{\mu}_i, \cdot)], \quad (21)$$

$$\hat{m}_{G,\tau}^{SWW}(x) = \tilde{\psi}_\tau^{-1} \left[\underset{\gamma \in \Gamma_\Theta}{\operatorname{argmin}} \hat{M}_G^{SWW}(\gamma, x) \right], \quad \hat{M}_G^{SWW}(\cdot, x) = n^{-1} \sum_{i=1}^n [s_{iG}(x) d_{DW}^2(\tilde{\psi}(\hat{\mu}_i), \cdot)]. \quad (22)$$

Sample version estimators of the local smoothing models for SAW and SWW, along with an analysis of the bandwidth selection, can be found in Section S.4.2 in the Supplement.

A practical data-driven approach to select the tuning parameter τ when an i.i.d. sample of random pairs $\{(X_i, \mu_i)\}_{i=1}^n$ is available can be obtained by leave-one-out cross-validation. Specifically, we aim to minimize the discrepancy between predicted and observed distributions, given by

$$\hat{\tau} = \underset{\tau}{\operatorname{argmin}} \sum_{i=1}^n d_{SW}^2(\mu_i, \hat{m}_{G,\tau,-i}^{SWW}(X_i)),$$

where $\hat{m}_{G,\tau,-i}^{SWW}(X_i)$ is the prediction at X_i from the GSWW regression of the i th-left-out sample $\{(X_{i'}, \mu_{i'})\}_{i' \neq i}$. When the sample size n exceeds 30, we substitute leave-one-out cross-validation with 5-fold cross-validation to strike a balance between computational efficiency and the accuracy.

We define a slice-averaged Wasserstein R^2 coefficient to quantify the discrepancy between observed distributions and predicted distributions from the regression model as

$$R_\oplus^2 = 1 - \frac{E[d_{SW}^2(\mu, m(x))]}{E[d_{SW}^2(\mu, \mu_\oplus)]},$$

where $m(x)$ is a regression object through either SAW or SWW regression and μ_\oplus is the slice-averaged Wasserstein Fréchet mean $\mu_\oplus = \underset{\omega \in \mathcal{F}}{\operatorname{argmin}} d_{SW}^2(\mu, \omega)$, with empirical estimates

$$\hat{R}_\oplus^2 = 1 - \frac{\sum_{i=1}^n d_{SW}^2(\mu_i, \hat{m}(x))}{\sum_{i=1}^n d_{SW}^2(\mu_i, \hat{\mu}_\oplus)}, \quad (23)$$

for a sample $\{(X_i, \mu_i)\}_{i=1}^n$. Here $\hat{\mu}_\oplus = \operatorname{argmin}_{\omega \in \mathcal{F}} n^{-1} \sum_{i=1}^n d_{SW}^2(\mu_i, \omega)$ is the sample Fréchet mean and $\hat{m}(x)$ is the sample estimator of the regression object $m(x)$ for SAW or SWW regression.

6 ASYMPTOTIC CONVERGENCE

To study the convergence of SAW/SWW regression, we require a curvature condition at the true minimizer, as is commonly assumed for M estimators. For Fréchet regression such a curvature condition has been established for the case of univariate distributions but not for multivariate distributions. Convexity assumptions have also been invoked in previous work (Fan and Müller, 2021; Boissard et al., 2015; Zhou and Müller, 2022). Specifically, we require

(A1) $\tilde{\psi}(\mathcal{F})$ is closed and convex.

(A2) $\operatorname{argmin}_{\gamma \in \Gamma_\Theta} M_G^{SWW}(\gamma, x)$ as per (18) is in $\tilde{\psi}(\mathcal{F})$.

Assumption (A1) guarantees the existence and uniqueness of the minimizer of the SAW regression, while assumption (A2) ensures the underlying minimizer of the GSWW regression belongs to the image space of the slicing transform. The following results are for global SAW and SWW regression for the two scenarios where densities are known or must be estimated from data. In the latter case, we require additional assumptions (P1), (K1), (K2) and (F1') that are provided in the Supplement Section S.3, which also contains details about the construction of the density estimates, as well as the results for local SAW and local SWW regression in Theorems S1 and S3 for known densities and in Theorems S2 and S4 for the case where densities must be estimated.

Theorem 2. *(Convergence of global SAW regression). Assume (D1), (F1)-(F2), (A1) and (T0)-(T2). For a fixed $x \in \mathbb{R}^q$, it holds for $m_G^{SAW}(x)$, $\check{m}_G^{SAW}(x)$ and $\hat{m}_G^{SAW}(x)$ as per (16), (19) and (21) that*

$$d_{SW}(m_G^{SAW}(x), \check{m}_G^{SAW}(x)) = O_p(n^{-1/2}), \quad \sup_{\|x\|_E \leq B} d_{SW}(m_G^{SAW}(x), \check{m}_G^{SAW}(x)) = O_p(n^{-1/(2+\epsilon)}),$$

for a given $B > 0$ and any $\epsilon > 0$. For the case where densities need to be estimated, under the

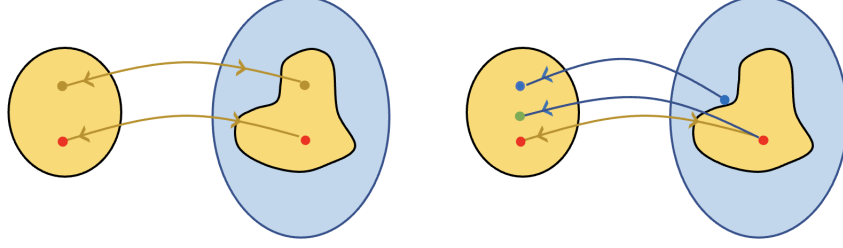


Figure 3: Diagram for SAW (left) and SWW (right) sample estimation. The red dots are population minimizers, the yellow dots are the sample SAW minimizer, the blue dots are the sample SWW minimizers and the green dot is the intermediate state used to facilitate the error analysis of SWW. Bidirectional yellow maps represent $\tilde{\psi}$ and $\tilde{\psi}^{-1}$ while directional blue maps represent the regularized inverse $\tilde{\psi}_\tau^{-1}$.

additional assumptions (P1), (F1'), (K1)-(K2) in Section S.3 of the Supplement,

$$d_{SW} (m_G^{SAW}(x), \hat{m}_G^{SAW}(x)) = O_p(n^{-1/2}), \quad \sup_{\|x\|_E \leq B} d_{SW} (m_G^{SAW}(x), \hat{m}_G^{SAW}(x)) = O_p(n^{-1/(2+\epsilon)}).$$

Using global Fréchet regression for tracking the global SAW target thus yields a parametric convergence rate that does not depend on the dimension of the distribution space. For SAW, convergence in terms of the sup norm is not possible due to the inverse transform $\tilde{\psi}^{-1}$, which amplifies estimation error in the image space, as exemplified above for the Radon transform. Since the regularized inverse transform $\tilde{\psi}_\tau^{-1}$ is continuous due to (T3), it is possible to obtain sup norm convergence for SWW. Under assumption (A2), the population-level target m_G^{SWW} is

$$m_G^{SWW} = \tilde{\psi}^{-1} \left[\operatorname{argmin}_{\gamma \in \Gamma_\Theta} M_G^{SWW}(\gamma, x) \right], \quad (24)$$

where M_G^{SWW} is as in (18).

Theorem 3. (Convergence of global SWW regression). Assume (D1), (F1), (F3), (A2), (T0)-(T4). For a fixed $x \in \mathbb{R}^q$, for $m_G^{SWW}(x)$, $\check{m}_{G,\tau}^{SWW}(x)$ and $\hat{m}_{G,\tau}^{SWW}(x)$ as per (24), (20) and (22), $C_1(\tau)$ and $C_2(\tau)$ from (T3),

$$d_\infty (m_G^{SWW}(x), \check{m}_{G,\tau}^{SWW}(x)) = O_p(C_1(\tau) + C_2(\tau)n^{-2/7}).$$

Furthermore, for a given $B > 0$ and any $\epsilon > 0$,

$$\sup_{\|x\|_E \leq B} d_\infty (m_G^{SWW}(x), \check{m}_{G,\tau}^{SWW}(x)) = O_p (C_1(\tau) + C_2(\tau)n^{-2/(\tau+\epsilon)}).$$

For estimated densities one obtains the same rates under (P1), (F1'), (K1)-(K2) in Section S.3 of the Supplement, for $d_\infty (m_G^{SWW}(x), \hat{m}_{G,\tau}^{SWW}(x))$ and $\sup_{\|x\|_E \leq B} d_\infty (m_G^{SWW}(x), \hat{m}_{G,\tau}^{SWW}(x))$.

The reconstruction error has two parts. The first term $C_1(\tau)$ is linked to the approximation bias in the reconstruction, while the second term $C_2(\tau)$ ensures that the approximation in the transformed space Γ_Θ is not excessively amplified (see Figure 3). If the slicing transform is the Radon transform, Corollary 1 shows that the curse of dimensionality is manifested in both $C_1(\tau)$ and $C_2(\tau)$, as the required order of smoothness increases with the dimension of the distribution to achieve the same convergence rate. We only provide the more intricate scenario when densities are not fully observed; analogous results hold for the case of known densities.

Corollary 1. *When taking the Radon transform \mathcal{R} and the corresponding regularized inverse \mathcal{R}_τ^{-1} as per (3) and (6), under the assumptions of Theorem 3,*

$$\begin{aligned} d_\infty (m_G^{SWW}(x), \hat{m}_{G,\tau}^{SWW}(x)) &= O_p (\tau^{-(k-p)} + \tau^p n^{-2/7}), \\ \sup_{\|x\|_E \leq B} d_\infty (m_G^{SWW}(x), \hat{m}_{G,\tau}^{SWW}(x)) &= O_p (\tau^{-(k-p)} + \tau^p n^{-2/(\tau+\epsilon)}), \end{aligned}$$

and with $\tau \sim n^{2/7k}$,

$$d_\infty (m_G^{SWW}(x), \hat{m}_{G,\tau}^{SWW}(x)) = O_p \left(n^{-2\frac{k-p}{7k}} \right), \quad \sup_{\|x\|_E \leq B} d_\infty (m_G^{SWW}(x), \hat{m}_{G,\tau}^{SWW}(x)) = O_p \left(n^{-2\frac{k-p}{7k+\epsilon}} \right).$$

7 NUMERICAL ALGORITHM

7.1 SAW Regression

To solve problem (21) in practice, we use a numerical optimization process proposed in [Bonnel et al. \(2015\)](#) that involves parametrizing a probability measure with equal weights. Specifically,

we use random observations $\mathbf{W} = \{\mathbf{W}_j\}_{j=1}^N \in \mathbb{R}^{p \times N}$ where each observation $\mathbf{W}_j \in \mathbb{R}^p$ follows a distribution characterized by a density function $f_{\mathbf{W}}$ in \mathcal{F} . We introduce the Radon slicing operation $\langle \cdot, \theta \rangle : \mathbb{R}^p \rightarrow \mathbb{R}$ for each random observation, resulting in a univariate distribution with the density function $\mathcal{R} \circ f_{\mathbf{W}}(\theta)$. The multivariate distribution μ corresponding to the density $f_{\mathbf{W}}$ can be represented as a discrete input measure $\mu_{\mathbf{W}} = \frac{1}{N} \sum_{j=1}^N \delta_{\mathbf{W}_j}$. Similarly, we represent the i -th distribution μ_i as a discrete input measure $\mu_{\mathbf{W}^{(i)}} = \frac{1}{N} \sum_{j=1}^N \delta_{\mathbf{W}_{ij}}$ where $\mathbf{W}^{(i)} = \{\mathbf{W}_{ij}\}_{j=1}^{n_i} \in \mathbb{R}^{p \times N}$ and $\mathbf{W}_{ij} \sim \mu_i$. The GSAW regression of (21) given $X = x$ can be represented as

$$\operatorname{argmin}_{\mathbf{W} \in \mathbb{R}^{p \times N}} \mathcal{M}_G(\mathbf{W}, x) = n^{-1} \sum_{i=1}^n [s_{iG}(x) d_{SW}^2(\mu_{\mathbf{W}^{(i)}}, \mu_{\mathbf{W}})]. \quad (25)$$

It is known that the target function is smooth for the Radon transform, a result that we state below for reference. We use the notation $\mathbf{W}(\theta) = (\langle \mathbf{W}_j, \theta \rangle)_{j=1}^N \in \mathbb{R}^N$ and similarly $\mathbf{W}^{(i)}(\theta) = (\langle \mathbf{W}_{ij}, \theta \rangle)_{j=1}^{n_i} \in \mathbb{R}^{n_i}$. For any $A = \{A_j\}_{j=1}^N \in \mathbb{R}^N$ where $A_j \in \mathbb{R}$, Π_A is a permutation operator on A , such that $\Pi_A(A) = (A_{\Pi(1)}, A_{\Pi(2)}, \dots, A_{\Pi(N)})^T$ with $A_{\Pi(1)} \leq A_{\Pi(2)} \leq \dots \leq A_{\Pi(N)}$.

Proposition 5 (Theorem 1 (Bonneel et al., 2015)). *For each fixed x and $N_i \equiv N$, $\mathcal{M}_G(\mathbf{W}, x) : \mathbb{R}^{p \times N} \rightarrow \mathbb{R}$ is a L^1 function with a uniformly ρ_G -Lipschitz gradient for some $\rho_G > 0$ given by*

$$\nabla \mathcal{M}_G(\mathbf{W}, x) = n^{-1} \sum_{i=1}^n \left[s_{iG}(x) \int_{\Theta} \theta \left(\mathbf{W}(\theta) - \Pi_{\mathbf{W}(\theta)}^{-1} \circ \Pi_{\mathbf{W}^{(i)}(\theta)} \circ \mathbf{W}^{(i)}(\theta) \right)^T d\theta \right].$$

The operation $\Pi_{\mathbf{W}(\theta)}^{-1} \circ \Pi_{\mathbf{W}^{(i)}(\theta)} \circ \mathbf{W}^{(i)}(\theta)$ aligns $\mathbf{W}^{(i)}(\theta)$ with $\mathbf{W}(\theta)$ in the sense of non-decreasing order for calculating the empirical Wasserstein distance. In practice, an equidistant grid $(\theta_1, \theta_2, \dots, \theta_L)$ along the angular coordinate θ is used to approximate the integration over Θ . Note that (25) is non-convex and Algorithm 1 uses gradient descent to find a stationary point.

Since the algorithm implied by Proposition 5 requires that the sample sizes N_i at which each distribution is sampled are identical, we set $N = \min_{i=1, \dots, n} N_i$ in step 2 of the following algorithm. In instances where $N_i > N$, we choose a randomly selected subsample of size N , referred to as downsampling in the following. For an additional discussion about the local modeling approach for SAW, we refer to Section S.4.4 in the Supplement.

Algorithm 1 GSAW Algorithm when using the Radon Transform

- 1: Initialize a grid $(\theta_1, \theta_2, \dots, \theta_L)$ along Θ
- 2: Set $N = \min_{i=1, \dots, n} N_i$, convergence threshold ε and learning rate η
- 3: For each $\mu_{\mathbf{W}^{(i)}}$, downsample $\mathbf{W}^{(i)}$ such that all $\mathbf{W}^{(i)} \in \mathbb{R}^{p \times N}$
- 4: Initialize $\mathbf{W}^{[0]} \in \mathbb{R}^{p \times N}$ arbitrarily and fix the output predictor $X = x$
- 5: **repeat**
- 6: Calculate $\nabla \mathcal{M}_G(\mathbf{W}^{[k]}, x)$

$$\nabla \mathcal{M}_G(\mathbf{W}^{[k]}, x) = (nL)^{-1} \sum_{i=1}^n \sum_{l=1}^L s_{iG}(x) \theta_l \left(\mathbf{W}(\theta_l) - \Pi_{\mathbf{W}(\theta_l)}^{-1} \circ \Pi_{\mathbf{W}^{(i)}(\theta_l)} \circ \mathbf{W}^{(i)}(\theta_l) \right)^T$$

- 7: $\mathbf{W}^{[k+1]} = \mathbf{W}^{[k]} - \eta \nabla \mathcal{M}_G(\mathbf{W}^{[k]}, x)$
 - 8: **until** Algorithm converges with $\|\mathbf{W}^{[k+1]} - \mathbf{W}^{[k]}\|_2 / \|\mathbf{W}^{[k]}\|_2 < \varepsilon$ to $\mathbf{W}^{[\infty]}$
 - 9: Consider each column of $\mathbf{W}^{[\infty]}$ as a sample from $\hat{m}_G^{SAW}(x)$ and apply the kernel density estimator (S.1) in the Supplement to derive the density estimator \hat{f}
-

7.2 SWW Regression

Since SWW regression is split into completely separate slicewise regression steps, one can leverage parallel computing to enhance computing efficiency; the permutation operator is not needed. We note that the local model for the SWW approach can be implemented analogously simply by using local instead of global Fréchet regression in the algorithm.

Algorithm 2 GSWW Algorithm for the Radon Transform

- 1: Initialize a grid $(\theta_1, \theta_2, \dots, \theta_L)$ along Θ and fix the output predictor $X = x$
 - 2: Perform a Radon slicing operation over random observations, i.e. $\langle \mathbf{W}^{(i)}, \theta_l \rangle$, $i = 1, \dots, n$, $l = 1, \dots, L$
 - 3: **for** $l = 1, \dots, L$ **do** in parallel
 - 4: Apply the Fréchet regression for sliced random pairs, $(X_i, \langle \mathbf{W}^{(i)}, \theta_l \rangle)$, $i = 1, \dots, n$ (Petersen and Müller, 2019; Chen et al., 2023b)
 - 5: Calculate the fitted density on the output $X = x$ as $\hat{\lambda}(\theta_l)$
 - 6: **end for**
 - 7: Apply the regularized Radon reconstruction $\hat{f} = \mathcal{R}_\tau^{-1}(\hat{\lambda})$ through (6)
-

8 SIMULATION STUDY

We studied two simulation scenarios, one of which is inspired by Fan and Müller (2021) and involves bivariate Gaussian distributions with mean and covariance depending linearly on a predictor vari-

able $x \in [-0.5, 0.5]$, with distributions truncated on the compact support $[-1, 1] \times [-1, 1]$. For both scenarios we used covariance matrices depending on the predictor x of the form $\mathcal{V}(x) = V\mathcal{D}(x)V^T$, $V = \begin{bmatrix} \frac{\sqrt{2}}{2} & \frac{\sqrt{2}}{2} \\ -\frac{\sqrt{2}}{2} & \frac{\sqrt{2}}{2} \end{bmatrix}$, $\mathcal{D}(x) = \text{diag}(\xi_1(x), \xi_2(x))$. In the first simulation scenario, we generated a scalar predictor X from a uniform distribution on $[-0.5, 0.5]$ and the distributional trajectories as

$$\alpha|X = x \sim \mathcal{N}((0.4x, 0.4x)^T, \mathcal{V}(x)), (\xi_1(x), \xi_2(x)) \sim \frac{1}{100}\mathcal{N}((1.25 + 0.5x, 0.75 - 0.5x)', 0.01\mathbf{I}_2) \quad (26)$$

In the second simulation scenario we used the same covariance matrix $\mathcal{V}(x)$ as in (26) and generated distributional trajectories as

$$\begin{aligned} \alpha|X = x &\sim \mathcal{N}(0.4x, 0.4x - 0.05 \sin(\pi x/0.5))^T, \mathcal{V}(x), \\ (\xi_1(x), \xi_2(x)) &\sim \frac{1}{100}\mathcal{N}((0.75 + x^2, 0.625 + x^3)', 0.01\mathbf{I}_2). \end{aligned} \quad (27)$$

We performed simulations with sample sizes $n = 50$ and $n = 100$, each with two sets of random observations, $N = 50$ and $N = 100$. The mean integrated sliced Wasserstein error (MISWE) is used as the evaluation metric, $\text{MISWE} = E \left[\int_0^1 d_{SW}^2(\hat{m}(x), m(x)) dx \right]$, where $\hat{m}(x)$ is the fitted and $m(x)$ the true model. The empirical MISWE is estimated through Monte Carlo runs,

$$\text{EMISWE} = \frac{1}{M_c} \sum_{k=1}^{M_c} \int_0^1 d_{SW}^2(\hat{m}_k(x), m(x)) dx, \quad (28)$$

where $\hat{m}_k(x)$ is the fit for the k -th Monte Carlo run. The results for all four methods (global slice-wise Wasserstein GSWW, global slice-average Wasserstein GSAW, and the local versions LSWW and LSAW, with details in Supplement Section S.4) are shown in Tables 1 and 2.

In all settings, SWW shows superior performance compared to SAW. Specifically, GSWW outperforms all other methods in the first simulation scenario where the global model tracks the true model, while LSWW outperforms all other methods in the second simulation scenario, where the local model is better suited to track the underlying nonlinear model. The overall superior behavior of SWW can be attributed to the fact that it seeks a unique minimizer for each slice where

the objective function is guaranteed to be convex, and when aggregating the slice-wise information, the regularized inverse controls the error that is introduced when inverting the slicing transform. In contrast, SAW employs gradient descent to directly search for a multivariate distribution target and is constrained by an overall convexity assumption.

Methods	$n = 50$		$n = 100$	
	$N = 50$	$N = 100$	$N = 50$	$N = 100$
GSWW	7.84	7.36	6.92	6.80
GSAW	13.2	11.0	12.0	10.8
LSWW	11.5	10.0	9.20	7.82
LSAW	14.1	11.8	13.9	11.6

Table 1: Simulation results for the first simulation scenario (26). The values of EMISWE as per (28) are reported for various sample sizes of distributions (n), numbers of random observations (N) and methods. The results are averaged over 100 Monte Carlo runs and reported in units of 10^{-4} .

Methods	$n = 50$		$n = 100$	
	$N = 50$	$N = 100$	$N = 50$	$N = 100$
GSWW	10.5	9.70	9.80	9.52
GSAW	13.4	11.9	13.1	11.7
LSWW	10.4	9.59	9.57	8.55
LSAW	12.2	10.3	11.9	9.97

Table 2: Same as Table 1 but for the second simulation scenario (27).

9 DATA ANALYSIS

9.1 Excess Winter Deaths in Europe

Excess winter deaths are a social and health challenge. For European countries, they have become an acute problem due to rapidly rising heating costs. It is known that in general Northern European countries have lower excess winter mortality rates compared to Southern European countries (Healy, 2003; Fowler et al., 2015). Our goal in this analysis was to follow up on this by modeling conditional distributions directly, rather than characterizing mortality effects through summary statistics such as sample mean or standard deviation, as was done in previous studies. Simply applying the conventional regression model to the scatter plot between excess winter mortality rates

and the absolute winter temperature (see Figure 4) makes the analysis susceptible to Simpson’s paradox, creating a misleading perception of an association between increased excess winter death rates and higher winter temperature. A better approach is to separate the observations by country.

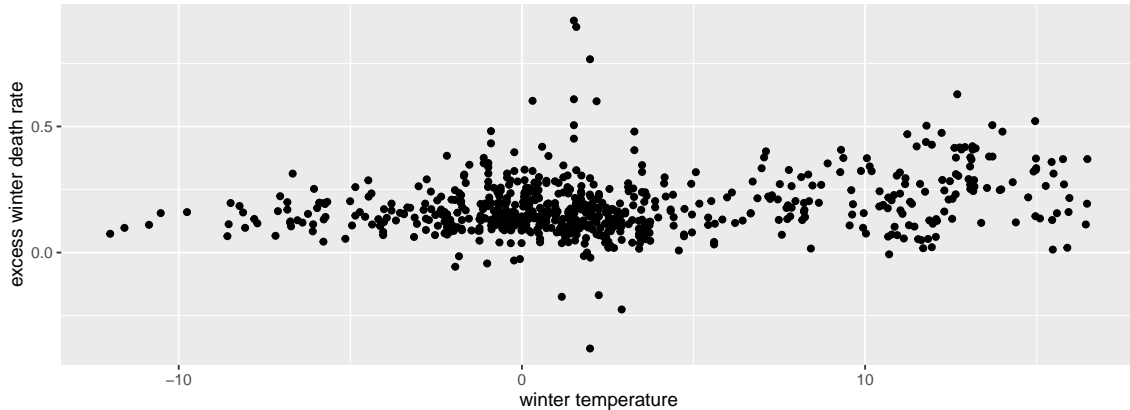


Figure 4: Scatterplot of excess winter death rates (y -axis) against winter temperature (x -axis)

We focused on $n = 31$ countries with available data from 1999 to 2021, for which we adopted the proposed GSWW and GSAW models with the country-level base winter temperature averaged from 1961-90 as predictor and the country-level bivariate distribution between the excess rate of winter mortality relative to the previous summer and winter temperature anomaly relative to the base winter temperature from 1961-90 as the response. We chose standardized winter temperature anomalies to ensure better overlap of shared subdomains within country-specific bivariate distributions. The absolute number of deaths in each of the 31 European countries from 1999 to 2021 was obtained from the Eurostat database <https://ec.europa.eu/eurostat/web/main/data/database> and the winter temperature anomalies and base winter temperatures from 1961-90 from <https://www.uea.ac.uk/groups-and-centres/climatic-research-unit/data>. The observed smoothed bivariate distributions are in Figure 5 for a few selected countries.

The fitted densities obtained from the GSWW model are shown in Figure 6, where the corresponding sliced Wasserstein fraction of variance explained is 0.53; the fitted densities when fitting GSAW for the same countries can be found in Section S.9 in the Supplement. Countries with warmer climates typically experience a higher rate of excess deaths during the winter season compared to colder countries for the same temperature anomaly. For instance, in Spain, a country

with a warm climate, there is a roughly 30% increase in the number of deaths during the winter months compared to the preceding summer. However, in Sweden, a country with a colder climate, this increase is only around 15%.

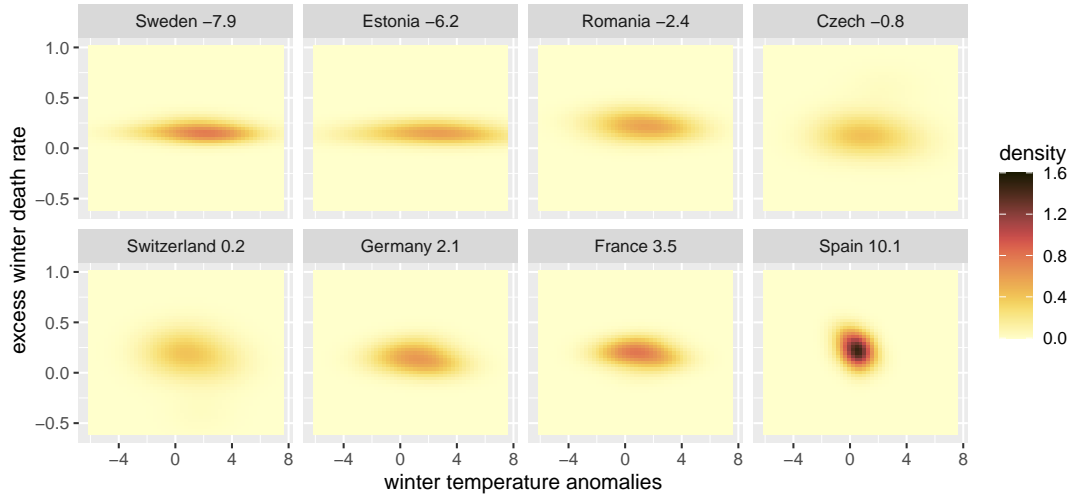


Figure 5: Observed smoothed densities of the joint distributions of excess winter death rates (y -axis) and winter temperature anomaly (x -axis) for a few European countries, arranged in order of their base winter temperature. Each panel is labeled by the name of the country; the corresponding average base winter temperature (in degrees C) from 1961-1990 is also indicated.

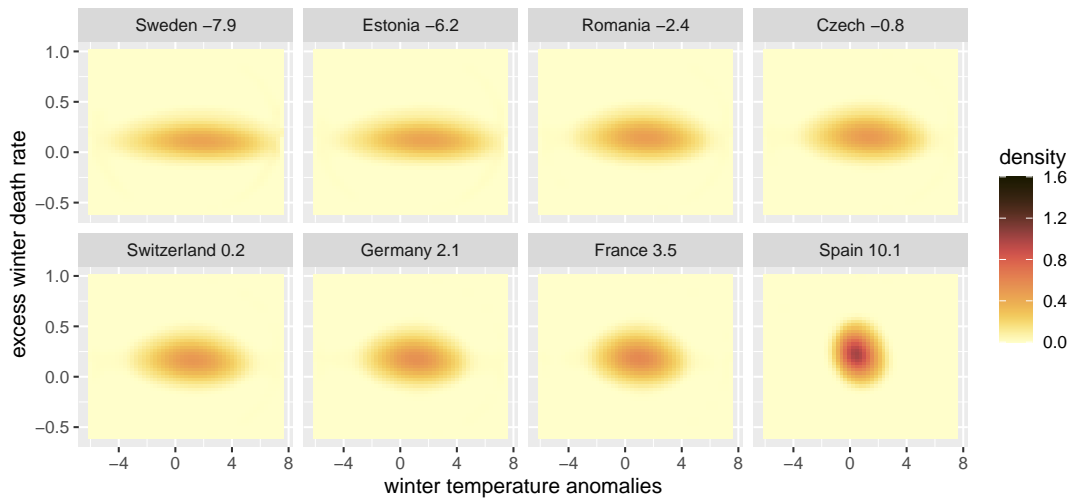


Figure 6: Fitted density surfaces for randomly selected countries obtained by global sliced Wasserstein regression (GSWW). The sliced Wasserstein fraction of variance explained is 0.53.

Figure 7 illustrates the Fréchet regression steps for one-dimensional distributions for some

representative projections. As the base temperature increases, the variance of the temperature anomalies decreases and the excess winter death rates shift to a higher level. The slice corresponding to the projection angle at 135 degrees illustrates the main effect of the regression, which is a shift to the right as winter base temperature goes up, leading to higher winter mortality, and effect that is most pronounced for Spain. Most likely, populations used to a relatively warm winter contain a higher fraction of individuals who are more susceptible to cold temperatures than populations accustomed to a cold winter.

9.2 S&P500 and VIX Index Joint Modeling

In the realm of financial markets, the application of distributional data modeling techniques holds promise, particularly concerning assets like stocks, exchange-traded funds or derivatives (Officer, 1972; Madan, 2020). One central challenge for modeling of financial market modeling stems from complex market dynamics featuring non-normality, low signal-to-noise ratio, and sudden, unpredictable changes in volatility (Madan and Wang, 2017). Traditional modeling of multivariate distribution in finance has centered on copula-based approaches that link marginal univariate distributions such as bilateral gamma marginals through a pre-specified copula function (Cherubini et al., 2004; Küchler and Tappe, 2008; Madan, 2020). The promise of sliced Wasserstein regression is that it eliminates the need to decompose the bivariate distribution into marginal distributions and to specify a copula function by directly targeting the bivariate distributions and their relation with predictors. In this context, there is growing interest in exploring the joint distribution between weekly returns of two crucial financial indices, the S&P 500 index and the Volatility Index (VIX), where the latter tracks expected volatility in the stock market over the subsequent 30 days (Madan, 2020). The objective is to gain a deeper understanding of this joint distribution and its connection with the Gross Domestic Product (GDP) of the United States, which is a annual monetary measure of final goods or services. The S&P 500 and VIX index data are sourced from Yahoo Finance (<https://finance.yahoo.com/>). The observed smoothed bivariate distributions are in Figure 8 for a few selected years, ordered by the associated GDP growth rate.

Consistent with the findings in the prior study by Madan (2020), the VIX returns are seen

to exhibit more variation than the S&P 500 returns, along with an evident negative correlation between these two returns. This inverse relationship occurs because elevated VIX levels, indicating market turbulence, typically coincide with lower stock prices, reflecting investor anxiety. In contrast, periods of market stability or upward trends in stock prices are associated with lower VIX values. The fitted densities obtained from the GSWW model are shown in Figure 9. They are seen to generally track the observed trends but not the sharpness of the density peaks; the Wasserstein fraction of variance explained is low at 0.15. Details of how the sliced regression works can be seen in Figure 10, which illustrates the (global) Fréchet regression step for the univariate distributions corresponding to a few representative slices.

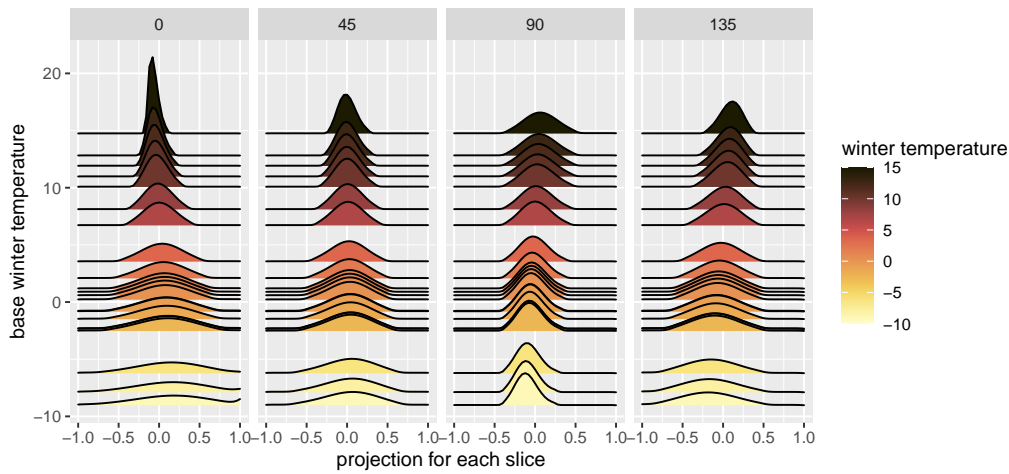


Figure 7: Fréchet regression between the base winter temperature (predictor, on the y -axis) and the slicing distributions (responses, on the x -axis) for various projections. The number at the top of each panel indicates the angle of the respective projection with the x -axis in Figure 5.

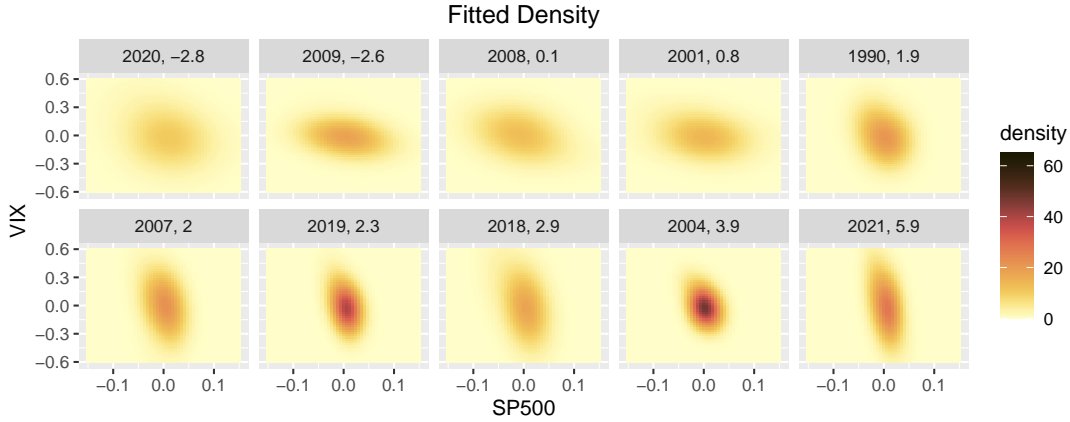


Figure 8: Observed smoothed densities of the joint distributions of the weekly returns of the VIX index, which reflects expected market volatility (y -axis) and of the SP&500 index (x -axis) for selected years, arranged in order of the associated yearly GDP growth rate. Each panel is labeled by year; the corresponding yearly GDP growth rate (as a percentage) is also indicated.

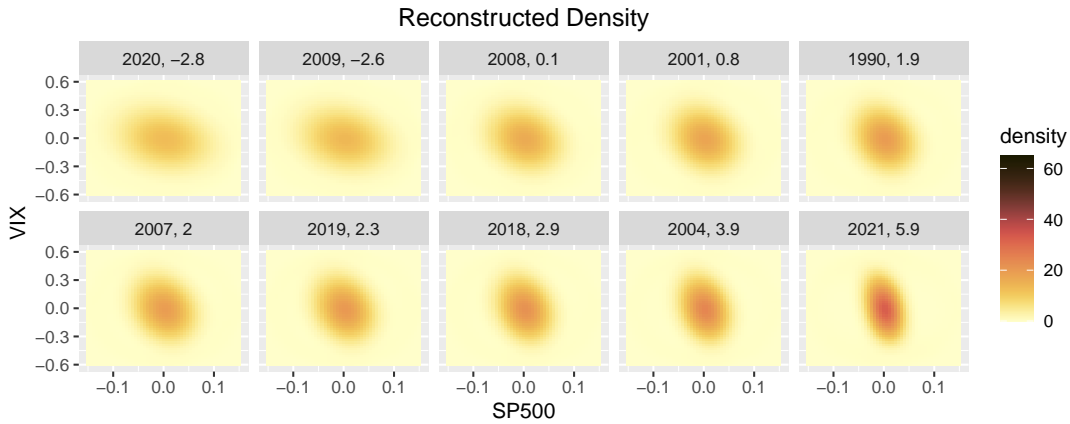


Figure 9: Fitted density surfaces for selected years obtained by the GSWW version of sliced Wasserstein regression. Each panel is labeled by year; the corresponding yearly GDP growth rate (as a percentage) is also indicated.

Further results for GSAW (instead of GSWW) and the local models (LSWW and LSAW) can be found in Section S.9 in the Supplement. The slice-wise fits elucidate the association between the GDP growth rate and the bivariate distributions, showcasing the profound influence of GDP growth on the marginal distribution of the S&P 500 index’s weekly return and its relationship with the VIX index. In Figure 10, an increase in the GDP growth rate coincides with a substantial decrease in the variance of the S&P 500 index return, contrasting with the relatively stable variance of the VIX index. Moreover, as depicted in Figure 9, a higher GDP growth rate intensifies the

responsiveness of VIX index upticks to downticks in the S&P 500 index. In essence, during times of robust economic health (indicated by higher GDP growth rates), declines in the S&P 500 index are more likely to associate with market turbulence, resulting in an increase in the VIX index.

For instance, during challenging periods such as 1990 (amidst the Gulf War), 2001 (following the September 11 terrorist attacks), 2008-2009 (amidst the financial crisis and substantial recession), and 2020 (amidst the COVID-19 pandemic), when the US economy faced significant hardships, a notable increase in the variance of the S&P 500 index was expected. In contrast, during more favorable economic phases like 2004 (highlighted by solid economic performance and low inflation rates), 2018-2019 (marked by sustained economic expansion and robust GDP growth), and 2021 (notably aided by fiscal stimulus to rebound from the pandemic’s impact), when the US economy was thriving, downturns in the S&P 500 index were more prone to coincide with surges in the VIX index. This association potentially stems from fears regarding an impending economic downturn.

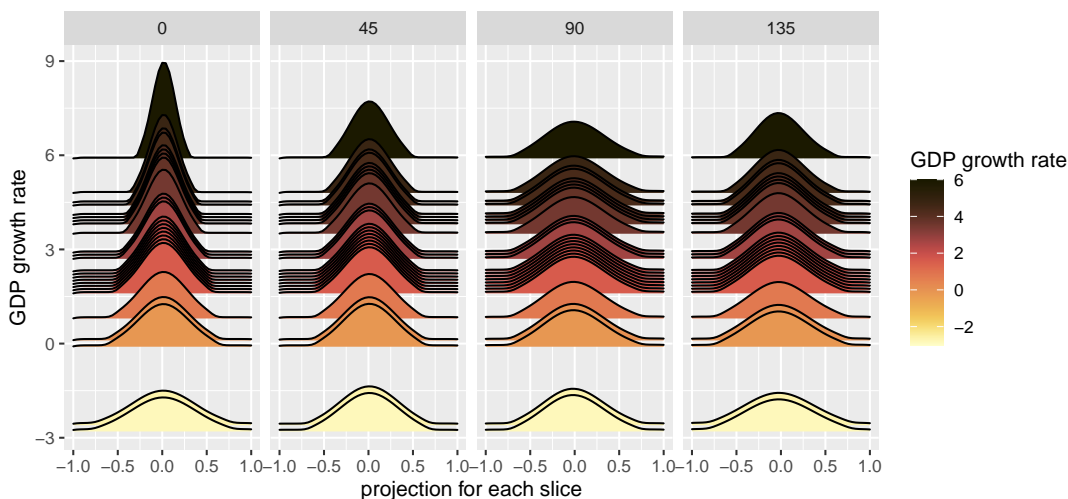


Figure 10: Fréchet regression between the GDP growth rate (predictor, on the y -axis) and the slicing distributions (responses, on the x -axis) for various projections. The number at the top of each panel indicates the angle of the respective projection with the x -axis in Figure 8.

9.3 Exchange Traded Funds

An additional data illustration is presented in the Supplement Section S.5 to highlight the application of the local versions LSWW and LSAW of the sliced Wasserstein regression models.

10 DISCUSSION AND OUTLOOK

The proposed SAW and SWW regression approaches are new tools for the statistical analysis of multivariate distributional data that come with theoretical guarantees and with the flexibility to employ both global and local Fréchet regression methods. The SAW regression model employs Fréchet regression over the multivariate distribution space equipped with the established slice-averaged Wasserstein distance, where the pointwise rates of convergence are optimal for both global and local SAW regression models under certain regularity conditions. The SWW approach offers a new perspective on how slicing transforms can be utilized for the analysis of data that consist of multivariate distributions. SWW regression is based on a regression step for each slice, thus allowing for parallel computation and avoiding the entanglement of the slices that is a characteristic of SAW regression. SWW is coupled with a regularized inverse transform from the sliced space to the original distribution space and is motivated by the idea that executing a regression step for each slice minimizes the slice-wise prediction error and when integrating this error it is smaller than the SAW error, as the latter seeks to minimize the aggregated error across all slices.

A downside of SWW regression is that it is associated with a slower rate of convergence. This is due to the fact that the slice-wise minimizers are not necessarily in the image space $\tilde{\mathcal{F}}$, necessitating to employ a generalized version of the inverse slicing transform $\tilde{\psi}_\tau^{-1}$ when transforming back to \mathcal{F} , which requires a regularization parameter τ and slows down the convergence of the final distribution estimates in the distribution space \mathcal{F} . Additionally, SWW requires a higher order of smoothness for the densities of the underlying distributions to achieve comparable convergence rates to SAW, since the convergence rates of SWW depend crucially on the convergence of the Fourier transform, where the undesirable assumption $k \geq p+1$ is required to ensure sufficiently fast convergence. However, these disadvantages are mitigated by the improved performance of SWW regression compared to SAW regression in both simulation settings and real data applications. This superior performance likely is due to smaller constants in the error rates for the slice-wise optimization in SWW as compared to the slice-averaged optimization in SAW, where the better rates of convergence of SAW cannot overcome this advantage for moderate sample sizes as typically

encountered in statistical data analysis.

We investigated two cases, the theoretically ideal case where the underlying densities are all known, an assumption that has been routinely made in previous research on sliced Wasserstein methods, and a more realistic case where the densities are not known and must be estimated from data that they generate. When densities need to be estimated, several additional issues arise. One of these is that uniform convergence of the estimators over the entire domain D is required, while the resulting estimates also need to be bona fide densities on D . While we offer a valid approach by truncating distributions to suitable subdomains, in order to keep the focus of the paper on the sliced Wasserstein approaches, a full resolution of this issue is left for future research. Commonly available estimators such as kernel estimators and their many variants do not achieve both properties over the entire domain; see [Petersen and Müller \(2016\)](#) for an in-depth discussion of the analogous issue for the one-dimensional case.

An ideal solution would lead to a bona fide density estimator that takes advantage of the additional order of smoothness k in the SWW case. However, our practical experience with kernel density estimation has shown that faster rates of convergence that are theoretically attainable for higher order smoothness of the underlying density functions coupled with higher order kernels rarely materialize for moderate sample sizes typically encountered in statistical data analysis. The reason for this is the same as mentioned above for the superiority of SWW over SAW in practical applications: The improvement in the rate of convergence is not strong enough to mitigate the effect of the larger constants associated with higher order kernels and one also incurs the problem of negative-valued density estimates (since higher order kernels cannot be non-negative).

In view of these considerations, we implemented a simple approach: We assume all distributions have nice smooth densities f on domains $D_f \supset D_\epsilon \supset D$, where D is a convex compact and reasonably nice set, densities are estimated with positive kernels (of order 2) on D_ϵ and the truncated versions of these estimates on domain D are used as estimates of the densities on D , which are assumed to be the targets. This allows for boundary-effect free estimation, yielding bona fide densities on D that satisfy the requisite assumptions. The individual domains D_f may be known or unknown, and more often than not they will be unknown. In such cases subject-matter

knowledge and common statistical sense will guide the choice of D .

Concurrent with our work, geometric properties associated with the so-called disintegrated distributional space have been recently studied ([Kitagawa and Takatsu, 2023](#)) and it was shown that the SAW representation and metric associated with the slice-averaged Wasserstein distance does not lead to a geodesic space ([Park and Slepčev, 2023](#)). In contrast, the SWW representation and associated distribution-slicing Wasserstein metric permits geodesics and thus is a geodesic space; this is a straightforward consequence of the fact that the Wasserstein space for univariate distributions is a geodesic space with the McCann interpolants serving as geodesics ([Gangbo and McCann, 1996](#)). A geodesic space is a prerequisite for adopting promising intrinsic approaches for principal component analysis ([Bigot et al., 2017](#)), regression ([Zhu and Müller, 2023b](#)) and extrapolation ([Fan and Müller, 2021](#)). The geodesic structure of the novel slice-wise methodology that we introduced in this paper is thus a major advantage of this approach and exploiting this structure is a promising avenue for future research.

SUPPLEMENT TO "SLICED WASSERSTEIN REGRESSION"

S.1 ABBREVIATIONS, NOTATIONS AND SUMMARY OF MODELS

Notation	Explanation
D	known support of multivariate distribution
$ D $	Lebesgue measure of the support D
p	dimension of the multivariate distribution
q	dimension of the predictor X
$f(z), \mathcal{F}$	multivariate density functions (space)
$g(u), \mathcal{G}$	univariate density functions (space)
$I(g)$	support of univariate distribution, $g \in \mathcal{G}$
$q(s), \mathcal{Q}$	quantile functions (space)
μ, \mathcal{F}	multivariate distributions (space)
ν, \mathcal{G}	univariate distributions (space)
θ, Θ	slicing parameter (set)
λ, Λ_Θ	density slicing functions (space) from Θ to \mathcal{G}
γ, Γ_Θ	quantile slicing functions (space) from Θ to \mathcal{G}
ψ, ψ_τ	slicing (regularized slicing) transform from \mathcal{F} to Λ_Θ
$\mathcal{R}, \mathcal{R}_\tau$	Radon (regularized Radon) transform from \mathcal{F} to Λ_Θ
$\phi_\tau(r)$	a regularizing function on Fourier domain
Δ_τ	reconstruction error
$\mathcal{I}_1, \mathcal{I}_p$	univariate (multivariate) Fourier transform
φ	map from \mathcal{F} to \mathcal{F} or from \mathcal{G} to \mathcal{G}
ϱ	map from Γ_Θ to Λ_Θ
G	map from \mathcal{G} to \mathcal{Q}
$\tilde{\psi}, \tilde{\psi}_\tau$	induced slicing (regularized slicing) transform from \mathcal{F} to Γ_Θ

Table S3: List of notations (1). The bracketed explanation corresponds to the second half of the notation.

Notation	Explanation
d	metric on \mathcal{F}
d_W	Wasserstein distance on \mathcal{F} or \mathcal{G}
d_{DW}	distribution-slicing Wasserstein metric on Γ_Θ
d_{SW}	slice-averaged Wasserstein distance on \mathcal{F}
d_2	L^2 norm
d_∞	L^∞ norm
Z_1, Z_2	random variables on \mathbb{R}^p
$\mathcal{P}(\mu_1, \mu_2)$	probability measure with marginal distributions μ_1, μ_2
μ, X	random pair with $\mu \in \mathcal{F}, X \in \mathbb{R}^q$
F	joint distribution of X and μ
F_X, F_μ	marginal distribution of X (of μ)
$m(x)$	Fréchet minimizer
$M(\cdot, x)$	conditional Fréchet function
$s_G(X, x), s_{i,G}(x)$	(sample) weight function of global Fréchet regression
SAW, GSAW	(global) slice-averaged Wasserstein
SWW, GSWW	(global) slice-wise Wasserstein
$m_G^{SAW}(x), m_G^{SWW}$	GSAW (GSWW) regression minimizer
$M_G^{SAW}(\cdot, x), M_G^{SWW}(\cdot, x)$	GSAW (GSWW) conditional Fréchet function
$\gamma_{G,x}$	minimizer of $M_G^{SWW}(\cdot, x)$
$\{(X_i, \mu_i)\}_{i=1}^n$	a sample of random pairs of predictors and measures
$\hat{\mu}_i, \hat{f}(x)$	estimated distribution (density function)
$\bar{X}, \hat{\Sigma}$	sample mean (variance) of $\{X_i\}_{i=1}^n$
R_\oplus^2	slice-averaged Wasserstein R^2 coefficient
$\mathbf{W} = \{\mathbf{W}_j\}_{j=1}^N$	random observations
$\mathbf{W}^{(i)} = \{\mathbf{W}_{ij}\}_{j=1}^{n_i}$	random observations from μ_i
$\mathbf{W}(\theta), \mathbf{W}^{(i)}(\theta)$	sliced observation (observations from μ_i)
$\mathcal{M}_G(\mathbf{W}, x)$	GSAW objective function
$\langle \cdot, \theta \rangle$	Radon slicing operation on random observation in \mathbb{R}^p
Π_A	permutation operator on $A \in \mathbb{R}^N$
η	step parameter in the gradient descent

Table S4: List of notations (2). The bracketed explanation corresponds to the second half of the notation.

Notation	Explanation
$\alpha X = x$	distribution trajectory
$\mathcal{V}(x) = V\mathcal{D}V^T$	covariance matrix
$\mathcal{D} = (\xi_1, \xi_2)$	eigenvalues
M_c	Monte Carlo run
MISWE, EMISWE	(empirical) mean integrated sliced Wasserstein error

Table S5: Notations for the simulation. The bracketed explanation corresponds to the second half of the notation.

Notation	Explanation
D_ϵ	neighborhood surrounding the common support D
D_f	support of the density function f
D_i	support of the i -th distribution
f_{i,D_i}, μ_{i,D_i}	the i -th sample density (distribution) on support D_i
$f_{i,D_i D_\epsilon}$	the i -th sample density on the subdomain D_ϵ
N_i, \tilde{N}_i	number of observations on D_i (D_ϵ)
κ, b	kernel function (bandwidth) for density estimation
$\mathcal{E}_{X \mu}, \mathcal{E}_X$	conditional (marginal) density of X
K, h	kernel function (bandwidth) for local regression
\mathcal{T}	domain of the predictor X when $q = 1$
$s_L(X, x, h), s_{iL,h}(x)$	(sample) weight function of local Fréchet regression
LSAW	local slice-averaged Wasserstein
LSWW	local slice-wise Wasserstein
$m_{L,h}^{SAW}(x), m_{L,h,\tau}^{SWW}$	LSAW (LSWW) regression minimizer
$M_{L,h}^{SAW}(\cdot, x), M_{L,h}^{SWW}(\cdot, x)$	LSAW (LSWW) conditional Fréchet function
$\gamma_{L,h,x}$	minimizer of $M_{L,h}^{SWW}(\cdot, x)$
$\mathcal{M}_{L,h}(\mathbf{W}, x)$	GSAW objective function
\mathcal{D}^k	differentiation operator on \mathcal{F}
\mathcal{K}, a	kernel function (bandwidth) used for a proof
$N(\epsilon, \mathcal{F}, d)$	covering number using balls of size ϵ
$B_\delta[m_G^{SAW}(x)]$	δ -ball in \mathcal{F} centered at $m_G^{SAW}(x)$
$B_G(x)$	best approximation
Ψ	map from quantile functions to distribution functions
$\eta_0, \eta_1, \eta_2, \beta_0, \beta_1, \beta_2$	constants
A_1, A_2, A_3, B_0, B_1	constants
$\tau_0, \tau_1, \tau_2, C_0, C_1, C_2, C, \zeta$	constants

Table S6: List of notations for the Supplementary material. The bracketed explanation corresponds to the second half of the notation.

Type	Regression	Object	Result
Global		weight function	$s_G(X, x) = 1 + (X - E(X))^T \text{Var}(X)^{-1}(x - E(X))$
	SAW	target function	$m_G^{SAW}(x) = \text{argmin}_{\omega \in \mathcal{F}} M_G^{SAW}(\omega, x)$ $M_G^{SAW}(\cdot, x) = E[s_G(X, x)d_{SW}^2(\mu, \cdot)]$
		convergence	$d_{SW}(m_G^{SAW}(x), \hat{m}_G^{SAW}(x)) = O_p(n^{-1/2})$
	SWW	target function	$m_{G,\tau}^{SWW}(x) = \tilde{\psi}_\tau^{-1} [\text{argmin}_{\gamma \in \Gamma_\Theta} M_G^{SWW}(\gamma, x)]$ $M_G^{SWW}(\cdot, x) = E[s_G(X, x)d_{DW}^2(\tilde{\psi}(\mu), \cdot)]$
		convergence	$d_\infty(m_{G,\tau}^{SWW}(x), \hat{m}_{G,\tau}^{SWW}(x)) = O_p(C_1(\tau) + C_2(\tau)n^{-2/7})$
Local		weight function	$s_L(X, x, h) = K_h(X - x)[v_2 - v_1(X - x)]/\sigma_0^2$
	SAW	target function	$m^{SAW}(x) = \text{argmin}_{\omega \in \mathcal{F}} M^{SAW}(\omega, x)$ $M^{SAW}(\cdot, x) = E[d_{SW}^2(\mu, \cdot) X = x]$
		local target	$m_{L,h}^{SAW}(x) = \text{argmin}_{\omega \in \mathcal{F}} M_{L,h}^{SAW}(\omega, x)$ $M_{L,h}^{SAW}(\cdot, x) = E[s_L(X, x, h)d_{SW}^2(\mu, \cdot)]$
		convergence	$d_{SW}(m^{SAW}(x), \hat{m}^{SAW}(x)) = O_p(n^{-2/5})$
	SWW	target function	$m^{SWW} = \tilde{\psi}^{-1} [\text{argmin}_{\gamma \in \Gamma_\Theta} M^{SWW}(\gamma, x)]$ $M^{SWW}(\cdot, x) = E[d_{DW}^2(\tilde{\psi}(\mu), \cdot) X = x]$
		local target	$m_{L,h,\tau}^{SWW}(x) = \tilde{\psi}_\tau^{-1} [\text{argmin}_{\gamma \in \Gamma_\Theta} M_{L,h}^{SWW}(\gamma, x)]$ $M_{L,h}^{SWW}(\cdot, x) = E[s_L(X, x, h)d_{DW}^2(\tilde{\psi}(\mu), \cdot)]$
		convergence	$d_\infty(m^{SWW}(x), \hat{m}_{L,h,\tau}^{SWW}(x)) = O_p(C_1(\tau) + C_2(\tau)n^{-8/35})$

Table S7: Summary of the global and local regression models.

S.2 ADDITIONAL ASSUMPTIONS

(A3) $\text{argmin}_{\gamma \in \Gamma_\Theta} M_{L,h}^{SWW}(\gamma, x) \in \tilde{\psi}(\mathcal{F})$ as per (S.6).

(L1) The kernel K used in the definition of the local sliced Wasserstein regression in Section S.4 is a probability density function and is symmetric around zero. Furthermore, defining $K_{kj} = \int_{\mathbb{R}} K^k(u)u^j du$, $|K_{14}|$ and $|K_{26}|$ are both finite.

(L2) The marginal density of X denoted as $\mathcal{E}_X(x)$ and the conditional density of X given $\mu = \omega$, $\mathcal{E}_{X|\mu}(\cdot, \omega)$, exist and are twice continuously differentiable, the latter for all $\omega \in \mathcal{F}$, with $\sup_{x,\omega} |(\partial^2 \mathcal{E}_{X|\mu}/\partial x^2)(x, \omega)| < \infty$. Additionally, for any open $U \subset \mathcal{F}$, $\int_U dF_{\mu|X}(x, \omega)$ is continuous as a function of x .

(L3) The derivative K' exists and is bounded on the support of K , i.e., $\sup_{K(u)>0} |K'(u)| < \infty$; additionally, $\int_{\mathbb{R}} u^2 |K'(u)| (|u \log |u||)^{1/2} du < \infty$.

(L4) Let \mathcal{T} be a closed interval in \mathbb{R} and \mathcal{T}° be its interior. Denote $\mathcal{E}_X(s)$ and $\mathcal{E}_{X|\mu}(\cdot, \omega)$ as per (L2), which exist and are twice continuously differentiable on \mathcal{T}° , the latter for all $\omega \in \mathcal{F}$. The marginal density $\mathcal{E}_X(x)$ is bounded away from zero on \mathcal{T} , $\inf_{x \in \mathcal{T}} \mathcal{E}_X(x) > 0$. The second-order derivative $\mathcal{E}_X''(x)$ is bounded, $\sup_{x \in \mathcal{T}^\circ} |\mathcal{E}_X''(x)| < \infty$. The second-order partial derivatives

$(\partial^2 \mathcal{E}_{X|\mu}(x, \omega)/\partial x^2)(x, \omega)$ are uniformly bounded, i.e., $\sup_{x \in \mathcal{T}^o, \omega \in \mathcal{F}} |(\partial^2 \mathcal{E}_{X|\mu}/\partial x^2)(x, \omega)| < \infty$. Additionally, for any open set $U \subset \mathcal{F}$, $\int_U dF_{\mu|X}(x, \omega)$ is continuous as a function of x ; for any $x \in \mathcal{T}$, $M(\cdot, x)$ is equicontinuous, i.e.,

$$\limsup_{y \rightarrow x} \sup_{\omega \in \mathcal{F}} |M(\omega, y) - M(\omega, x)| = 0.$$

S.3 ADDITIONAL PRELIMINARY DENSITY ESTIMATION STEP

We assume for our main results that the multivariate distributions under consideration are well defined and possess density functions on a common domain D , satisfying (D1) and (F1). In practice, the common domain D will either be pre-specified in statistical applications or will be chosen by the analyst based on subject-matter or practical considerations. This is exemplified in our data examples. Once D has been selected, distributions truncated on D are the targets of the analysis and serve as responses for the SAW or SWW regression models. The actual distributions may have domains of which D is a subset and these domains may vary from distribution to distribution and could be unbounded.

For the practically important case where the distributions μ_i are not known but must be inferred from observations, we make some robust assumptions that will suffice to side-step the issue of boundary effects in density estimation without delving into complex technical details. A first assumption is that there exists $\epsilon > 0$ so that $D_\epsilon = \bigcup_{z \in D} B(z, \epsilon)$ is a subset of the domain of each underlying distribution, where $B(z, \epsilon)$ is a ball with radius ϵ centered at z . This assumption makes it possible to avoid a detailed discussion of boundary effects when estimating densities from available data they generate. We furthermore assume that the continuous differentiability assumption (F1) holds on D_ϵ . If a random distribution in the sample with density f_{D_f} has the (random) domain D_f , we require that $D_f \supset D_\epsilon$ and that on D_ϵ the density f_{D_f} is uniformly bounded from below and above, continuously differentiable of order k and has uniformly bounded partial derivatives, where the uniformity requirement extends across all f_{D_f} . Formally,

(F1') There exists a constant $M_0 > 0$ and an integer $k \geq 2$ such that for all $f \in \mathcal{F}$, the density function f is the density of a truncated distribution on the domain D , where the original distribution has a domain D_f with $D_f \supset D_\epsilon$ and a density f_{D_f} that is defined on D_f . It holds that $\max\{\|f_{D_f}\|_\infty, \|1/f_{D_f}\|_\infty\} \leq M_0$ on D_ϵ and that f_{D_f} is continuously differentiable of order k on D_ϵ , with uniformly bounded partial derivatives. The target distribution with density f is the truncated version of the f_{D_f} on D , so that for all $z \in D$ one has $f(z) = f_{D_f}(z)/\int_D f_{D_f}(u)du$.

Assume we have a sample of distributions $\mu_{1,D_1}, \dots, \mu_{n,D_n}$ with densities $f_{1,D_1}, \dots, f_{n,D_n}$ and domains $D_i \supset D_\epsilon$ and N_i i.i.d. observations generated by f_{i,D_i} by a random mechanism that is independent of the random mechanism that generates the μ_{i,D_i} . Let \tilde{N}_i be the number of observations made for f_{i,D_i} that fall inside the domain D_ϵ . We impose the following assumption (P1) on the N_i to ensure that the L^2 convergence rate of the density estimates is faster than or at least as fast as the parametric rate $n^{-1/2}$.

(P1) $N(n) = \min_{1 \leq i \leq n} N_i \gtrsim n^{(p+4)/4}$, where N_i is the number of random observations for the i -th

distribution μ_{i,D_i} .

The following proposition shows that \tilde{N}_i follows the same rate as (P1) with probability approaching one.

Proposition S1. *Assume (P1) and (F1'). Let $\tilde{N} = \min_{1 \leq i \leq n} \tilde{N}_i$. There exists a constant \tilde{c} such that*

$$P\left(\tilde{N} \geq \tilde{c}n^{(p+4)/4}\right) \rightarrow 1, \quad \text{as } n \rightarrow \infty.$$

To obtain the consistency of estimates of SAW regression and SWW regression when estimated densities are used, one needs to quantify the discrepancy between the true densities of the distributions $\{\mu_i\}_{i=1}^n$ and their estimates. This preliminary density estimation step can be implemented with standard density estimation methods, which have been extensively studied in the literature for both univariate and multivariate scenarios (Cowling and Hall, 1996; Hazelton and Marshall, 2009).

Let μ_{D_f} be a random probability distribution with density function f_{D_f} that satisfies (F1'), from which random observations Z_1, \dots, Z_N are independently sampled. Then a standard kernel estimator \check{f} for f_{D_f} and its truncated version \hat{f} for the density f truncated to the domain D is

$$\check{f}(z) = \frac{1}{Nb^p} \sum_{j=1}^N \kappa\left(\frac{z - Z_j}{b}\right), \quad \hat{f}(z) = \check{f}(z) / \int_D \check{f}(u) du, \quad z \in D \subset \mathbb{R}^p. \quad (\text{S.1})$$

Here, κ is a kernel function and b a positive bandwidth (tuning parameter) satisfying assumptions (K1) and (K2) listed below.

(K1) The kernel function κ as per (S.1) is a probability density function that has compact support and is symmetric, bounded and k times continuously differentiable (without loss of generality, the support is assumed to be contained in the unit cube of \mathbb{R}^p).

(K2) For some $A > 0$ and $\omega > 0$, the class of functions $\mathcal{I}_b = \{\kappa\left(\frac{z-\cdot}{b}\right), z \in \mathbb{R}^p, b > 0\}$ satisfies

$$\sup_{\mathcal{P}} M\left(\mathcal{I}_b, L_2(\mathcal{P}), \varepsilon \|F\|_{L_2(\mathcal{P})}\right) \leq \left(\frac{A}{\varepsilon}\right)^\omega,$$

where $M(T, d, \varepsilon)$ denotes the ε -covering number of the metric space (T, d) , F is the envelope function of \mathcal{I}_b and the supremum is taken over the set of all probability measures on \mathbb{R}^p .

Proposition S2. *Assume (D1), (F1') and (K1). Choosing $b \sim N^{-\frac{1}{p+4}}$, the kernel density estimator \hat{f} in (S.1) satisfies that*

$$\sup_{f \in \mathcal{F}} E \left[d_2\left(\hat{f}, f\right)^2 \middle| f \right] = O(N^{-4/(4+p)}). \quad (\text{S.2})$$

We note that by construction, $\hat{f} \geq 0$, $\int_D \hat{f}(z) dz = 1$ and since $b \rightarrow 0$ as $N \rightarrow \infty$, we only need

to consider the scenario where $b < \epsilon$, when due to the compactness of the support of the kernel κ there are no boundary effects when estimating f , as for any $x \in D$ one has $B(x, \epsilon) \subset D_\epsilon$. The following proposition formalizes this in terms of a uniform convergence rate.

Proposition S3. *Assume (D1), (F1') and (K1)-(K2) and $b \sim N^{-\frac{1}{p+4}}$. The kernel density estimator \hat{f} in (S.1) satisfies*

$$\sup_{f \in \mathcal{F}} d_\infty(\hat{f}, f) = O_p(\sqrt{\log N} N^{-\frac{2}{p+4}}). \quad (\text{S.3})$$

We have assumed symmetric non-negative kernel functions, thus their first non-zero moments are of order two (alternatively one can also use products of kernels that are one-dimensional symmetric densities). If one wants to take full advantage of the higher order smoothness of the density function f in view of assumptions (F2) or (F3), one can use higher order kernels κ of order k , where the order of the first non-zero moments is k . We refer to [Müller and Stadtmüller \(1999\)](#) for a more detailed account on multivariate kernels and boundary effects in multivariate density estimation. It is well known that such higher order kernel functions cannot be non-negative valued and thus it is not guaranteed anymore that the resulting kernel density estimates on D satisfy $\hat{f} \geq 0$, however one can still show that, since boundary effects can be ignored,

$$\sup_{f \in \mathcal{F}} E \left[d_2(\hat{f}, f)^2 \middle| f \right] = O(N^{-2k/(2k+p)}).$$

For example, under the condition $k \geq p + 1$ in (F3) one has

$$\sup_{f \in \mathcal{F}} E \left[d_2(\hat{f}, f)^2 \middle| f \right] = O(N^{-2/3}).$$

Under (F3), the condition (P1) can then be replaced by a dimension-independent rate, if one adopts the following condition (P1').

(P1') $N(n) = \min_{1 \leq i \leq n} N_i \gtrsim n^{3/2}$, where N_i is the number of random observations for the i -th distribution μ_i when densities need to be estimated.

The fact that $\hat{f} \geq 0$ is not guaranteed for these faster converging estimates makes this option less practical for our setting where the density estimates must be bona fide densities. The gains for higher order kernels are a consequence of their bias-reducing property, while the variance typically suffers a substantial increase through larger constants that are associated with these kernels. One can artificially enforce bona fide density estimates by modifying the estimator ([Gajek, 1986](#)) but this leads to new problems. If one nevertheless follows through with these adjustments, it may be possible to relax condition (P1) to (P1').

S.4 LOCAL SLICED WASSERSTEIN REGRESSION

S.4.1 Regression Model

For local Fréchet regression (Petersen and Müller, 2019) we consider the case of a scalar predictor $X \in \mathbb{R}$ while the extension to $X \in \mathbb{R}^q$ with $q > 1$ is easily possible but tedious and for $q > 3$ usually subject to the curse of dimensionality, just like ordinary nonparametric regression approaches. For a smoothing kernel $K(\cdot)$ corresponding to a probability density and $K_h = h^{-1}K_h(\cdot/h)$, where h is a bandwidth, local Fréchet regression at x is defined as

$$m_{L,h}(x) = \operatorname{argmin}_{\omega \in \mathcal{F}} M_{L,h}(\omega, x), \quad M_{L,h}(\cdot, x) = E \left[s_L(X, x, h) d^2(\mu, \cdot) \right], \quad (\text{S.4})$$

where $s_L(X, x, h) = K_h(X - x)[v_2 - v_1(X - x)]/\sigma_0^2$ with $v_j = E[K_h(X - x)(X - x)^j]$ for $j = 0, 1, 2$ and $\sigma_0^2 = v_0v_2 - v_1^2$. The proposed local slice-averaged Wasserstein (LSAW) regression at x is

$$m_{L,h}^{SAW}(x) = \operatorname{argmin}_{\omega \in \mathcal{F}} M_{L,h}^{SAW}(\omega, x), \quad M_{L,h}^{SAW}(\cdot, x) = E \left[s_L(X, x, h) d_{SW}^2(\mu, \cdot) \right]. \quad (\text{S.5})$$

The proposed local slice-wise Wasserstein (LSWW) regression at x is defined as

$$m_{L,h,\tau}^{SWW}(x) = \tilde{\psi}_\tau^{-1} \left[\operatorname{argmin}_{\gamma \in \Gamma_\Theta} M_{L,h}^{SWW}(\gamma, x) \right], \quad M_{L,h}^{SWW}(\cdot, x) = E \left[s_L(X, x, h) d_{DW}^2(\tilde{\psi}(\mu), \cdot) \right]. \quad (\text{S.6})$$

In analogy to Proposition 4 for GSWW, the following result shows that the LSWW regression is equivalent to applying the Fréchet regression along each slice θ followed by an inverse transform.

Proposition S4. *The minimizing argument $\gamma_{L,h,x} = \operatorname{argmin}_{\gamma \in \Gamma_\Theta} M_{L,h}^{SWW}(\gamma, x)$, see (S.6), is characterized as*

$$\gamma_{L,h,x}(\theta) = \operatorname{argmin}_{\nu \in \mathcal{G}} E \left[s_L(X, x, h) d_W^2 \left(G^{-1} \left(\tilde{\psi}(\mu)(\theta) \right), \nu \right) \right], \quad \text{for almost all } \theta \in \Theta.$$

S.4.2 Estimation

Suppose we have a sample of independent random pairs $\{(X_i, \mu_i)\}_{i=1}^n \sim F$, then the sample mean and variance are

$$\bar{X} = n^{-1} \sum_{i=1}^n X_i, \quad \hat{\Sigma} = n^{-1} \sum_{i=1}^n (X_i - \bar{X})(X_i - \bar{X})^T.$$

If random distributions μ_i are fully observed, sample estimators of LSAW and LSWW are obtained as

$$\check{m}_{L,h}^{SAW}(x) = \operatorname{argmin}_{\omega \in \mathcal{F}} \check{M}_{L,h}^{SAW}(\omega, x), \quad \check{M}_{L,h}^{SAW}(\cdot, x) = n^{-1} \sum_{i=1}^n [s_{iL,h}(x) d_{SW}^2(\mu_i, \cdot)], \quad (\text{S.7})$$

$$\check{m}_{L,h,\tau}^{SWW}(x) = \tilde{\psi}_\tau^{-1} \left[\operatorname{argmin}_{\gamma \in \Gamma_\Theta} \check{M}_{L,h}^{SWW}(\gamma, x) \right], \quad \check{M}_{L,h}^{SWW}(\cdot, x) = n^{-1} \sum_{i=1}^n [s_{iL,h}(x) d_{DW}^2(\tilde{\psi}(\mu_i), \cdot)], \quad (\text{S.8})$$

where $s_{iL,h}(x) = K_h(X_i - x)[\hat{v}_2 - \hat{v}_1(X_i - x)]/\hat{\sigma}_0^2$ with $\hat{v}_j = n^{-1} \sum_{i=1}^n K_h(X_i - x)(X_i - x)^j$, $j = 0, 1, 2$ and $\hat{\sigma}_0^2 = \hat{v}_0 \hat{v}_2 - \hat{v}_1^2$. If the random distributions μ_i are estimated by $\hat{\mu}_i$ as per (S.1), the corresponding estimators are

$$\hat{m}_{L,h}^{SAW}(x) = \operatorname{argmin}_{\omega \in \mathcal{F}} \hat{M}_{L,h}^{SAW}(\omega, x), \quad \hat{M}_{L,h}^{SAW}(\cdot, x) = n^{-1} \sum_{i=1}^n [s_{iL,h}(x) d_{SW}^2(\hat{\mu}_i, \cdot)]; \quad (\text{S.9})$$

$$\hat{m}_{L,h,\tau}^{SWW}(x) = \tilde{\psi}_\tau^{-1} \left[\operatorname{argmin}_{\gamma \in \Gamma_\Theta} \hat{M}_{L,h}^{SWW}(\gamma, x) \right], \quad \hat{M}_{L,h}^{SWW}(\cdot, x) = n^{-1} \sum_{i=1}^n [s_{iL,h}(x) d_{DW}^2(\tilde{\psi}(\hat{\mu}_i), \cdot)]. \quad (\text{S.10})$$

A practical data-driven approach to select the tuning parameter τ and bandwidth h when an i.i.d. sample of random pairs $\{(X_i, \mu_i)\}_{i=1}^n$ is available can be obtained through leave-one-out cross-validation. Specifically, we aim to minimize the discrepancy between predicted and observed distributions, given by

$$\hat{\tau}, \hat{h} = \operatorname{argmin}_{\tau, h} \sum_{i=1}^n d_{SW}^2(\mu_i, \hat{m}_{L,h,\tau,-i}^{SWW}(X_i)),$$

where $\hat{m}_{L,h,\tau,-i}^{SWW}(X_i)$ is the prediction at X_i from the LSWW regression of the i th-left-out sample $\{(X_{i'}, \mu_{i'})\}_{i' \neq i}$. When the sample size n exceeds 30, we substitute leave-one-out cross-validation with 5-fold cross-validation to strike a balance between computational efficiency and the accuracy of the tuning parameter selection.

S.4.3 Asymptotic Convergence

Some additional assumptions listed in Section S.2 are required to derive asymptotic convergence result for the local models. Assumption (A3) ensures the underlying minimizer of the LSWW regression belongs to the image space of the slicing transform. Additional kernel and distributional assumptions (L1)-(L4) are standard for local regression estimation. We provide the following convergence result for LSAW. Here Theorem S1 provides rates of convergence for the case where the densities in the random sample are known and Theorem S2 for the case where they are unknown and must be estimated from the data.

Theorem S1. (*LSAW for known distributions*). Assume (D1), (F1)-(F2), (A1), (T0)-(T2) and (L1)-(L2). When adopting the slice-averaged Wasserstein distance, for a fixed $x \in \mathbb{R}$ and

$m^{SAW}(x)$, $m_{L,h}^{SAW}(x)$, and $\check{m}_{L,h}^{SAW}(x)$ as per (15), (S.5) and (S.7),

$$\begin{aligned} d_{SW}(m^{SAW}(x), m_{L,h}^{SAW}(x)) &= O(h^2), \\ d_{SW}(m_{L,h}^{SAW}(x), \check{m}_{L,h}^{SAW}(x)) &= O_p\left((nh)^{-1/2}\right), \end{aligned}$$

and when taking $h \sim n^{-1/5}$,

$$d_{SW}(m^{SAW}(x), \check{m}_{L,h}^{SAW}(x)) = O_p(n^{-2/5}).$$

Furthermore, assuming (L3)-(L4) for a closed interval $\mathcal{T} \subset \mathbb{R}$, if $h \rightarrow 0$, $nh^2(-\log h)^{-1} \rightarrow \infty$ as $n \rightarrow \infty$, for any $\epsilon > 0$,

$$\begin{aligned} \sup_{x \in \mathcal{T}} d_{SW}(m^{SAW}(x), m_{L,h}^{SAW}(x)) &= O(h^2), \\ \sup_{x \in \mathcal{T}} d_{SW}(m_{L,h}^{SAW}(x), \check{m}_{L,h}^{SAW}(x)) &= O_p(\max\{(nh^2)^{-1/(2+\epsilon)}, [nh^2(-\log h)^{-1}]^{-1/2}\}), \end{aligned}$$

and when taking $h \sim n^{-1/(6+2\epsilon)}$,

$$\sup_{x \in \mathcal{T}} d_{SW}(m^{SAW}(x), \check{m}_{L,h}^{SAW}(x)) = O_p(n^{-1/(3+\epsilon)}).$$

Theorem S2. (LSAW for estimated distributions). Assume (D1), (F1)-(F2), (A1), (T0)-(T2), (L1)-(L2) and assumptions based on kernel density estimation (P1), (F1'), (K1)-(K2). When adopting the slice-averaged Wasserstein distance, for a fixed $x \in \mathbb{R}$ and $m^{SAW}(x)$, $m_{L,h}^{SAW}(x)$, and $\hat{m}_{L,h}^{SAW}(x)$ as per (15), (S.5) and (S.9),

$$\begin{aligned} d_{SW}(m^{SAW}(x), m_{L,h}^{SAW}(x)) &= O(h^2), \\ d_{SW}(m_{L,h}^{SAW}(x), \hat{m}_{L,h}^{SAW}(x)) &= O_p\left((nh)^{-1/2}\right), \end{aligned}$$

and when taking $h \sim n^{-1/5}$,

$$d_{SW}(m^{SAW}(x), \hat{m}_{L,h}^{SAW}(x)) = O_p(n^{-2/5}).$$

Furthermore, assuming (L3)-(L4) for a closed interval $\mathcal{T} \subset \mathbb{R}$, if $h \rightarrow 0$, $nh^2(-\log h)^{-1} \rightarrow \infty$ as $n \rightarrow \infty$, for any $\epsilon > 0$,

$$\begin{aligned} \sup_{x \in \mathcal{T}} d_{SW}(m^{SAW}(x), m_{L,h}^{SAW}(x)) &= O(h^2), \\ \sup_{x \in \mathcal{T}} d_{SW}(m_{L,h}^{SAW}(x), \hat{m}_{L,h}^{SAW}(x)) &= O_p(\max\{(nh^2)^{-1/(2+\epsilon)}, [nh^2(-\log h)^{-1}]^{-1/2}\}), \end{aligned}$$

and when taking $h \sim n^{-1/(6+2\epsilon)}$,

$$\sup_{x \in \mathcal{T}} d_{SW}(m^{SAW}(x), \hat{m}_{L,h}^{SAW}(x)) = O_p(n^{-1/(3+\epsilon)}).$$

The pointwise convergence rate of the LSAW estimator achieves the optimal rates established for local linear estimators for the special case of real-valued responses.

Turning to the convergence of LSWW, under assumption (A3), we define the population-level targets m^{SWW} as

$$m^{SWW} = \tilde{\psi}^{-1} \left[\operatorname{argmin}_{\gamma \in \Gamma_{\Theta}} M^{SWW}(\gamma, x) \right]. \quad (\text{S.11})$$

For LSWW we again obtain results for two scenarios, when the densities are known in Theorem S3 and when they are unknown and must be estimated in Theorem S4.

Theorem S3. (*LSWW for known distributions*). Assume (D1), (F1), (F3), (A3), (T0)-(T4) and (L1)-(L2). When adopting the slice-averaged Wasserstein distance, for a fixed $x \in \mathbb{R}$ and $m^{SWW}(x)$, $m_{L,h,\tau}^{SWW}(x)$ and $\check{m}_{L,h,\tau}^{SWW}(x)$ as per (S.11), (S.6) and (S.8), with $C_1(\tau)$ and $C_2(\tau)$ from (T3),

$$\begin{aligned} d_{\infty}(m^{SWW}(x), m_{L,h,\tau}^{SWW}(x)) &= O(C_1(\tau) + C_2(\tau)h^{8/7}), \\ d_{\infty}(m_{L,h,\tau}^{SWW}(x), \check{m}_{L,h,\tau}^{SWW}(x)) &= O_p(C_2(\tau)(nh)^{-2/7}), \end{aligned}$$

and when taking $h \sim n^{-1/5}$,

$$d_{\infty}(m^{SWW}(x), \check{m}_{L,h,\tau}^{SWW}(x)) = O_p(C_1(\tau) + C_2(\tau)n^{-8/35}).$$

Furthermore, assume (L3)-(L4) for a closed interval $\mathcal{T} \subset \mathbb{R}$, if $h \rightarrow 0$, $nh^2(-\log h)^{-1} \rightarrow \infty$ as $n \rightarrow \infty$, then for any $\epsilon > 0$,

$$\begin{aligned} \sup_{x \in \mathcal{T}} d_{\infty}(m^{SWW}(x), m_{L,h,\tau}^{SWW}(x)) &= O(C_1(\tau) + C_2(\tau)h^{8/7}), \\ \sup_{x \in \mathcal{T}} d_{\infty}(m_{L,h,\tau}^{SWW}(x), \check{m}_{L,h,\tau}^{SWW}(x)) &= O_p\left(C_2(\tau) \max\left\{(nh^2)^{-2/(7+\epsilon)}, [nh^2(-\log h)^{-1}]^{-2/7}\right\}\right), \end{aligned}$$

and when taking $h \sim n^{-1/(6+\epsilon)}$,

$$\sup_{x \in \mathcal{T}} d_{\infty}(m^{SWW}(x), \check{m}_{L,h,\tau}^{SWW}(x)) = O_p(C_1(\tau) + C_2(\tau)n^{-4/(21+\epsilon)}).$$

Theorem S4. (*LSWW for estimated distributions*). Assume (D1), (F1), (F3), (A3), (T0)-(T4), (L1)-(L2) and assumptions based on kernel density estimation (P1), (F1'), (K1)-(K2). When adopting the slice-averaged Wasserstein distance, for a fixed $x \in \mathbb{R}$ and $m^{SWW}(x)$, $m_{L,h,\tau}^{SWW}(x)$ and

$\hat{m}_{L,h,\tau}^{SWW}(x)$ as per (S.11), (S.6) and (S.10), with $C_1(\tau)$ and $C_2(\tau)$ from (T3),

$$\begin{aligned} d_\infty(m^{SWW}(x), m_{L,h,\tau}^{SWW}(x)) &= O(C_1(\tau) + C_2(\tau)h^{8/7}), \\ d_\infty(m_{L,h,\tau}^{SWW}(x), \hat{m}_{L,h,\tau}^{SWW}(x)) &= O_p\left(C_2(\tau)(nh)^{-2/7}\right), \end{aligned}$$

and when taking $h \sim n^{-1/5}$,

$$d_\infty(m^{SWW}(x), \hat{m}_{L,h,\tau}^{SWW}(x)) = O_p(C_1(\tau) + C_2(\tau)n^{-8/35}).$$

Furthermore, assume (L3)-(L4) for a closed interval $\mathcal{T} \subset \mathbb{R}$, if $h \rightarrow 0$, $nh^2(-\log h)^{-1} \rightarrow \infty$ as $n \rightarrow \infty$, then for any $\epsilon > 0$,

$$\begin{aligned} \sup_{x \in \mathcal{T}} d_\infty(m^{SWW}(x), m_{L,h,\tau}^{SWW}(x)) &= O(C_1(\tau) + C_2(\tau)h^{8/7}), \\ \sup_{x \in \mathcal{T}} d_\infty(m_{L,h,\tau}^{SWW}(x), \hat{m}_{L,h,\tau}^{SWW}(x)) &= O_p\left(C_2(\tau) \max\left\{(nh^2)^{-2/(7+\epsilon)}, [nh^2(-\log h)^{-1}]^{-2/7}\right\}\right), \end{aligned}$$

and when taking $h \sim n^{-1/(6+\epsilon)}$,

$$\sup_{x \in \mathcal{T}} d_\infty(m^{SWW}(x), \hat{m}_{L,h,\tau}^{SWW}(x)) = O_p(C_1(\tau) + C_2(\tau)n^{-4/(21+\epsilon)}).$$

This result demonstrates the convergence rate of LSWW regression and provides a decomposition of the reconstruction error into two components, similar to the situation for GSWW. In the special case of a Radon transform, Corollary S1 below shows that the curse of dimensionality is manifested in both $C_1(\tau)$ and $C_2(\tau)$, as a higher order of smoothness is required for a higher dimensional distribution to achieve the same convergence rate. Here we only give an explicit result for the more intricate scenario where densities are not fully observed and must be estimated; however, analogous results are available for scenarios with fully observed densities.

Corollary S1. *When taking the Radon transform \mathcal{R} and the corresponding regularized inverse \mathcal{R}_τ^{-1} as per (3) and (6), under the assumptions of Theorem S4,*

$$\begin{aligned} d_\infty(m^{SWW}(x), \hat{m}_{L,h,\tau}^{SWW}(x)) &= O_p(\tau^{-(k-p)} + \tau^p n^{-8/35}), \\ \sup_{x \in \mathcal{T}} d_\infty(m^{SWW}(x), \hat{m}_{L,h,\tau}^{SWW}(x)) &= O_p(\tau^{-(k-p)} + \tau^p n^{-4/(21+\epsilon)}), \end{aligned}$$

and with $\tau \sim n^{8/(35k)}$,

$$d_\infty(m^{SWW}(x), \hat{m}_{L,h,\tau}^{SWW}(x)) = O_p(n^{-8(k-p)/35k}).$$

Furthermore, for $\tau \sim n^{4/(21k)}$,

$$\sup_{x \in \mathcal{T}} d_\infty(m^{SWW}(x), \hat{m}_{L,h,\tau}^{SWW}(x)) = O_p(n^{-4(k-p)/(21k+\epsilon)}).$$

S.4.4 Numerical Algorithm

Following the notations in Section 7, the LSAW regression of (S.9) given $X = x$ is defined as,

$$\operatorname{argmin}_{\mathbf{W} \in \mathbb{R}^{p \times N}} \mathcal{M}_{L,h}(\mathbf{W}, x) = n^{-1} \sum_{i=1}^n [s_{iL,h}(x) d_{SW}^2(\mu_{\mathbf{W}^{(i)}}, \mu_{\mathbf{W}})]. \quad (\text{S.12})$$

The following proposition states that the target function of LSAW is smooth for the case of the Radon transform.

Proposition S5 (Theorem 1 (Bonnel et al., 2015)). *For each fixed x and $N_i \equiv N$, $\mathcal{M}_{L,h}(\mathbf{W}, x) : \mathbb{R}^{p \times N} \rightarrow \mathbb{R}$ is a L^1 function with a uniformly ρ_L -Lipschitz gradient for some $\rho_L > 0$ given by*

$$\nabla \mathcal{M}_{L,h}(\mathbf{W}, x) = n^{-1} \sum_{i=1}^n \left[s_{iL,h}(x) \int_{\Theta} \theta \left(\mathbf{W}(\theta) - \Pi_{\mathbf{W}(\theta)}^{-1} \circ \Pi_{\mathbf{W}^{(i)}(\theta)} \circ \mathbf{W}^{(i)}(\theta) \right)^T d\theta \right].$$

In analogy to Algorithm 1, we use the following gradient descent algorithm to find a stationary point.

Algorithm S3 LSAW Algorithm when using the Radon Transform

- 1: Initialize a grid $(\theta_1, \theta_2, \dots, \theta_L)$ along Θ
- 2: Set $N = \min_{i=1, \dots, n} N_i$, convergence threshold ε and learning rate η
- 3: For each $\mu_{\mathbf{W}^{(i)}}$, downsample $\mathbf{W}^{(i)}$ such that $\mathbf{W}^{(i)} \in \mathbb{R}^{p \times N}$
- 4: Initialize $\mathbf{W}^{[0]} \in \mathbb{R}^{p \times N}$ arbitrarily and fix the output predictor $X = x$
- 5: **repeat**
- 6: Calculate $\nabla \mathcal{M}_{L,h}(\mathbf{W}^{[k]}, x)$ through

$$\nabla \mathcal{M}_{L,h}(\mathbf{W}^{[k]}, x) = (nL)^{-1} \sum_{i=1}^n \sum_{l=1}^L s_{iL,h}(x) \theta_l \left(\mathbf{W}(\theta_l) - \Pi_{\mathbf{W}(\theta_l)}^{-1} \circ \Pi_{\mathbf{W}^{(i)}(\theta_l)} \circ \mathbf{W}^{(i)}(\theta_l) \right)^T$$

- 7: $\mathbf{W}^{[k+1]} = \mathbf{W}^{[k]} - \eta \nabla \mathcal{M}_{L,h}(\mathbf{W}^{[k]}, x)$
 - 8: **until** Algorithm converges with $\|\mathbf{W}^{[k+1]} - \mathbf{W}^{[k]}\|_2 / \|\mathbf{W}^{[k]}\|_2 < \varepsilon$ to $\mathbf{W}^{[\infty]}$
 - 9: Consider each column of $\mathbf{W}^{[\infty]}$ as a sample from $\hat{m}_{L,h}^{SAW}(x)$ and apply the kernel density estimator (S.1) to derive the density estimator \hat{f}
-

S.5 ADDITIONAL DATA APPLICATION

S.5.1 Exchange Traded Funds Modeling

We provide an additional data application to further illustrate the LSAW and LSWW regression models, aiming to demonstrate that these models can be used for the smoothing (nonparametric regression) of multivariate distributional against a one-dimensional covariate, for which we use calendar year in this application. Exchange Traded Funds (ETFs) are investment vehicle that

invests assets to track a benchmark, such as a general index, sector, bonds, fixed income, etc. Sector ETFs that track a particular industry have become popular among investors and are widely used for hedging and statistical arbitrage. Historical data for sector ETFs can be obtained from Yahoo finance <https://finance.yahoo.com/>. For each year, we model the bivariate distribution between the weekly return of iShares Biotechnology ETF (IBB) and the weekly return of iShares U.S. Real Estate ETF (IYR). Kernel density estimates of the data are in Figure S1.

Figure S4 displays the local Fréchet regressions for representative angles for LSWW. The variance of weekly returns for the two included sectors increased during the financial crisis of 2008-2009 and the COVID-19 pandemic in 2020, indicating increased market uncertainty during these periods. The real estate market was impacted more significantly than biotechnology, likely due to its sensitivity to economic and financial conditions.

Reconstructed density surfaces obtained from LSWW are shown in Figure S2 while those obtained from LSAW are shown in Figure S3. The sliced Wasserstein fraction of variance explained for LSWW and LSAW models, as per (23), is 0.95 and 0.74. During periods of economic expansion and positive investor sentiment, the biotech and real estate sectors both benefit and become positively correlated, as was the case during the housing bubble from 2002 to 2008 and the post-crisis period from 2010 to 2018. Conversely, during times of economic uncertainty or market volatility, correlations between sectors tend to decrease as investors shift toward safe-haven assets. This was evident during the financial crisis of 2008-2009 and the COVID-19 pandemic in 2020. Both LSWW and LSAW models reveal the general trends of the joint distribution and achieve satisfactory values of the sliced Wasserstein fraction of variance explained.

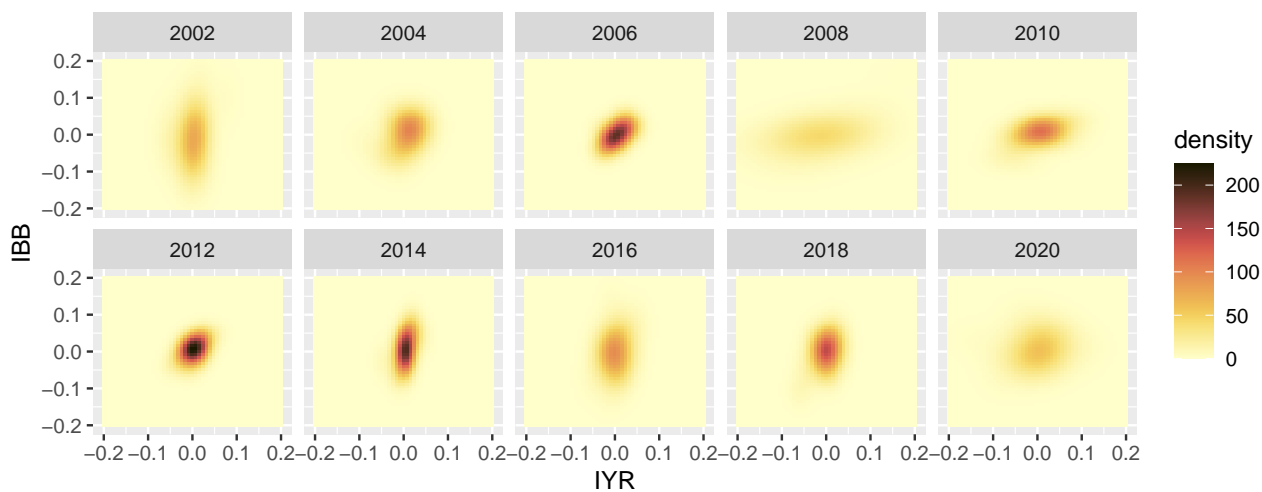


Figure S1: Kernel smoothed densities across different years for Biotechnology (IBB) and Real Estate (IYR) ETFs.

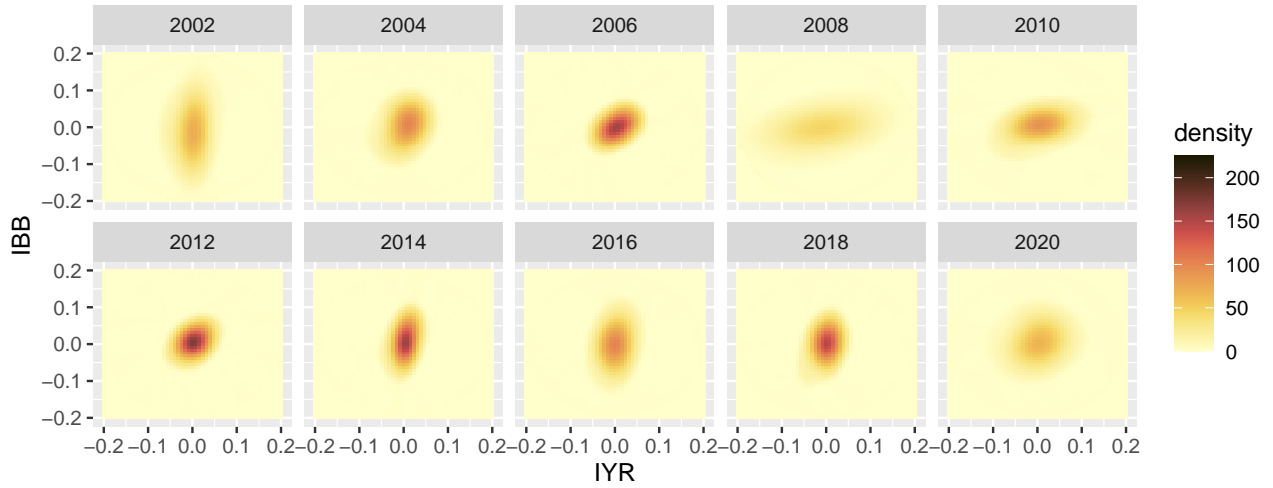


Figure S2: Fitted density surfaces for different years obtained by the LSWW version of sliced Wasserstein regression with sliced Wasserstein fraction of variance explained at level 0.95 for Biotechnology (IBB) and Real Estate (IYR) ETFs.

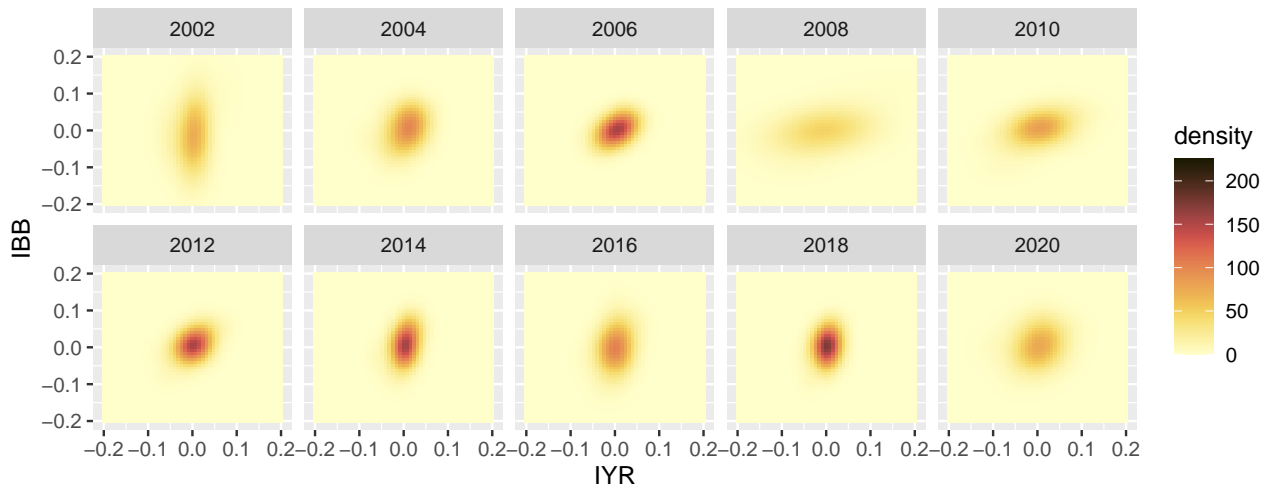


Figure S3: Fitted density surfaces for different years obtained by the LSAW version of sliced Wasserstein regression with sliced Wasserstein fraction of variance explained at level 0.74 for Biotechnology (IBB) and Real Estate (IYR) ETFs.

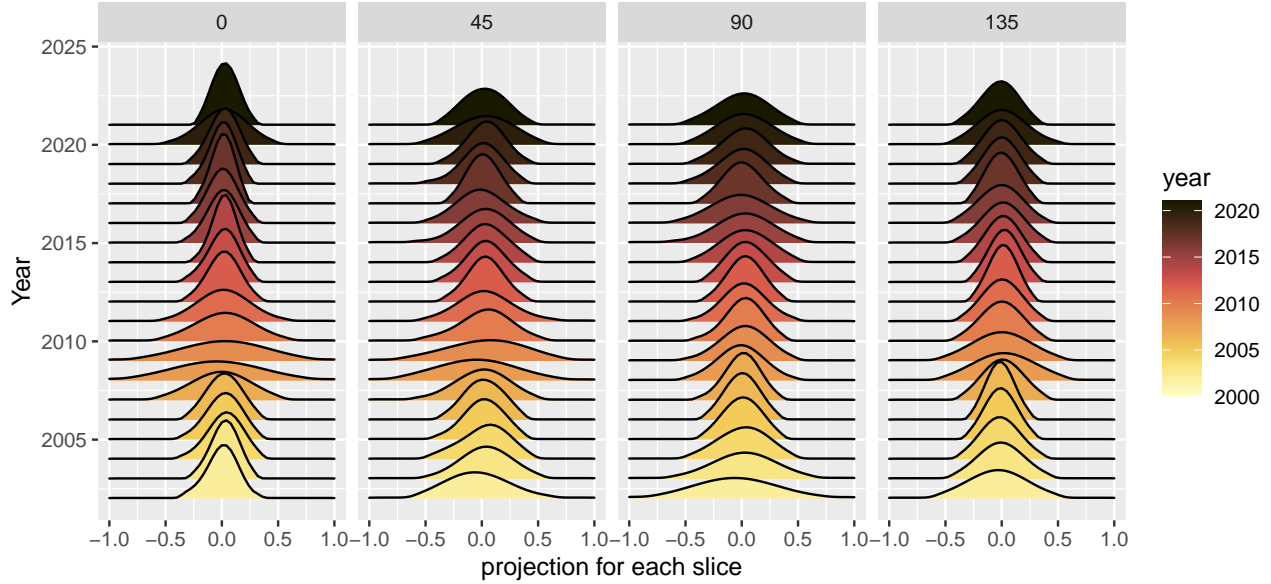


Figure S4: Fréchet regressions for LSWW between year (predictor, on the y -axis) and fitted slicing distributions (response, on the x -axis) for various projections. The number at the top of each panel indicates the angle of the respective projection with the x -axis (IYR) in Figure S1.

S.6 SLICING TRANSFORMS

Various slicing transforms besides the Radon transform may be of interest. One of these is the circular Radon transform \mathcal{CR} (Kuchment, 2006). This transform is the integral of a function f over a sphere centered at $\theta \in \Theta$, where

$$\mathcal{CR}(f)(\theta, u) = \int_{|z-\theta|=u} f(z) d\sigma(z), \quad \theta \in \Theta.$$

The injectivity property of the circular Radon transform has been studied previously, especially for the case when Θ is a unit sphere (Agranovsky and Quinto, 1996; Ehrenpreis, 2003). However, the analytic inverse formulas for even dimensions are still unknown (Finch and Patch, 2004).

Another transform of interest is the generalized Radon transform, which extends the classic Radon transform (Beylkin, 1984; Ehrenpreis, 2003). The generalized Radon transform \mathcal{GR} is defined as an integral over $I_{u,\theta} = \{z \in D | \chi(z, \theta) = u\}$,

$$\mathcal{GR}(f)(\theta, u) = \int_{\chi(z,\theta)=u} f(z) d\sigma(z),$$

where $d\sigma(z)$ integrates the surface area on $I_{u,\theta}$ and χ is a so-called defining function if it satisfies some regularity conditions (Beylkin, 1984). The sliced Wasserstein distance has been extended to the generalized Radon transform (Kolouri et al., 2019).

S.7 AUXILIARY LEMMAS AND PROPOSITIONS

Lemma S1. *Assume (D1) and (F1). For any vector $\mathbf{k} = (k_1, \dots, k_p)$ of p non-negative integers with $\sum_{l=1}^p k_l = k$ let $\mathcal{D}^{\mathbf{k}} = \frac{\partial^k}{\partial z_{k_1} \dots \partial z_{k_p}}$. It holds that $\mathcal{R}(f)(\theta, \cdot)$, $f \in \mathcal{F}$, is k -times differentiable, and*

$$\mathcal{R}[\mathcal{D}^{\mathbf{k}} f](\theta, u) = (-1)^k \left(\prod_{l=1}^p \theta_l^{k_l} \right) \frac{\partial^k (\mathcal{R}(f))}{\partial u^k}(\theta, u), \quad (\text{S.13})$$

for each $\theta = (\theta_1, \dots, \theta_p) \in \Theta$. Furthermore,

$$\left| \frac{\partial^k (\mathcal{R}(f))}{\partial u^k}(\theta, u) \right| \leq B_1 p^{k/2} < \infty,$$

for each $\theta \in \Theta$ where the constant B_1 does not depend on f or θ .

Proof. Assumptions (D1) and (F1) imply f has bounded support and continuous partial derivatives of order k , and formula (S.13) follows from Proposition 6.1.3 in Epstein (2007). For each $\theta = (\theta_1, \dots, \theta_p) \in \Theta$, $\sum_{j=1}^p \theta_j^2 = 1$,

$$\max_{j=1, \dots, p} |\theta_j| \geq p^{-1/2}.$$

Let $j(\theta) = \operatorname{argmax}_{j=1, \dots, p} |\theta_j|$. Taking $\mathbf{k}(\theta) = (0, \dots, 0, k, 0, \dots, 0)$ with all components equal to 0 except the $j(\theta)$ -th as k , so that

$$\left| \left(\prod_{l=1}^p \theta_l^{k_l} \right) \right| = \left(\prod_{l=1}^p |\theta_l|^{k_l} \right) \geq p^{-k/2}.$$

Since $\|\mathcal{D}^{\mathbf{k}(\theta)} f\|_{\infty} \leq B_1$ for a constant B_1 from (F1), it follows from the definition of the Radon transform that $\|\mathcal{R}[\mathcal{D}^{\mathbf{k}(\theta)} f](\theta, u)\|_{\infty} \leq B_1$. Hence,

$$\left| \frac{\partial^k (\mathcal{R}(f))}{\partial u^k}(\theta, u) \right| \leq B_1 p^{k/2}.$$

□

Lemma S2. *Suppose h_1, h_2 are three times continuously differentiable on $[0, 1]$ with $\max\{\|h_1^{(3)}(s)\|_{\infty}, \|h_2^{(3)}(s)\|_{\infty}\} \leq B_0$ where B_0 is a constant, then*

$$|h_1'(s) - h_2'(s)| \leq C(B_0) d_2^{4/7}(h_1, h_2), \quad \forall z \in [0, 1].$$

Proof. Consider a kernel function $\mathcal{K}(\cdot)$ that is a symmetric probability density function with compact support on $[-1, 1]$ and a bounded derivative \mathcal{K}' . Furthermore, assume \mathcal{K} satisfies that $\sigma^2(\mathcal{K}) = \int u^2 \mathcal{K}(u) du < \infty$ and $\sigma^3(\mathcal{K}) = \int |u|^3 \mathcal{K}(u) du < \infty$. From Lemma 1 in Chen et al. (2020),

arbitrarily fix $s \in (0, 1)$, and assume for the bandwidth a that $a \leq \min\{s, 1 - s\}$. As $a \rightarrow 0$,

$$\int_0^1 a^{-1} h_1(u) \mathcal{K} \left(\frac{s-u}{a} \right) du = h_1(s) + \frac{1}{2} a^2 \sigma^2(\mathcal{K}) h_1^{(2)}(s) + R_{11}(a), \quad (\text{S.14})$$

$$\int_0^1 a^{-2} h_1(u) \mathcal{K}' \left(\frac{s-u}{a} \right) du = h_1'(s) + \frac{1}{2} a^2 \sigma^2(\mathcal{K}) h_1^{(3)}(s) + R_{12}(a). \quad (\text{S.15})$$

Expanding $h_1(u)$,

$$h_1(u) = h_1(s) + h_1'(s)(u-s) + h_1^{(2)}(s)(u-s)^2/2 + \int_s^u \frac{h_1^{(3)}(t)(u-t)^2}{3!} dt.$$

Combining the expansion of $h_1(u)$ with (S.14) and (S.15), the remainder terms $R_{11}(a), R_{12}(a)$ can be bounded as follows

$$|R_{11}(a)| = \left| \int_0^1 a^{-1} \mathcal{K} \left(\frac{s-u}{a} \right) \int_s^u \frac{h_1^{(3)}(t)(u-t)^2}{3!} dt du \right| \lesssim B_0 a^3,$$

$$\begin{aligned} R_{12}(a) &= \int_0^1 a^{-2} \mathcal{K}' \left(\frac{s-u}{a} \right) \int_s^u \frac{h_1^{(3)}(t)(u-t)^2}{3!} dt du \\ &\quad - \int_0^1 a^{-1} \mathcal{K} \left(\frac{s-u}{a} \right) \frac{h_1^{(3)}(s)(u-s)^2}{3!} du \lesssim B_0 a^2. \end{aligned}$$

Similarly for $h_2(u)$, we have

$$\int_0^1 a^{-2} h_2(u) \mathcal{K}' \left(\frac{s-u}{a} \right) du = h_2'(s) + \frac{1}{2} a^2 \sigma^2(\mathcal{K}) h_2^{(3)}(s) + R_{22}(a).$$

Then

$$\begin{aligned} |h_1'(s) - h_2'(s)| &\leq a^{-2} \int_0^1 |h_1(u) - h_2(u)| \mathcal{K}' \left(\frac{s-u}{a} \right) du + \frac{1}{2} a^2 \sigma^2(\mathcal{K}) |h_1^{(3)}(s) - h_2^{(3)}(s)| \\ &\quad + |R_{12}(a) - R_{22}(a)| \\ &\leq a^{-3/2} d_2(h_1, h_2) \left(\int (\mathcal{K}'(u))^2 du \right)^{1/2} + B_0 a^2 \sigma^2(\mathcal{K}) + |R_{12}(a) + R_{22}(a)| \\ &\lesssim C_1(B_0) (a^{-3/2} d_2(h_1, h_2)) + C_2(B_0) a^2, \end{aligned}$$

for constants $C_1(B_0), C_2(B_0)$ which only depend on B_0 . By choosing $a \sim d_2^{2/7}(h_1, h_2)$,

$$|h_1'(s) - h_2'(s)| \leq C(B_0) d_2^{4/7}(h_1, h_2).$$

□

Lemma S3. *If D is compact, the univariate Wasserstein distance is bounded by the L^2 distance of the corresponding densities*

$$d_W(\nu_1, \nu_2) \lesssim d_2(\varphi(\nu_1), \varphi(\nu_2)), \quad \nu_1, \nu_2 \in \mathcal{G}. \quad (\text{S.16})$$

Proof. From Theorem 4 in [Gibbs and Su \(2002\)](#),

$$d_W(\nu_1, \nu_2) \leq \text{diam}(D) d_{TV}(\nu_1, \nu_2), \quad \nu_1, \nu_2 \in \mathcal{G},$$

where $\text{diam}(D) = \sup\{d(z_1, z_2) : z_1, z_2 \in D\}$ and $d_{TV}(\nu_1, \nu_2)$ represents the total variation distance $d_{TV} = \sup_{S \subset D} |\nu_1(S) - \nu_2(S)|$. Note that when ν_1 and ν_2 have densities $\varphi(\nu_1)$ and $\varphi(\nu_2)$, it follows that

$$d_{TV}(\nu_1, \nu_2) = \frac{1}{2} \int_D |\varphi(\nu_1)(u) - \varphi(\nu_2)(u)| du \leq \frac{1}{2} \sqrt{\text{diam}(D)} d_2(\varphi(\nu_1), \varphi(\nu_2)).$$

If D is a compact set, $\text{diam}(D)$ is bounded. We conclude that

$$d_W(\nu_1, \nu_2) \lesssim d_2(\varphi(\nu_1), \varphi(\nu_2)). \quad (\text{S.17})$$

□

Proposition S6. *Assume (T0) and (T2), for m_G^{SAW} as per (16) and M_G^{SWW} as per (18),*

$$m_G^{SAW}(x) = \tilde{\psi}^{-1} \left[\underset{\gamma \in \Gamma_\Theta \cap \tilde{\psi}(\mathcal{F})}{\text{argmin}} M_G^{SWW}(\gamma, x) \right].$$

Similarly, for $m_{L,h}^{SAW}$ as per (S.5) and $M_{L,h}^{SWW}$ as per (S.6),

$$m_{L,h}^{SAW}(x) = \tilde{\psi}^{-1} \left[\underset{\gamma \in \Gamma_\Theta \cap \tilde{\psi}(\mathcal{F})}{\text{argmin}} M_{L,h}^{SWW}(\gamma, x) \right].$$

Proof. The change of variable $\gamma = \tilde{\psi}(\omega) \in \tilde{\psi}(\mathcal{F})$, $\omega \in \mathcal{F}$ is a bijection because of the injectivity of the transform $\tilde{\psi}$. Hence,

$$\begin{aligned} m_G^{SAW}(x) &= \underset{\omega \in \mathcal{F}}{\text{argmin}} E \left[s_G(X, x) d_{SW}^2(\mu, \omega) \right] \\ &= \underset{\omega \in \mathcal{F}}{\text{argmin}} E \left[s_G(X, x) d_{DW}^2(\tilde{\psi}(\mu), \tilde{\psi}(\omega)) \right] \\ &= \tilde{\psi}^{-1} \left(\underset{\gamma \in \Gamma_\Theta \cap \tilde{\psi}(\mathcal{F})}{\text{argmin}} E \left[s_G(X, x) d_{DW}^2(\tilde{\psi}(\mu), \gamma) \right] \right) \\ &= \tilde{\psi}^{-1} \left[\underset{\gamma \in \Gamma_\Theta \cap \tilde{\psi}(\mathcal{F})}{\text{argmin}} M_G^{SWW}(\omega, x) \right]. \end{aligned}$$

Similarly,

$$m_{L,h}^{SAW}(x) = \tilde{\psi}^{-1} \left[\operatorname{argmin}_{\gamma \in \Gamma_{\Theta} \cap \tilde{\psi}(\mathcal{F})} M_{L,h}^{SWW}(\gamma, x) \right].$$

□

S.8 PROOFS

S.8.1 Proof of Proposition S1

Proof. Denoting by \tilde{N}_i the number of observations made for $f_{i,D_i|D_\epsilon}$ that fall within the domain D_ϵ , it is clear that each \tilde{N}_i follows a binomial distribution $\mathcal{B}(p_i, N_i)$, where $p_i = \int_{D_\epsilon} f_{i,D_i|D_\epsilon}(z) dz \geq M_0^{-1}|D_\epsilon|$ according to (F1'). From (P1), there exists a constant $c > 0$, such that $\min_{1 \leq i \leq n} N_i \geq cn^{1+p/4}$. Let $\tilde{c} = c \cdot |D_\epsilon|/(2M_0)$. Hoeffding's inequality (Hoeffding, 1994) implies that for any $\rho \leq N_i p_i$,

$$P\left(\tilde{N}_i \leq \rho\right) \leq \exp\left(-2N_i\left(p_i - \frac{\rho}{N_i}\right)^2\right).$$

Whence,

$$\begin{aligned} P\left(\min_{1 \leq i \leq n} \tilde{N}_i > \tilde{c}n^{1+p/4}\right) &= \prod_{i=1}^n P\left(\tilde{N}_i > \tilde{c}n^{1+p/4}\right) \\ &= \prod_{i=1}^n \left(1 - P\left(\tilde{N}_i \leq \tilde{c}n^{1+p/4}\right)\right) \\ &\geq \prod_{i=1}^n \left(1 - e^{-2N_i(p_i - |D_\epsilon|/(2M_0))^2}\right). \end{aligned}$$

Denote $\tilde{m}_i = p_i - |D_\epsilon|/(2M_0) \geq |D_\epsilon|/(2M_0) > 0$, then

$$\begin{aligned} P\left(\min_{1 \leq i \leq n} \tilde{N}_i > \tilde{c}n^{1+p/4}\right) &\geq \left(1 - e^{-2N_i \tilde{m}_i^2}\right)^n \\ &\geq \left(1 - e^{-2c\tilde{m}_i^2 n^{1+p/4}}\right)^n \\ &= e^{n \log\left(1 - e^{-2c\tilde{m}_i^2 n^{1+p/4}}\right)} \\ &\rightarrow 1 \text{ as } n \rightarrow \infty. \end{aligned}$$

□

S.8.2 Proof of Proposition 2

Proof. First, we show that if assumptions (D1), (F1) are satisfied, $\mathcal{R}(\mathcal{F})$ satisfies assumptions (D2) and (G1). It is clear that $\mathcal{R}(f) \geq 0$ and $\int_u \mathcal{R}(f)(\theta, u) du = 1$, where we denote $\mathcal{R}(f)(\theta, u)$ as $\mathcal{R}(f)(\theta)(u)$ for simplicity. The validity of (D2) follows from (D1) and the definition of the Radon transform. Furthermore, (G1) holds based on (D1), (F1) and the implications of Lemma S1. Next, we prove that (T0) and (T1) are satisfied. The injectivity of the Radon transform is evident from the definition. Hence, (T0) is satisfied. Since D is compact, there exists a constant C such that $\|D\|_\infty \leq C$. Computing the L^2 -distance between $\mathcal{R}(f_1)$ and $\mathcal{R}(f_2)$ for fixed $\theta \in \Theta$,

$$\begin{aligned} & \int_{\mathbb{R}} |\mathcal{R}(f_1)(\theta, u) - \mathcal{R}(f_2)(\theta, u)|^2 du \\ &= \int_{-C}^C \left(\int_{-C}^C \cdots \int_{-C}^C \left((f_1 - f_2) \left(u\theta + \sum_{j=1}^{p-1} s_j e_j \right) \right) ds_1 \cdots ds_p \right)^2 du \\ &\leq (2C)^{p-1} \int_{-C}^C \cdots \int_{-C}^C \left((f_1 - f_2) \left(u\theta + \sum_{j=1}^{p-1} s_j e_j \right) \right)^2 ds_1 \cdots ds_p du \\ &\leq (2C)^{p-1} d_2^2(f_1, f_2). \end{aligned}$$

The first inequality follows from the Cauchy-Schwarz inequality. Thus, (T1) holds as well. Assumptions (T2) and (T3) naturally follow as a corollary from Theorem 1. \square

S.8.3 Proof of Theorem 1

Proof. Set $\overline{\mathcal{R}(f)}(\theta, r) = \mathcal{J}_1(\mathcal{R}(f)(\theta))(r)$, $r \in \mathbb{R}$ and $\check{\Delta}_{\tau,1} = f - \check{\mathcal{R}}_\tau(\mathcal{R}(f))$. Then we have

$$\check{\Delta}_{\tau,1} = \frac{1}{2(2\pi)^p} \int_{\Theta} \int_{|r|>\tau} \overline{\mathcal{R}(f)}(\theta, r) e^{ir\langle \theta, z \rangle} |r|^{p-1} dr d\theta.$$

Since $\mathcal{R}(f)(\theta)(\cdot)$ has uniform bounded k -derivative for each $\theta \in \Theta$ from (G1), it follows from Proposition 4.2.1 in Epstein (2007) that

$$|\overline{\mathcal{R}(f)}(\theta, r)| \leq M_3 |r|^{-k},$$

where M_3 is a constant such that $\|\mathcal{R}(f)(\theta)(\cdot)\|_\infty \leq M_3$. Therefore, we get

$$\begin{aligned} \|\check{\Delta}_{\tau,1}\|_\infty &\leq \frac{1}{2(2\pi)^p} \int_{\Theta} \int_{|r|>\tau} |\overline{\mathcal{R}(f)}(\theta, r)| |r|^{p-1} dr d\theta \\ &\leq \frac{M_3}{2(2\pi)^p} \int_{\Theta} d\theta \int_{|r|>\tau} |r|^{p-k-1} dr \\ &= O(\tau^{-(k-p)}), \end{aligned}$$

where we note that $k \geq p + 1$ from (F3). Since $\int_D f(z)dz = 1 > 0$ and $\|f\|_\infty \leq M_0$ from (F1), we obtain $\|\Delta_{\tau,1}\|_\infty = O(\tau^{-(k-p)})$.

Next, set $\lambda_f = \mathcal{R}(f)$, $\lambda_f^* = \widetilde{\mathcal{R}(f)} \in \Lambda_\Theta$ and $\check{\Delta}_{\tau,2} = \check{\mathcal{R}}_\tau^{-1}(\lambda_f) - \check{\mathcal{R}}_\tau^{-1}(\lambda_f^*)$. This yields

$$\begin{aligned} \|\check{\Delta}_{\tau,2}\|_\infty &= \frac{1}{2(2\pi)^p} \int_\Theta \int_{|r| \leq \tau} (\overline{\lambda_f}(\theta, r) - \overline{\lambda_f^*}(\theta, r)) |r|^{p-1} e^{ir\langle \theta, z \rangle} dr d\theta \\ &\leq \frac{\tau^{p-1}}{2(2\pi)^p} \int_\Theta \int_{|r| \leq \tau} |\overline{\lambda_f}(\theta, r) - \overline{\lambda_f^*}(\theta, r)| dr d\theta \\ &\leq \frac{\tau^{p-1}}{2(2\pi)^p} \int_\Theta \int_{|r| \leq \tau} \int_{\mathbb{R}} |\lambda_f(\theta, u) - \lambda_f^*(\theta, u)| du dr d\theta \\ &\lesssim \frac{\tau^p}{2(2\pi)^p} d_2(\lambda_f, \lambda_f^*). \end{aligned}$$

The last inequality follows from the bounded support of Λ_Θ and \mathcal{F} . Note that $\|\check{\mathcal{R}}_\tau(\mathcal{R}(f)) - f\|_\infty = O(\tau^{-(k-p)})$ as $\tau \rightarrow \infty$. The boundedness of $\Delta_{\tau,2}$ follows from the fact $\int_D f(z)dz = 1$ and the condition that $d_2(\lambda_f^*, \lambda_f) \rightarrow 0$, whence

$$\|\Delta_{\tau,2}\|_\infty = O(\tau^p d_2(\lambda_f, \lambda_f^*)) = O\left(\tau^p d_2\left(\mathcal{R}(f), \widetilde{\mathcal{R}(f)}\right)\right).$$

□

S.8.4 Proof of Proposition 3

This proof follows a similar approach as Proposition 1 of [Kolouri et al. \(2019\)](#), but we present it for a more generalized version of the slicing transform as follows. If $\mu_1 = \mu_2$, $\mu_1, \mu_2 \in \mathcal{F}$, the slice-averaged Wasserstein distance satisfies $d_{SW}(\mu_1, \mu_2) = 0$. The non-negativity and symmetry properties of the slice-averaged Wasserstein distance are direct consequences of the Wasserstein distance being a metric. We next consider the triangle inequality. For any $\mu_1, \mu_2, \mu_3 \in \mathcal{F}$,

$$\begin{aligned} d_{SW}(\mu_1, \mu_3) &= \left(\int_\Theta d_W^2(G^{-1}(\tilde{\psi}(\mu_1)(\theta)), G^{-1}(\tilde{\psi}(\mu_3)(\theta))) \right)^{1/2} \\ &\leq \left(\int_\Theta d_W^2(G^{-1}(\tilde{\psi}(\mu_1)(\theta)), G^{-1}(\tilde{\psi}(\mu_2)(\theta))) \right)^{1/2} \\ &\quad + \left(\int_\Theta d_W^2(G^{-1}(\tilde{\psi}(\mu_2)(\theta)), G^{-1}(\tilde{\psi}(\mu_3)(\theta))) \right)^{1/2} \\ &= d_{SW}(\mu_1, \mu_2) + d_{SW}(\mu_2, \mu_3) \end{aligned}$$

The last inequality is obtained using the Minkowski inequality. We have thus established that the slice-averaged Wasserstein distance satisfies non-negativity, symmetry and the triangle inequality,

hence it is a pseudo-metric. If $d_{SW}(\mu_1, \mu_2) = 0$,

$$d_W \left(G^{-1} \left(\tilde{\psi}(\mu_1)(\theta) \right), G^{-1} \left(\tilde{\psi}(\mu_2)(\theta) \right) \right) = 0, \quad \text{for almost all } \theta \in \Theta.$$

Equivalently, considering that the Wasserstein distance is a metric, we have $\tilde{\psi}(\mu_1) = \tilde{\psi}(\mu_2)$. Therefore, the slice-averaged Wasserstein distance is a distance if and only if $\tilde{\psi}(\mu_1) = \tilde{\psi}(\mu_2)$ implies $\mu_1 = \mu_2$, which is equivalent to the injectivity of $\tilde{\psi}$. Note that $\tilde{\psi}$ is induced from ψ , and since φ and ϱ are bijective, the injectivity of $\tilde{\psi}$ is equivalent to (T0).

S.8.5 Proof of Proposition 4 and Proposition S4

Proof. For any $\gamma_1, \gamma_2 \in \Gamma_\Theta$,

$$\begin{aligned} d_{DW}^2(\gamma_1, \gamma_2) &= \int_{\Theta} d_W^2(G^{-1}(\gamma_1(\theta)), G^{-1}(\gamma_2(\theta))) d\theta \\ &\lesssim \int_{\Theta} d_2^2(\varrho(\gamma_1)(\theta), \varrho(\gamma_2)(\theta)) d\theta, \\ &\lesssim \int_{\Theta} d_\infty^2(\varrho(\gamma_1)(\theta), \varrho(\gamma_2)(\theta)) d\theta. \end{aligned}$$

The first inequality comes from the distance relationship discussed in Lemma S3. Following the boundedness condition in (D1) and (G1), $d_{DW}(\gamma_1, \gamma_2)$ is bounded from above. Therefore,

$$\begin{aligned} &E \left[s_G(X, x) d_{DW}^2(\tilde{\psi}(\mu), \gamma) \right] \\ &= \int_{X, \mu} s_G(X, x) \int_{\Theta} d_W^2 \left(G^{-1} \left(\tilde{\psi}(\mu)(\theta) \right), G^{-1}(\gamma(\theta)) \right) d\theta d_F(X, \mu) \\ &= \int_{\Theta} \int_{X, \mu} s_G(X, x) d_W^2 \left(G^{-1} \left(\tilde{\psi}(\mu)(\theta) \right), G^{-1}(\gamma(\theta)) \right) d_F(X, \mu) d\theta \\ &= \int_{\Theta} E \left[s_G(X, x) d_W^2 \left(G^{-1} \left(\tilde{\psi}(\mu)(\theta) \right), G^{-1}(\gamma(\theta)) \right) \right] d\theta. \end{aligned}$$

Since $s_G(X, x) > 0$, the second equation follows from the Fubini theorem. The last equation indicates that finding the minimum in $E \left[s_G(X, x) d_{DW}^2(\tilde{\psi}(\mu), \gamma) \right]$ is equivalent to finding the minimum in $E \left[s_G(X, x) d_W^2 \left(G^{-1} \left(\tilde{\psi}(\mu)(\theta) \right), G^{-1}(\gamma(\theta)) \right) \right]$ for almost all $\theta \in \Theta$. The result for the local slice-wise Wasserstein regression can be derived analogously. \square

S.8.6 Proof of Proposition S2 and Proposition S3

Proof. Set $z = (z_1, \dots, z_p)^T \in D \subset D_\epsilon$, $t = (t_1, \dots, t_p)^T \in D_\epsilon$ and the density f_{D_f} on domain D_ϵ as $f_{D_\epsilon} = f_{D_f} \mathbf{1}_{D_\epsilon}$. We can express the expected value as follows

$$E[\check{f}(z)|f] = \frac{1}{b^p} \int_{D_\epsilon} \kappa\left(\frac{z-t}{b}\right) f_{D_\epsilon}(t) dt, \quad z \in D. \quad (\text{S.18})$$

Expanding the multivariate density function $f_{D_\epsilon}(t)$ yields

$$f_{D_\epsilon}(t) = f_{D_\epsilon}(z) + \sum_{s=1}^p \frac{\partial f_{D_\epsilon}(z)}{\partial z_s} (t_s - z_s) + \sum_{s_1=1}^p \sum_{s_2=1}^p \frac{\partial^2 f_{D_\epsilon}(z^*)}{\partial z_{s_1} \partial z_{s_2}} (t_{s_1} - z_{s_1})(t_{s_2} - z_{s_2})/2, \quad t \in D_\epsilon,$$

where $z^* = z + \alpha(t - z) \in D_\epsilon$ for a $\alpha \in (0, 1)$. With (S.18),

$$E[\check{f}(z)|f] = f_{D_\epsilon}(z) + \frac{1}{2b^p} \sum_{s=1}^p \int_{D_\epsilon} \frac{\partial^2 f_{D_\epsilon}(z^*)}{\partial z_s^2} \kappa\left(\frac{z-t}{b}\right) (z_s - t_s)^2 dt, \quad z \in D.$$

Here we use the symmetry property (K1) of the kernel function. From (F1'), there exists a constant M_3 that does not depend on the function f_{D_ϵ} such that the partial derivative $|\partial^2 f_{D_\epsilon}(z^*)/\partial z_s^2|$ is uniformly bounded by M_3 for $s = 1, \dots, p$. Then

$$\sup_{z \in D} \sup_{f \in \mathcal{F}} |E[\check{f}(z)|f] - f_{D_\epsilon}(z) \mathbf{1}_D| = O(b^2). \quad (\text{S.19})$$

Next, we establish the boundedness of the variance of $\check{f}(z)$,

$$\begin{aligned} \text{Var}(\check{f}(z)|f) &= \frac{1}{N} \text{Var}\left(\kappa\left(\frac{z - Z_j}{b}\right) b^{-p} \middle| f\right) \\ &\leq \frac{1}{N} \int_{D_\epsilon} \kappa\left(\frac{z-t}{b}\right)^2 b^{-2p} f_{D_\epsilon}(t) dt \\ &\leq \frac{M_0}{N} \int_{D_\epsilon} \kappa\left(\frac{z-t}{b}\right)^2 b^{-2p} dt, \end{aligned}$$

where M_0 from assumption (F1) is a constant that does not depend on the density function f_{D_ϵ} . From (K2),

$$\sup_{z \in D} \sup_{f \in \mathcal{F}} \text{Var}(\check{f}(z)|f) = O\left(\frac{1}{Nb^p}\right).$$

Combining the above results, we obtain

$$\sup_{f \in \mathcal{F}} E\left(d_2(\check{f}, f_{D_\epsilon} \mathbf{1}_D)^2 \middle| f\right) = O\left(\frac{1}{Nb^p} + b^4\right).$$

Choosing $b \sim N^{-\frac{1}{p+4}}$ leads to

$$\sup_{f \in \mathcal{F}} E \left(d_2(\check{f}, f_{D_\epsilon} \mathbf{1}_D)^2 \middle| f \right) = O(N^{-4/(4+p)}).$$

For a fixed $f \in \mathcal{F}$ and the corresponding f_{D_ϵ} , by (S.19) and Proposition 9 in [Rinaldo and Wasserman \(2010\)](#),

$$\sup_{f \in \mathcal{F}} d_\infty(\check{f}, f_{D_\epsilon} \mathbf{1}_D) = O(b^2) + O_p \left(\sqrt{\frac{\log N}{Nb^p}} \right) = O_p(\sqrt{\log N} N^{-\frac{2}{p+4}}).$$

The error of uniform bound can be decomposed into a deterministic term $E[\check{f}(z)] - f_{D_\epsilon}(z)$ and a probabilistic term $\check{f} - E[\check{f}(z)]$. The first part depends on smoothness properties of f_{D_ϵ} only while the second part is characterized via empirical process techniques ([Rinaldo and Wasserman, 2010](#); [Jiang, 2017](#); [Chen, 2017](#)).

Note that the truncated density on domain D is presented as $f(z) = f_{D_\epsilon}(z) / \int_D f_{D_\epsilon}(u) du, z \in D$. We can then provide the convergence result for the truncated density \hat{f} . Note that when N is large enough we have,

$$\int_D f_{D_\epsilon}(u) du \geq \frac{|D|}{M_0}, \quad \int_D \check{f}(u) du \geq \frac{|D|}{2M_0}.$$

Whence,

$$\begin{aligned} d_2(\hat{f}, f) &\leq d_2 \left(\frac{\check{f}(z)}{\int_D \check{f}(u) du}, \frac{f_{D_\epsilon}(z) \mathbf{1}_D}{\int_D \check{f}(u) du} \right) + d_2 \left(\frac{f_{D_\epsilon}(z) \mathbf{1}_D}{\int_D \check{f}(u) du}, \frac{f_{D_\epsilon}(z) \mathbf{1}_D}{\int_D f_{D_\epsilon}(u) du} \right) \\ &\leq \frac{2M_0}{|D|} d_2(\check{f}, f_{D_\epsilon} \mathbf{1}_D) + \frac{2M_0^3}{|D|^{3/2}} d_2(\check{f}, f_{D_\epsilon} \mathbf{1}_D). \end{aligned}$$

Similarly, we have

$$d_\infty(\hat{f}, f) \leq \frac{2M_0}{|D|} d_\infty(\check{f}, f_{D_\epsilon} \mathbf{1}_D) + \frac{2M_0^3}{|D|} d_\infty(\check{f}, f_{D_\epsilon} \mathbf{1}_D).$$

It follows that when choosing $b \sim N^{-\frac{1}{p+4}}$

$$\begin{aligned} \sup_{f \in \mathcal{F}} E \left[d_2(\hat{f}, f)^2 \right] &= O(N^{-4/(4+p)}), \\ \sup_{f \in \mathcal{F}} d_\infty(\hat{f}, f) &= O_p(\sqrt{\log N} N^{-\frac{2}{p+4}}). \end{aligned}$$

□

S.8.7 Proof of Theorem 2

Proof. The proof proceeds in two steps.

Step 1. We first prove $d_{SW}(m_G^{SAW}(x), \check{m}_G^{SAW}(x)) = O_p(n^{-1/2})$ and establish the following three properties for the SAW estimator $\check{m}_G^{SAW}(x)$.

(R1): The objects $m_G^{SAW}(x)$ and $\check{m}_G^{SAW}(x)$ exist and are unique, the latter almost surely, and, for any $\epsilon > 0$,

$$\inf_{d_{SW}(m_G^{SAW}(x), \omega) > \epsilon} M_G^{SAW}(\omega, x) > M_G^{SAW}(m_G^{SAW}(x), x).$$

(R2): Let $B_\delta[m_G^{SAW}(x)]$ be the δ -ball in \mathcal{F} centered at $m_G^{SAW}(x)$ and $N(\epsilon, \mathcal{F}, d_{SW})$ its covering number using balls of size ϵ . Then

$$\int_0^1 (1 + \log N\{\delta\epsilon, B_\delta[m_G^{SAW}(x)], d_{SW}\})^{1/2} d\epsilon = O(1) \quad \text{as } \delta \rightarrow 0.$$

(R3) There exists $\eta_0 > 0, \beta_0 > 0$, possibly depending on x , such that

$$\inf_{d_{SW}(m_G^{SAW}(x), \omega) < \eta_0} \left\{ M_G^{SAW}(\omega, x) - M_G^{SAW}(m_G^{SAW}(x), x) - \beta_0 d_{SW}(m_G^{SAW}(x), \omega)^2 \right\} \geq 0.$$

Proof of (R2): We note that $d_W^2(\nu_1, \nu_2) = O(d_2(\varphi(\nu_1), \varphi(\nu_2)))$ from Lemma S3, whence

$$\begin{aligned} d_{SW}(\mu_1, \mu_2) &= \left(\int_{\Theta} d_W^2(G^{-1}(\tilde{\psi}(\mu_1)(\theta)), G^{-1}(\tilde{\psi}(\mu_2)(\theta))) d\theta \right)^{1/2} \\ &\lesssim \left(\int_{\Theta} d_2^2(\psi \circ \varphi(\mu_1)(\theta), \psi \circ \varphi(\mu_2)(\theta)) d\theta \right)^{1/2} \\ &\lesssim d_2(\varphi(\mu_1), \varphi(\mu_2)), \end{aligned} \tag{S.20}$$

where the last inequality follows from (T1) and the compactness of Θ . Using Theorem 2.7.1 of Vaart and Wellner (1996), there exists a constant A_1 depending only on k and p such that

$$\log N(\epsilon, \mathcal{F}, \|\cdot\|_\infty) \leq A_1 \epsilon^{-p/k},$$

for every $\epsilon > 0$ and $k > p/2$ from (F2). Note that $d_{SW}(\mu_1, \mu_2) = O(d_2(\varphi(\mu_1), \varphi(\mu_2))) = O(d_\infty(\varphi(\mu_1), \varphi(\mu_2)))$ and from the boundedness of the support set D , we have $B_{A_2\epsilon}(\mu, \|\cdot\|_\infty) \subset B_\epsilon(\mu, d_{SW})$ for some constant A_2 . Thus, we have $N(\epsilon, \mathcal{F}, d_{SW}) \leq A_3 N(\epsilon, \mathcal{F}, \|\cdot\|_\infty)$. For $\tilde{k} = p/k < 2$

it follows that

$$\begin{aligned} \int_0^1 \sqrt{1 + \log N\{\delta\epsilon, B_\delta[m_G^{SAW}(x)], d_{SW}\}} d\epsilon &< \int_0^1 \sqrt{1 + \log N\{\delta\epsilon, \mathcal{F}, d_{SW}\}} d\epsilon \\ &\leq \int_0^1 \sqrt{1 + A_3 A_1 \epsilon^{-p/k}} d\epsilon \end{aligned} \quad (\text{S.21})$$

$$\lesssim \int_0^1 \epsilon^{-\tilde{k}/2} < \infty. \quad (\text{S.22})$$

Proof of (R1) and (R3): We define the Hilbert space \mathcal{H} as the set of all functions

$$\mathcal{H} := \{\varsigma \in \mathcal{H} : \Theta \times [0, 1] \rightarrow \mathbb{R}, \int_\Theta \int_{[0,1]} \varsigma^2(\theta, s) ds d\theta < \infty\}$$

with the inner product

$$\langle \varsigma_1, \varsigma_2 \rangle = \int_\Theta \int_{[0,1]} \varsigma_1(\theta, s) \varsigma_2(\theta, s) ds d\theta.$$

Here the integral is well defined due to the Cauchy-Schwarz inequality. It is easy to verify that the space \mathcal{H} is a vector space over the field \mathbb{R} . The inner product satisfies the conditions of conjugate symmetry, linearity, and positive definiteness. The compactness of the Hilbert space follows from the fact that \mathcal{H} consists of measurable functions that are square integrable. We define the L^2 distance between two functions $\varsigma_1, \varsigma_2 \in \mathcal{H}$ as $d_2(\varsigma_1, \varsigma_2) = \langle \varsigma_1 - \varsigma_2, \varsigma_1 - \varsigma_2 \rangle$. Note that the quantile slicing space Γ_Θ is a subspace of \mathcal{H} and the distribution slicing Wasserstein metric coincides with the L^2 distance, i.e., $d_{DW}(\gamma_1, \gamma_2) = d_2(\gamma_1, \gamma_2)$ for $\gamma_1, \gamma_2 \in \Gamma_\Theta$. Let $B_G(x) = E[s_G(X, x)\tilde{\psi}(\mu)]$, then for any fixed $\omega \in \mathcal{F}$,

$$\begin{aligned} M_G^{SAW}(\omega, x) &= E[s_G(X, x)d_{SW}^2(\mu, \omega)] \\ &= E[s_G(X, x)d_2^2(\tilde{\psi}(\mu), \tilde{\psi}(\omega))] \\ &= E[s_G(X, x)\langle \tilde{\psi}(\mu) - \tilde{\psi}(\omega), \tilde{\psi}(\mu) - \tilde{\psi}(\omega) \rangle] \\ &= E[s_G(X, x)\langle \tilde{\psi}(\mu) - B_G(x), \tilde{\psi}(\mu) - B_G(x) \rangle] \\ &\quad + E[s_G(X, x)\langle B_G(x) - \tilde{\psi}(\omega), B_G(x) - \tilde{\psi}(\omega) \rangle] \\ &\quad + 2E[s_G(X, x)\langle \tilde{\psi}(\mu) - B_G(x), B_G(x) - \tilde{\psi}(\omega) \rangle] \\ &= E[s_G(X, x)d_2^2(\tilde{\psi}(\mu), B_G(x))] + E[s_G(X, x)d_2^2(B_G(x), \tilde{\psi}(\omega))] \\ &= E[s_G(X, x)d_2^2(\tilde{\psi}(\mu), B_G(x))] + d_2^2(B_G(x), \tilde{\psi}(\omega)), \end{aligned}$$

where the last equation follows from the fact that $E[s_G(X, x)] = 1$. Thus,

$$m_G^{SAW}(x) = \underset{\omega \in \mathcal{F}}{\operatorname{argmin}} d_2^2(B_G(x), \tilde{\psi}(\omega)).$$

Using $n^{-1} \sum_{i=1}^n s_{iG}(x) = 1$, one can similarly show that

$$\check{m}_G^{SAW}(x) = \operatorname{argmin}_{\omega \in \mathcal{F}} d_2^2(\check{B}_G(x), \tilde{\psi}(\omega)), \quad (\text{S.23})$$

where $\check{B}_G(x) = n^{-1} \sum_{i=1}^n s_{iG}(x) \tilde{\psi}(\mu_i)$. From the convexity and closedness of space $\tilde{\psi}(\mathcal{F})$, the minimizers $m_G^{SAW}(x)$ and $\check{m}_G^{SAW}(x)$ exist and are unique for any $x \in \mathbb{R}^q$, so that (R1) is satisfied. The best approximation $m_G^{SAW}(x) \in \mathcal{F}$ can be characterized by (Deutsch, 2012, chap.4)

$$\langle B_G(x) - \tilde{\psi}(m_G^{SAW}(x)), \tilde{\psi}(\omega) - \tilde{\psi}(m_G^{SAW}(x)) \rangle \leq 0, \text{ for all } \omega \in \mathcal{F}. \quad (\text{S.24})$$

Consequently, $d_2^2(B_G(x), \tilde{\psi}(\omega)) \geq d_2^2(B_G(x), \tilde{\psi}(m_G^{SAW}(x))) + d_2^2(\tilde{\psi}(m_G^{SAW}(x)), \tilde{\psi}(\omega))$. Then,

$$\begin{aligned} M_G^{SAW}(\omega, x) &\geq M_G^{SAW}(m_G^{SAW}(x), x) + d_2^2(\tilde{\psi}(m_G^{SAW}(x)), \tilde{\psi}(\omega)) \\ &= M_G^{SAW}(m_G^{SAW}(x), x) + d_{SW}^2(m_G^{SAW}(x), \omega), \end{aligned}$$

for all $\omega \in \mathcal{F}$. Hence, we may choose $\beta_0 = 1$.

Under Properties (R1)-(R3), it follows from Petersen and Müller (2019) that

$$d_{SW}(m_G^{SAW}(x), \check{m}_G^{SAW}(x)) = O_p(n^{-1/2}). \quad (\text{S.25})$$

Step 2. Here we show that $d_{SW}(m_G^{SAW}(x), \hat{m}_G^{SAW}(x)) = O_p(n^{-1/2})$. As before, $\varphi(\mu_i)$ and $\varphi(\hat{\mu}_i)$ denote the density functions of the i -th sample distribution μ_i and the estimator $\hat{\mu}_i$ (see (S.1)). From Proposition S2,

$$\max_{i=1, \dots, n} d_2(\varphi(\mu_i), \varphi(\hat{\mu}_i)) = O_p(N^{-2/(4+p)}),$$

and the derivation of (S.20) implies

$$d_2(\tilde{\psi}(\mu_i), \tilde{\psi}(\hat{\mu}_i)) = d_{SW}(\mu_i, \hat{\mu}_i) \lesssim d_2(\varphi(\mu_i), \varphi(\hat{\mu}_i)).$$

Consequently,

$$\max_{i=1, \dots, n} d_2(\tilde{\psi}(\mu_i), \tilde{\psi}(\hat{\mu}_i)) = O_p(N^{-2/(4+p)}).$$

Setting $\hat{B}_G(x) = n^{-1} \sum_{i=1}^n s_{iG}(x) \tilde{\psi}(\hat{\mu}_i)$ and noting that $n^{-1} \sum_{i=1}^n s_{iG}(x) = 1$,

$$d_2(\check{B}_G(x), \hat{B}_G(x)) = O_p(N^{-2/(4+p)}).$$

Similarly from the derivation of (S.23), we have

$$\hat{m}_G^{SAW}(x) = \operatorname{argmin}_{\omega \in \mathcal{F}} d_2(\hat{B}_G(x), \tilde{\psi}(\omega)).$$

By Theorem 5.3 of [Deutsch \(2012\)](#), considering the closeness and convexity of $\tilde{\psi}(\mathcal{F})$, we obtain

$$d_2(\tilde{\psi}(\check{m}_G^{SAW}(x)), \tilde{\psi}(\hat{m}_G^{SAW}(x))) = O_p(N^{-2/(4+p)}),$$

whence

$$d_{SW}(\check{m}_G^{SAW}(x), \hat{m}_G^{SAW}(x)) = O_p(N^{-2/(4+p)}). \quad (\text{S.26})$$

From [\(S.25\)](#) and assumption (P1), we conclude that

$$d_{SW}(m_G^{SAW}(x), \hat{m}_G^{SAW}(x)) = O_p(n^{-1/2}).$$

Uniform convergence results require stronger versions of these properties provided by (R4)-(R6) as stated below. Let $\|\cdot\|_E$ be the Euclidean norm on \mathbb{R}^q and $B > 0$ a constant.

(R4) Almost surely, for all $\|x\|_E \leq B$, the objects $m_G^{SAW}(x)$ and $\check{m}_G^{SAW}(x)$ exist and are unique. Additionally, for any $\epsilon > 0$,

$$\inf_{\|x\|_E \leq B} \inf_{d_{SW}(m_G^{SAW}(x), \omega) > \epsilon} \{M_G^{SAW}(\omega, x) - M_G^{SAW}[m_G^{SAW}(x), x]\} > 0$$

and there exists $\zeta = \zeta(\epsilon) > 0$ such that

$$\text{pr} \left(\inf_{\|x\|_E \leq B} \inf_{d_{SW}[\check{m}_G^{SAW}(x), \omega] > \epsilon} \{\check{M}_G^{SAW}(\omega, x) - \check{M}_G^{SAW}[\check{m}_G^{SAW}(x), x]\} \geq \zeta \right) \rightarrow 1.$$

(R5) With $B_\delta[m_G^{SAW}(x)]$ and $N\{\epsilon, B_\delta[m_G^{SAW}(x)], d_{SW}\}$ as in condition (R2),

$$\int_0^1 \sup_{\|x\|_E \leq B} (1 + \log N\{\delta\epsilon, B_\delta[m_G^{SAW}(x)], d_{SW}\})^{1/2} d\epsilon = O(1) \quad \text{as } \delta \rightarrow 0.$$

(R6) There exist $\tau_0 > 0$, $C_0 > 0$, possibly depending on B , such that

$$\inf_{\substack{\|x\|_E \leq B, \\ d_{SW}(m_G^{SAW}(x), \omega) < \tau_0}} \{M_G^{SAW}(\omega, x) - M_G[m_G^{SAW}(x), x] - C_0 d_{SW}[m_G^{SAW}(x), \omega]^2\} \geq 0.$$

The derivation of (R1) and (R3) lead to (R4) and (R6) with $C_0 = 1$. From equation [\(S.21\)](#), we find that (R5) is satisfied. From Theorem 2 of [Petersen and Müller \(2019\)](#), we conclude that

$$\sup_{\|x\|_E \leq B} d_{SW}(m_G^{SAW}(x), \check{m}_G^{SAW}(x)) = O_p(n^{-1/(2+\epsilon)}).$$

Note that formula (S.26) is uniform for $\|x\| \leq B$, leading to

$$\sup_{\|x\|_E \leq B} d_{SW} (m_G^{SAW}(x), \hat{m}_G^{SAW}(x)) = O_p(n^{-1/(2+\epsilon)}).$$

□

S.8.8 Proof of Theorem S2

Proof. We first show that

$$d_{SW} (m^{SAW}(x), m_{L,h}^{SAW}(x)) = O(h^2), \quad (\text{S.27})$$

$$d_{SW} (m_{L,h}^{SAW}(x), \check{m}_{L,h}^{SAW}(x)) = O_p((nh)^{-1/2}). \quad (\text{S.28})$$

We establish the following three properties for the SAW estimator $\check{m}_{L,h}^{SAW}(x)$.

(U1) The minimizers $m^{SAW}(x)$, $m_{L,h}^{SAW}(x)$ and $\check{m}_{L,h}^{SAW}(x)$ exist and are unique, the last almost surely. Additionally, for any $\epsilon > 0$,

$$\begin{aligned} & \inf_{d_{SW}(m^{SAW}(x), \omega) > \epsilon} \{M^{SAW}(\omega, x) - M^{SAW}[m^{SAW}(x), x]\} > 0, \\ \liminf_{h \rightarrow 0} & \inf_{d_{SW}(m_{L,h}^{SAW}(x), \omega) > \epsilon} \{M_{L,h}^{SAW}(\omega, x) - M_{L,h}^{SAW}[m_{L,h}^{SAW}(x), x]\} > 0. \end{aligned}$$

(U2) Let $B_\delta[m^{SAW}(x)]$ be the ball of radius δ centered at $m^{SAW}(x)$ with covering number $N\{\delta\epsilon, B_\delta[m^{SAW}(x)], d_{SW}\}$. Then

$$\int_0^1 (1 + \log N\{\delta\epsilon, B_\delta[m^{SAW}(x)], d_{SW}\})^{1/2} d\epsilon = O(1) \quad \text{as } \delta \rightarrow 0.$$

(U3) There exists $\eta_1, \eta_2 > 0$, $\beta_1, \beta_2 > 0$ such that

$$\begin{aligned} & \inf_{d_{SW}(m^{SAW}(x), \omega) < \eta_1} \left\{ M^{SAW}(\omega, x) - M^{SAW}[m^{SAW}(x), x] - \beta_1 d_{SW}(m^{SAW}(x), \omega)^2 \right\} \geq 0, \\ & \liminf_{h \rightarrow 0} \inf_{d_{SW}(m_{L,h}^{SAW}(x), \omega) < \eta_2} \left\{ M_{L,h}^{SAW}(\omega, x) - M_{L,h}^{SAW}[m_{L,h}^{SAW}(x), x] \right. \\ & \quad \left. - \beta_2 d_{SW}(m_{L,h}^{SAW}(x), \omega)^2 \right\} \geq 0. \end{aligned}$$

Proof of (U2). Similar to the derivation of (S.21), we have

$$\begin{aligned} \int_0^1 \sqrt{1 + \log N\{\delta\epsilon, B_\delta[m^{SAW}(x)], d_{SW}\}} d\epsilon & < \int_0^1 \sqrt{1 + \log N\{\delta\epsilon, \mathcal{F}, d_{SW}\}} d\epsilon \\ & \leq \int_0^1 \sqrt{1 + A_3 A_1 \epsilon^{-p/k}} d\epsilon < \infty. \end{aligned}$$

Proof of (U1) and (U3). For any distribution $\mu \in \mathcal{F}$, let $\tilde{\psi}(\mu) \in \tilde{\psi}(\mathcal{F})$ and $B(x) = E[\tilde{\psi}(\mu)|X = x]$. Then

$$\begin{aligned} M^{SAW}(\omega, x) &= E[d_{SW}^2(\mu, \omega)|X = x] \\ &= E[d_2^2(\tilde{\psi}(\mu), \tilde{\psi}(\omega))|X = x] \\ &= E[d_2^2(\tilde{\psi}(\mu), B(x))|X = x] + E[d_2^2(B(x), \tilde{\psi}(\omega))|X = x] \\ &= M^{SAW}[B(x), x] + d_2^2(B(x), \tilde{\psi}(\omega)) \end{aligned}$$

for all $\omega \in \mathcal{F}$, whence

$$m^{SAW}(x) = \operatorname{argmin}_{\omega \in \mathcal{F}} d_2^2(B(x), \tilde{\psi}(\omega)).$$

Set $B_{L,h}(x) = E[s_L(X, x, h)\tilde{\psi}(\mu)]$, $\check{B}_{L,h}(x) = n^{-1} \sum_{i=1}^n s_{iL,h}(x)\tilde{\psi}(\mu_i)$. Considering $E[s_L(x, h)] = 1$ and $n^{-1} \sum_{i=1}^n s_{iL,h}(x) = 1$, one finds

$$\begin{aligned} m_{L,h}^{SAW}(x) &= \operatorname{argmin}_{\omega \in \mathcal{F}} d_2^2(B_{L,h}(x), \tilde{\psi}(\omega)), \\ \check{m}_{L,h}^{SAW}(x) &= \operatorname{argmin}_{\omega \in \mathcal{F}} d_2^2(\check{B}_{L,h}(x), \tilde{\psi}(\omega)). \end{aligned}$$

From the convexity and closedness of space $\tilde{\psi}(\mathcal{F})$, the minimizers $m^{SAW}(x)$, $m_{L,h}^{SAW}(x)$ and $\check{m}_{L,h}^{SAW}(x)$ exist uniquely for any $x \in \mathbb{R}$, so that (U1) is satisfied. Following the characterization of the best approximation as per (S.24), we have

$$M^{SAW}(\omega, x) \geq M^{SAW}(m^{SAW}(x), x) + d_{SW}^2(m^{SAW}(x), \omega).$$

Similarly,

$$M_{L,h}^{SAW}(\omega, x) \geq M_{L,h}^{SAW}(m_{L,h}^{SAW}(x), x) + d_{SW}^2(m_{L,h}^{SAW}(x), \omega).$$

Thus, (U3) is satisfied with $\beta_1 = \beta_2 = 1$ and η_1, η_2 chosen arbitrarily. Under conditions (L1)-(L2) and (U1)-(U3), it follows from Theorem 3 and Theorem 4 in Petersen and Müller (2019) that

$$\begin{aligned} d_{SW}(m^{SAW}(x), m_{L,h}^{SAW}(x)) &= O(h^2), \\ d_{SW}(m_{L,h}^{SAW}(x), \check{m}_{L,h}^{SAW}(x)) &= O_p((nh)^{-1/2}). \end{aligned}$$

Hence, we conclude that (S.27) and (S.28) are satisfied. Similarly to the derivation of (S.26), it follows that

$$d_{SW}(m_{L,h}^{SAW}(x), \hat{m}_{L,h}^{SAW}(x)) = O_p((nh)^{-1/2} + N^{-4/(4+p)}).$$

From assumption (P1), we conclude that

$$d_{SW} (m_{L,h}^{SAW}(x), \hat{m}_{L,h}^{SAW}(x)) = O_p \left((nh)^{-1/2} \right).$$

Next, we provide stronger versions of the assumptions and then show that the previous results can be extended to hold uniformly over a closed interval $\mathcal{T} \subset \mathbb{R}$.

(U4) For all $x \in \mathcal{T}$, the minimizers $m^{SAW}(x)$, $m_{L,h}^{SAW}(x)$ and $\check{m}_{L,h}^{SAW}(x)$ exist and are unique, the latter almost surely. Additionally, for any $\epsilon > 0$,

$$\begin{aligned} & \inf_{x \in \mathcal{T}} \inf_{d_{SW}(m(x), \omega) > \epsilon} \{M^{SAW}(\omega, x) - M^{SAW}[m^{SAW}(x), x]\} > 0, \\ \liminf_{h \rightarrow 0} \inf_{x \in \mathcal{T}} \inf_{d_{SW}(m_{L,h}^{SAW}(x), \omega) > \epsilon} \{M_{L,h}^{SAW}(\omega, x) - M_{L,h}^{SAW}[m_{L,h}^{SAW}(x), x]\} > 0, \end{aligned}$$

and there exists $\zeta = \zeta(\epsilon) > 0$ such that

$$\text{pr} \left(\inf_{x \in \mathcal{T}} \inf_{d_{SW}(\check{m}_{L,n}^{SAW}(x), \omega) > \epsilon} \{ \check{M}_{L,n}^{SAW}(\omega, x) - \check{M}_{L,n}^{SAW}[\check{m}_{L,n}^{SAW}(x), x] \} \geq \zeta \right) \rightarrow 1.$$

(U5) With $B_\delta[m^{SAW}(x)]$ and $N\{\delta\epsilon, B_\delta[m^{SAW}(x)], d_{SW}\}$ as in condition (R5),

$$\int_0^1 \sup_{x \in \mathcal{T}} (1 + \log N\{\delta\epsilon, B_\delta[m^{SAW}(x)], d_{SW}\})^{1/2} d\epsilon = O(1) \quad \text{as } \delta \rightarrow 0.$$

(U6) There exists $\tau_1, \tau_2 > 0$ and $C_1, C_2 > 0$, such that

$$\begin{aligned} & \inf_{x \in \mathcal{T}} \inf_{d_{SW}(m^{SAW}(x), \omega) < \tau_1} \{M^{SAW}(\omega, x) - M^{SAW}[m^{SAW}(x), x] - C_1 d_{SW}(m^{SAW}(x), \omega)^2\} \geq 0, \\ & \liminf_{h \rightarrow 0} \inf_{x \in \mathcal{T}} \inf_{d_{SW}(m_{L,h}^{SAW}(x), \omega) < \tau_2} \{M_{L,h}^{SAW}(\omega, x) - M_{L,h}^{SAW}[m_{L,h}^{SAW}(x), x] \\ & \quad - C_2 d_{SW}(m_{L,h}^{SAW}(x), \omega)^2\} \geq 0. \end{aligned}$$

The arguments provided for (U1) and (U3) lead to (U4) and (U6) with $C_1 = C_2 = 1$. Using (S.21), one finds that (U5) is satisfied. With assumptions (L1)-(L2) from Theorem 1 of [Chen and Müller \(2022\)](#), we may conclude that

$$\begin{aligned} & \sup_{x \in \mathcal{T}} d_{SW}(m^{SAW}(x), m_{L,h}^{SAW}(x)) = O(h^2), \\ & \sup_{x \in \mathcal{T}} d_{SW}(m_{L,h}^{SAW}(x), \check{m}_{L,h}^{SAW}(x)) = O_p \left(\max \left\{ (nh^2)^{-1/(2+\epsilon)}, [nh^2(-\log h)^{-1}]^{-1/2} \right\} \right). \end{aligned}$$

From (S.26) which holds uniformly for $x \in \mathcal{T}$ and assumption (P1),

$$\sup_{x \in \mathcal{T}} d_{SW} (m_{L,h}^{SAW}(x), \hat{m}_{L,h}^{SAW}(x)) = O_p \left(\max \left\{ (nh^2)^{-1/(2+\epsilon)}, [nh^2(-\log h)^{-1}]^{-1/2} \right\} \right).$$

□

S.8.9 Proof of Theorem 3

Proof. Let $\gamma_G = \operatorname{argmin}_{\gamma \in \Gamma_\Theta} M_G^{SWW}(\gamma, x)$ and $\hat{\gamma}_G = \operatorname{argmin}_{\gamma \in \Gamma_\Theta} \hat{M}_G^{SWW}(\gamma, x)$. Note that the space Γ_Θ is convex and bounded. Then applying the arguments used for Theorem 2 to the metric space (Γ_Θ, d_{DW}) , it follows that

$$d_{DW}^2(\gamma_G(x), \hat{\gamma}_G(x)) = \int_{\Theta} \int_{[0,1]} (\gamma_G(\theta)(s) - \hat{\gamma}_G(\theta)(s))^2 ds d\theta = O_p(n^{-1}). \quad (\text{S.29})$$

Recall that G maps a univariate distribution to the corresponding quantile function while G^{-1} maps a quantile function to the corresponding distribution. Let Ψ map the quantile function to the cumulative distribution function. The arguments given in the proof of Proposition 2 in Petersen and Müller (2016) lead to

$$\begin{aligned} & \int_{\Theta} \int_{\mathbb{R}} (\Psi(\gamma_G(\theta))(u) - \Psi(\hat{\gamma}_G(\theta))(u))^2 dud\theta \\ & \lesssim \int_{\Theta} \int_{[0,1]} (\gamma_G(\theta)(s) - \hat{\gamma}_G(\theta)(s))^2 ds d\theta, \end{aligned}$$

where we observe that by assumption (G1) the derivatives of $\Psi(\gamma_G(\theta))$ and $\Psi(\hat{\gamma}_G(\theta))$ are bounded above and below. From Lemma S2 and the fact that $\varphi(G^{-1}(\gamma_G(\theta))) = \partial \Psi(\gamma_G(\theta))(u)/\partial u$ we obtain

$$\begin{aligned} & \int_{\Theta} \|\varphi(G^{-1}(\gamma_G(\theta)))(u) - \varphi(G^{-1}(\hat{\gamma}_G(\theta)))(u)\|_{\infty}^2 d\theta \\ & \leq \int_{\Theta} \left(\int_{\mathbb{R}} (\Psi(\gamma_G(\theta))(u) - \Psi(\hat{\gamma}_G(\theta))(u))^2 du \right)^{4/7} d\theta \\ & \lesssim \left(\int_{\Theta} \int_{\mathbb{R}} (\Psi(\gamma_G(\theta))(u) - \Psi(\hat{\gamma}_G(\theta))(u))^2 dud\theta \right)^{4/7} = O_p(n^{-4/7}). \end{aligned}$$

Here the first inequality follows from Lemma S2 and the second inequality from Hölder's inequality and the compactness of Θ . By assumption (D2) the support of elements in \mathcal{G} is uniformly bounded, whence

$$\int_{\Theta} \int_{\mathbb{R}} (\varphi(G^{-1}(\gamma_G(\theta)))(u) - \varphi(G^{-1}(\hat{\gamma}_G(\theta)))(u))^2 dud\theta = O_p(n^{-4/7}).$$

Recalling the notation $\varrho(\gamma_G)(\theta) = \varphi(G^{-1}(\gamma_G(\theta)))$ and the definition of L^2 distance in (2), we conclude

$$d_2(\varrho(\gamma_G), \varrho(\hat{\gamma}_G)) = O_p(n^{-2/7}). \quad (\text{S.30})$$

By Theorem 1, we have

$$d_\infty(m_G^{SWW}(x), \hat{m}_{G,\tau}^{SWW}) = O_p(C_1(\tau) + C_2(\tau)n^{-2/7}).$$

Uniform convergence then follows similarly to the uniform convergence in Theorem 2,

$$\sup_{\|x\| \leq B} d_{DW}(\gamma_G(x), \hat{\gamma}_G(x)) = O_p(n^{-1/(2+\epsilon)}),$$

for a given $B > 0$ and any $\epsilon > 0$. Since this holds uniformly across x , we have

$$\sup_{\|x\| \leq B} d_\infty(m_G^{SWW}(x), \hat{m}_{G,\tau}^{SWW}) = O_p(C_1(\tau) + C_2(\tau)n^{-2/(7+\epsilon)}).$$

□

S.8.10 Proof of Theorem S4

Consider the following notations

$$\begin{aligned} \gamma_x &= \operatorname{argmin}_{\gamma \in \Gamma_\Theta} M^{SWW}(\gamma, x), \\ \gamma_{x,L,h} &= \operatorname{argmin}_{\gamma \in \Gamma_\Theta} M_{L,h}^{SWW}(\gamma, x), \\ \hat{\gamma}_{x,L,h} &= \operatorname{argmin}_{\gamma \in \Gamma_\Theta} \hat{M}_{L,h}^{SWW}(\gamma, x). \end{aligned}$$

Note that the space Γ_Θ is convex and closed. Applying the arguments in the proof of Theorem S2 to the metric space (Γ_Θ, d_{DW}) , it follows that

$$\begin{aligned} d_{DW}(\gamma_{x,L,h}, \gamma_x) &= O_p(h^2), \\ d_{DW}(\gamma_{x,L,h}, \hat{\gamma}_{x,L,h}) &= O_p((nh)^{-1/2}). \end{aligned}$$

In analogy to the derivation of (S.30), we have

$$\begin{aligned} d_2(\varrho(\gamma_{x,L,h}), \varrho(\gamma_x)) &= O_p(h^{8/7}), \\ d_2(\varrho(\gamma_{x,L,h}), \varrho(\hat{\gamma}_{x,L,h})) &= O_p((nh)^{-2/7}). \end{aligned}$$

From assumption (T3), we obtain

$$\begin{aligned} d_\infty(m^{SWW}(x), m_{L,h,\tau}^{SWW}(x)) &= O_p(C_1(\tau) + C_2(\tau)h^{8/7}), \\ d_\infty(m_{L,h,\tau}^{SWW}(x), \hat{m}_{L,h,\tau}^{SWW}(x)) &= O_p\left(C_2(\tau)(nh)^{-2/7}\right). \end{aligned}$$

When choosing $h \sim n^{-1/5}$, the resulting convergence rate is

$$d_\infty(m^{SWW}(x), \hat{m}_{L,h,\tau}^{SWW}(x)) = O_p(C_1(\tau) + C_2(\tau)n^{-8/35}).$$

Under the additional assumptions (L3)-(L4), the uniform convergence rate similarly is obtained as

$$\begin{aligned} \sup_{x \in \mathcal{T}} d_\infty(m^{SWW}(x), m_{L,h,\tau}^{SWW}(x)) &= O(C_1(\tau) + C_2(\tau)h^{8/7}), \\ \sup_{x \in \mathcal{T}} d_\infty(m_{L,h,\tau}^{SWW}(x), \hat{m}_{L,h,\tau}^{SWW}(x)) &= O_p\left(C_2(\tau) \max\left\{(nh^2)^{-2/(7+\epsilon)}, [nh^2(-\log h)^{-1}]^{-2/7}\right\}\right), \end{aligned}$$

and when taking $h \sim n^{-1/(6+\epsilon)}$,

$$\sup_{x \in \mathcal{T}} d_\infty(m^{SWW}(x), \hat{m}_{L,h,\tau}^{SWW}(x)) = O_p(C_1(\tau) + C_2(\tau)n^{-4/(21+\epsilon)}).$$

S.9 ADDITIONAL FIGURES

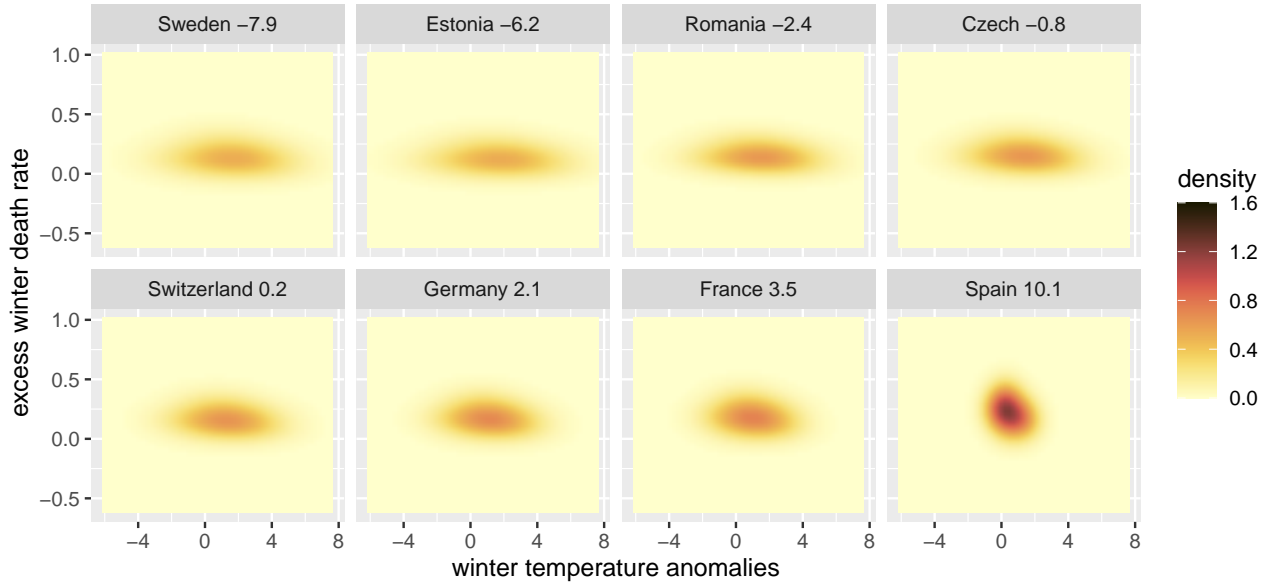


Figure S5: Excess Winter Death Rates: Fitted density surfaces for randomly selected countries obtained by the GSAW version of sliced Wasserstein regression with sliced Wasserstein fraction of variance explained at level 0.28.

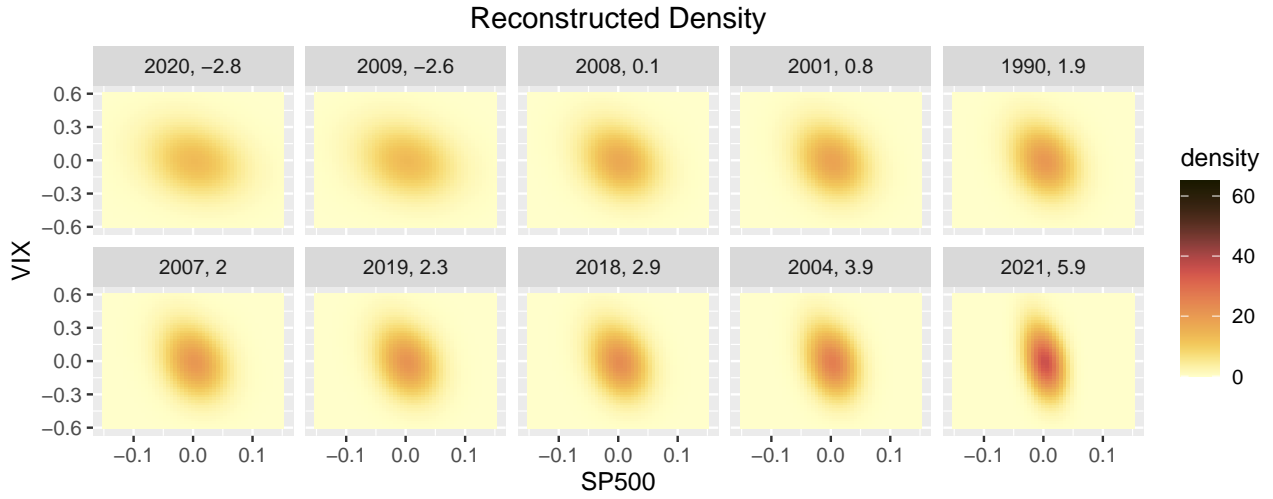


Figure S6: S&P500 and VIX Index Data: Fitted density surfaces for randomly selected years obtained by the GSAW version of sliced Wasserstein regression with sliced Wasserstein fraction of variance explained at level 0.13.

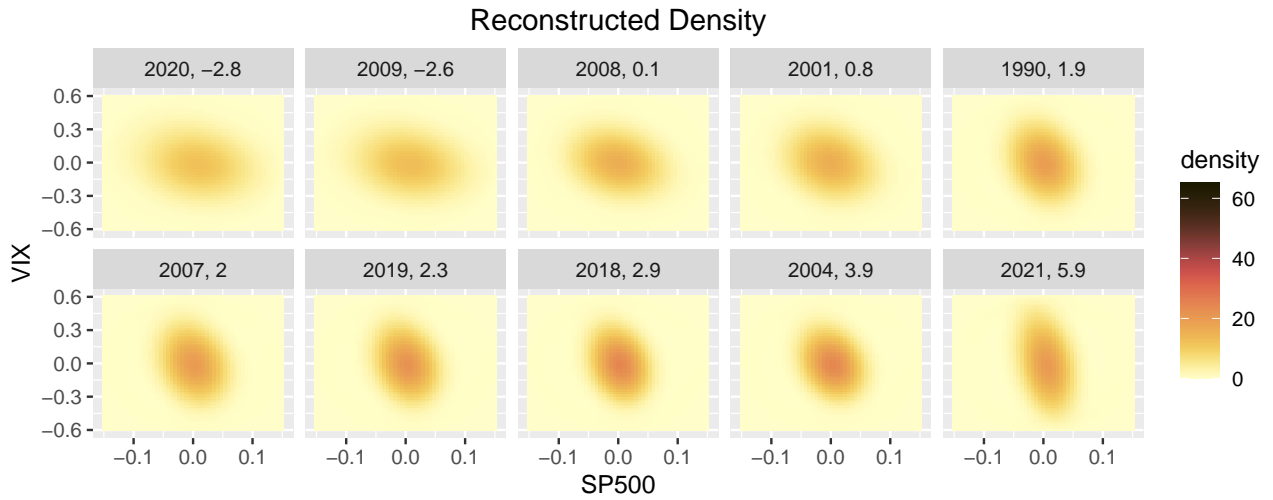


Figure S7: S&P500 and VIX Index data: Fitted density surfaces for randomly selected years obtained by the LSWW version of sliced Wasserstein regression with sliced Wasserstein fraction of variance explained at level 0.31.

REFERENCES

- Abeida, H., Zhang, Q., Li, J., and Merabtine, N. (2012), “Iterative sparse asymptotic minimum variance based approaches for array processing,” *IEEE Transactions on Signal Processing*, 61, 933–944.
- Agranovsky, M. L. and Quinto, E. T. (1996), “Injectivity sets for the Radon transform over circles and complete systems of radial functions,” *Journal of Functional Analysis*, 139, 383–414.
- Beylkin, G. (1984), “The inversion problem and applications of the generalized Radon transform,” *Communications on Pure and Applied Mathematics*, 37, 579–599.
- Bigot, J., Gouet, R., Klein, T., and López, A. (2017), “Geodesic PCA in the Wasserstein space by convex PCA,” *Annales de l’Institut Henri Poincaré B: Probability and Statistics*, 53, 1–26.
- Boissard, E., Gouic, T. L., and Loubes, J.-M. (2015), “Distribution’s template estimate with Wasserstein metrics,” *Bernoulli*, 21, 740–759.
- Bonneel, N., Rabin, J., Peyré, G., and Pfister, H. (2015), “Sliced and Radon Wasserstein barycenters of measures,” *Journal of Mathematical Imaging and Vision*, 51, 22–45.
- Bracewell, R. N. (1956), “Strip integration in radio astronomy,” *Australian Journal of Physics*, 9, 198–217.
- Chen, Y., Dawson, M., and Müller, H.-G. (2020), “Rank dynamics for functional data,” *Computational Statistics & Data Analysis*, 149, 106963.
- Chen, Y., Lin, Z., and Müller, H.-G. (2023a), “Wasserstein regression,” *Journal of the American Statistical Association*, 118, 869–882.
- Chen, Y. and Müller, H.-G. (2022), “Uniform convergence of local Fréchet regression with applications to locating extrema and time warping for metric space valued trajectories,” *The Annals of Statistics*, 50, 1573–1592.
- Chen, Y., Zhou, Y., Chen, H., Gajardo, A., Fan, J., Zhong, Q., Dubey, P., Han, K., Bhattacharjee, S., Zhu, C., Iao, S. I., Kundu, P., Alexander, P., and Müller, H.-G. (2023b), “Fréchet: Statistical Analysis for Random Objects and Non-Euclidean Data,” URL <https://CRAN.R-project.org/package=frechet>. R package version 0.3.0.
- Chen, Y.-C. (2017), “A tutorial on kernel density estimation and recent advances,” *Biostatistics & Epidemiology*, 1, 161–187.
- Cherubini, U., Luciano, E., and Vecchiato, W. (2004), *Copula Methods in Finance*, John Wiley & Sons.
- Courty, N., Flamary, R., Habrard, A., and Rakotomamonjy, A. (2017), “Joint distribution optimal transportation for domain adaptation,” *Advances in Neural Information Processing Systems*, 30.

- Cowling, A. and Hall, P. (1996), “On pseudodata methods for removing boundary effects in kernel density estimation,” *Journal of the Royal Statistical Society: Series B (Methodological)*, 58, 551–563.
- Dai, X. (2022), “Statistical inference on the Hilbert sphere with application to random densities,” *Electronic Journal of Statistics*, 16, 700–736.
- Deutsch, F. (2012), *Best Approximation in Inner Product Spaces*, CMS Books in Mathematics, Springer New York.
- Ehrenpreis, L. (2003), *The Universality of the Radon Transform*, Oxford University Press.
- Epstein, C. L. (2007), *Introduction to the Mathematics of Medical Imaging*, SIAM.
- Fan, J. and Müller, H.-G. (2021), “Conditional Wasserstein barycenters and interpolation/extrapolation of distributions,” *arXiv preprint arXiv:2107.09218*.
- (2022), “Conditional distribution regression for functional responses,” *Scandinavian Journal of Statistics*, 49, 502–524.
- Finch, D. and Patch, S. K. (2004), “Determining a function from its mean values over a family of spheres,” *SIAM Journal on Mathematical Analysis*, 35, 1213–1240.
- Fowler, T., Southgate, R. J., Waite, T., Harrell, R., Kovats, S., Bone, A., Doyle, Y., and Murray, V. (2015), “Excess Winter deaths in Europe: A multi-country descriptive analysis,” *The European Journal of Public Health*, 25, 339–345.
- Gajek, L. (1986), “On improving density estimators which are not bona fide functions,” *Annals of Statistics*, 14, 1612–1618.
- Gangbo, W. and McCann, R. J. (1996), “The geometry of optimal transportation,” *Acta Mathematica*, 177, 113–161.
- Ghodrati, L. and Panaretos, V. M. (2022), “Distribution-on-distribution regression via optimal transport maps,” *Biometrika*, 109, 957–974.
- (2023), “Transportation of measure regression in higher dimensions,” *arXiv preprint arXiv:2305.17503*.
- Ghosal, R., Varma, V. R., Volfson, D., Hillel, I., Urbanek, J., Hausdorff, J. M., Watts, A., and Zipunnikov, V. (2023), “Distributional data analysis via quantile functions and its application to modeling digital biomarkers of gait in Alzheimer’s Disease,” *Biostatistics*, 24, 539–561.
- Gibbs, A. L. and Su, F. E. (2002), “On choosing and bounding probability metrics,” *International Statistical Review*, 70, 419–435.

- Guégan, D. and Iacopini, M. (2018), “Nonparametric forecasting of multivariate probability density functions,” *arXiv preprint arXiv:1803.06823*.
- Hazelton, M. L. and Marshall, J. C. (2009), “Linear boundary kernels for bivariate density estimation,” *Statistics & Probability Letters*, 79, 999–1003.
- Healy, J. D. (2003), “Excess winter mortality in Europe: A cross country analysis identifying key risk factors,” *Journal of Epidemiology & Community Health*, 57, 784–789.
- Helgason, S. (2010), *Integral Geometry and Radon Transforms*, Springer New York.
- Herman, G. T. (2009), *Fundamentals of Computerized Tomography: Image Reconstruction from Projections*, Springer Science & Business Media.
- Hoeffding, W. (1994), “Probability inequalities for sums of bounded random variables,” *The collected works of Wassily Hoeffding*, 409–426.
- Horbelt, S., Liebling, M., and Unser, M. (2002), “Discretization of the Radon transform and of its inverse by spline convolutions,” *IEEE Transactions on Medical Imaging*, 21, 363–376.
- Hron, K., Machalová, J., and Menafoglio, A. (2023), “Bivariate densities in Bayes spaces: Orthogonal decomposition and spline representation,” *Statistical Papers*, 64, 1629–1667.
- Hron, K., Menafoglio, A., Templ, M., Hruzova, K., and Filzmoser, P. (2016), “Simplicial principal component analysis for density functions in Bayes spaces,” *Computational Statistics and Data Analysis*, 94, 330–350.
- Jiang, H. (2017), “Uniform convergence rates for kernel density estimation,” in *International Conference on Machine Learning*, PMLR, pp. 1694–1703.
- Kak, A. C. and Slaney, M. (2001), *Principles of Computerized Tomographic Imaging*, SIAM.
- Kantorovich, L. V. (2006), “On the translocation of masses,” *Journal of Mathematical Sciences*, 133, 1381–1382.
- Kitagawa, J. and Takatsu, A. (2023), “Two new families of metrics via optimal transport and barycenter problems,” *arXiv preprint arXiv:2311.15874*.
- Kolouri, S., Nadjahi, K., Simsekli, U., Badeau, R., and Rohde, G. (2019), “Generalized sliced Wasserstein distances,” *Advances in Neural Information Processing Systems*, 32.
- Kolouri, S., Zou, Y., and Rohde, G. K. (2016), “Sliced Wasserstein kernels for probability distributions,” in *Proceedings of the IEEE Conference on Computer Vision and Pattern Recognition*, pp. 5258–5267.
- Küchler, U. and Tappe, S. (2008), “Bilateral gamma distributions and processes in financial mathematics,” *Stochastic Processes and their Applications*, 118, 261–283.

- Kuchment, P. (2006), “Generalized transforms of Radon type and their applications,” in *Proceedings of Symposia in Applied Mathematics*, vol. 63, p. 67.
- Madan, D. B. (2020), “Multivariate distributions for financial returns,” *International Journal of Theoretical and Applied Finance*, 23, 2050041.
- Madan, D. B. and Wang, K. (2017), “Asymmetries in financial returns,” *International Journal of Financial Engineering*, 4, 1750045.
- Matabuena, M., Petersen, A., Vidal, J. C., and Gude, F. (2021), “Glucodensities: A new representation of glucose profiles using distributional data analysis,” *Statistical Methods in Medical Research*, 30, 1445–1464.
- Menafoglio, A., Grasso, M., Secchi, P., and Colosimo, B. M. (2018), “Profile monitoring of probability density functions via simplicial functional PCA with application to image data,” *Technometrics*, 60, 497–510.
- Mersereau, R. M. and Oppenheim, A. V. (1974), “Digital reconstruction of multidimensional signals from their projections,” *Proceedings of the IEEE*, 62, 1319–1338.
- Meunier, D., Pontil, M., and Ciliberto, C. (2022), “Distribution regression with sliced Wasserstein kernels,” *arXiv preprint arXiv:2202.03926*.
- Müller, H.-G. and Stadtmüller, U. (1999), “Multivariate boundary kernels and a continuous least squares principle,” *Journal of the Royal Statistical Society Series B*, 61, 439–458.
- Nadjahi, K., Durmus, A., Chizat, L., Kolouri, S., Shahrampour, S., and Simsekli, U. (2020), “Statistical and topological properties of sliced probability divergences,” *Advances in Neural Information Processing Systems*, 33, 20802–20812.
- Nadjahi, K., Durmus, A., Simsekli, U., and Badeau, R. (2019), “Asymptotic guarantees for learning generative models with the sliced-Wasserstein distance,” *Advances in Neural Information Processing Systems*, 32.
- Natterer, F. (2001), *The Mathematics of Computerized Tomography*, SIAM.
- Officer, R. R. (1972), “The distribution of stock returns,” *Journal of the American Statistical Association*, 67, 807–812.
- Okano, R. and Imaizumi, M. (2023), “Distribution-on-distribution regression with Wasserstein metric: Multivariate Gaussian case,” *arXiv preprint arXiv:2307.06137*.
- Park, S. and Slepčev, D. (2023), “Geometry and analytic properties of the sliced Wasserstein space,” *arXiv preprint arXiv:2311.05134*.
- Pegoraro, M. and Beraha, M. (2022), “Projected statistical methods for distributional data on the real line with the Wasserstein metric.” *Journal of Machine Learning Research*, 23, 37–1.

- Petersen, A. and Müller, H.-G. (2016), “Functional data analysis for density functions by transformation to a Hilbert space,” *The Annals of Statistics*, 44, 183–218.
- Petersen, A. and Müller, H.-G. (2019), “Fréchet regression for random objects with Euclidean predictors,” *The Annals of Statistics*, 47, 691–719.
- Petersen, A., Zhang, C., and Kokoszka, P. (2022), “Modeling probability density functions as data objects,” *Econometrics and Statistics*, 21, 159–178.
- Peyré, G., Cuturi, M., et al. (2019), “Computational optimal transport: With applications to data science,” *Foundations and Trends® in Machine Learning*, 11, 355–607.
- Quellmalz, M., Beinert, R., and Steidl, G. (2023), “Sliced optimal transport on the sphere,” *arXiv preprint arXiv:2304.09092*.
- Qureshi, S. A., Mirza, S. M., and Arif, M. (2005), “Inverse Radon transform-based image reconstruction using various frequency domain filters in parallel beam transmission tomography,” in *2005 Student Conference on Engineering Sciences and Technology*, IEEE, pp. 1–8.
- Rabin, J., Peyré, G., Delon, J., and Bernot, M. (2011), “Wasserstein barycenter and its application to texture mixing,” in *International Conference on Scale Space and Variational Methods in Computer Vision*, Springer, pp. 435–446.
- Radon, J. (1917), “Über die Bestimmung von Funktionen durch ihre Integralwerte längs gewisser Mannigfaltigkeiten,” *Akad. Wiss.*, 69, 262–277.
- Rinaldo, A. and Wasserman, L. (2010), “Generalized density clustering,” *The Annals of Statistics*, 38, 2678–2722.
- Rustamov, R. M. and Majumdar, S. (2023), “Intrinsic sliced Wasserstein distances for comparing collections of probability distributions on manifolds and graphs,” in *International Conference on Machine Learning*, PMLR, pp. 29388–29415.
- Shepp, L. A. and Vardi, Y. (1982), “Maximum likelihood reconstruction for emission tomography,” *IEEE Transactions on Medical Imaging*, 1, 113–122.
- Tanguy, E., Flamary, R., and Delon, J. (2023), “Reconstructing discrete measures from projections. Consequences on the empirical sliced Wasserstein distance,” *arXiv preprint arXiv:2304.12029*.
- Vaart, A. W. and Wellner, J. A. (1996), *Weak Convergence and Empirical Processes*, Springer.
- Villani, C. (2003), *Topics in Optimal Transportation*, American Mathematical Society.
- Zhang, Q., Li, B., and Xue, L. (2022), “Nonlinear sufficient dimension reduction for distribution-on-distribution regression,” *arXiv preprint arXiv:2207.04613*.

Zhou, Y. and Müller, H.-G. (2022), “Network regression with graph Laplacians,” *The Journal of Machine Learning Research*, 23, 14383–14423.

— (2023), “Wasserstein Regression with Empirical Measures and Density Estimation for Sparse Data,” *arXiv preprint arXiv:2308.12540*.

Zhu, C. and Müller, H.-G. (2023a), “Autoregressive optimal transport models,” *Journal of the Royal Statistical Society Series B: Statistical Methodology*, 85, 1012–1033.

— (2023b), “Geodesic Optimal Transport Regression,” *arXiv preprint arXiv:2312.15376*.

— (2023c), “Spherical autoregressive models, with application to distributional and compositional time series,” *Journal of Econometrics*.